A finite-difference analysis of turbulent, axisymmetric, buoyant jets and plumes

by

Imtiaz Kamil Madni

A Dissertation Submitted to the
Graduate Faculty in Partial Fulfillment of
The Requirements for the Degree of
DOCTOR OF PHILOSOPHY
Major: Mechanical Engineering

Approved:

Signature was redacted for privacy.

In Charge of Major Work

Signature was redacted for privacy.

For the Major Department

Signature was redacted for privacy.

For the Graduate College

Iowa State University
Ames, Iowa

1975

TABLE OF CONTENTS

LIST OF TABLES

LIST OF FIGURES

NOMENCLATURE

Latin Symbols

c_p	specific heat at constant pressure
d_o	diameter of jet or plume at discharge
F	velocity ratio function
$\vec{F}$	body force per unit volume
Fr_o	discharge Froude number, $u_o^2/[gd_o(\rho_{\infty_o} - \rho_o)/\rho_o]$, dimensionless
Fr	local Froude number, $u^2/[2g\delta(\rho_\infty - \rho)/\rho_o]$, dimensionless
f(y)	initial velocity distribution
F(Y)	dimensionless initial velocity distribution
g(y)	initial temperature distribution
G(Y)	dimensionless initial temperature distribution
g	acceleration of gravity
$\vec{g}$	gravity vector, $-g\vec{k}$
G	stability parameter, $g(\Gamma - \lambda)/T_{o,a}$
H	discharge depth
$\vec{i}_s, \vec{i}_y, \vec{i}_\phi$	unit vectors parallel to the s, y, ϕ axes, respectively
k	thermal conductivity
K_1, K_2, K_3, K_4	constants in models for turbulent viscosity
ℓ	mixing length
ℓ_o	unmodified mixing length in Monin-Oboukhov formula
n	total or effective kinematic voscosity
N	dimensionless total or effective kinematic viscosity, n/ν
n_H	total or effective diffusivity for heat

N_H	dimensionless total or effective diffusivity for heat, n_H/ν
NY	transverse grid number at jet half-width
NYT	transverse grid number at jet thermal half-width
NYJ	max(NY,NYT)
Pr	Prandtl number, ν/α
q	heat flux due to molecular and turbulent transport
R	velocity ratio, u_∞/u_o
$\bar{R}$	radius of curvature, $(d\theta/ds)^{-1}$
Re_o	Reynolds number at discharge, $u_o d_o/\nu$, dimensionless
Re_{cr}	critical Reynolds number above which flow is always turbulent, dimensionless
Ri	gradient Richardson number, $[g(\partial t/\partial y)]/[T_a(\partial u/\partial y)^2]$
r_o	radius of jet or plume at discharge
s	distance along jet or plume axis
S	dimensionless axial distance, $s u_o/\nu$
ΔS	increment of S
s_ℓ	starting length
t	temperature
T	non-dimensional temperature, $(t - t_\infty)/(t_o - t_\infty)$
$T_{o,a}$	discharge temperature, in degrees absolute
$\bar{T}$	stratification parameter, $(\rho_\infty - \rho_o)/[-r_o(d\rho_\infty/dz)]$
u	s-component of time mean velocity
U	dimensionless s-component of time mean velocity, u/u_o
v	y-component of time mean velocity
V	dimensionless y-component of time mean velocity, v/u_o
x	distance along x-axis

X	dimensionless distance along x-axis, $x u_o/\nu$
y	radial distance from jet centerline
Y	dimensionless radial distance from jet centerline, $y u_o/\nu$
$y_{1/2}$	radial distance from jet centerline to point at which $(u - u_\infty)/(u_c - u_\infty) = 0.5$
$y_{t_{1/2}}$	radial distance from jet centerline to point at which $(t - t_\infty)/(t_c - t_\infty) = 0.5$
y_{infl}	radial distance from jet centerline to velocity profile inflexion point
ΔY	increment of Y
z	vertical distance
Z	dimensionless vertical distance
z_M	zero momentum height
z_B	zero buoyancy height

Greek Symbols

α	thermal diffusivity, $k/\rho c_p$
β	isobaric volume expansivity, $-(\partial \rho/\partial t)_p/\rho_{ref}$
β'	constant in Monin-Oboukhov formula
γ	intermittency function, see Eq. (4.12)
δ	mixing layer thickness
μ	viscosity
ν	kinematic viscosity, μ/ρ
ρ	density
τ	total or effective shear stress in s-momentum equation
θ	angle between $\vec{i}_s$ and the horizontal
ϕ	azimuthal angle

λ	degree of ambient stratification, $-dt_\infty/dz$
Γ	adiabatic lapse rate of the atmosphere
$\Delta( )$	for dependent variables, this means $( ) - ( )_\infty$

Subscripts

c	evaluated at edge of core or at jet centerline if no. core exists
p	evaluated at constant pressure
e	evaluated at outer edge of jet
1/2	evaluated at velocity half-radius
o	value at jet discharge
ref	reference value
T	turbulent flow quantity
∞	free stream or ambient value
i,j	lattice or grid indices corresponding to S, Y directions, respectively
+,-	used in special notation, $\Delta Y_+ = (Y_{j+1} - Y_j)$, $\Delta Y_- = (Y_j - Y_{j-1})$, and similarly for ΔS
max	maximum
min	minimum

Superscripts

$( )'$	primes on dependent variables denote fluctuating quantities
$\overline{( )}$	bars on dependent variables denote time mean quantities
$(\rightarrow)$	denotes vector quantities

1. INTRODUCTION

1.1. Problem Description

The problem of the turbulent buoyant jet or plume issuing into flowing or quiescent ambients has received considerable theoretical and experimental attention in recent years. This interest is prompted by the occurrence of such flows as discharges from power plants and other industrial sources into the adjacent environment which can significantly alter the local ecosystem. Informative material on the general aspects of this problem can be found in Baumgartner and Trent [1], Harleman and Stolzenbach [2], Parker and Krenkel [3,4], and others.

In coastal waters, the most common pollutants are those associated with municipal and industrial wastes, but a non-material pollutant new to coastal waters and definitely of large dimensions already in rivers, lakes (and even the atmosphere), is heat. Over 70% of all water withdrawn for industrial use for cooling and condensing is used by thermal-electric power plants [3]. Petroleum, chemical, steel, and pulp-and-paper processing industries are examples of other, less significant users of cooling water. Power plants of today, being less than 40% efficient, produce more waste heat than electrical energy (the most efficient fossil-fuel stations achieve about 60% of the Carnot cycle efficiency for an overall thermal efficiency of 40%, and presently operating nuclear stations even lower - about 32%), and this heat can be most conveniently discharged into the immediate environment, be it a water body or the atmosphere. The demand for power in the United States has been doubling every 7 to 10 years, and, unless drastic steps are taken as are advocated by many

in response to the current "energy crisis," the electrical generating capacity is expected to continue doubling each decade. Regional economics and economics of scale have resulted in increases in plant size so that, where two 550 MW generating stations would have been adequate, they are being replaced by a single 1100 MW station. Thus, immense concentrations of waste heat have taken place, and discharge of these large quantities into the immediate environment will significantly increase the water temperature near the outfall.

A schematic diagram [5] of the thermal plant cycle is presented in Figure 1.1 to illustrate the sources of power and waste heat to the condenser. The boiler, either fossil or nuclear, converts water into high-pressure steam, which gives up some of its energy to drive the turbine. The turbine rotor is connected to the shaft of the generator where electrical energy is produced. The expanded steam from the turbine exhaust then goes to the condenser where it is cooled until it condenses to water which is returned to the boiler to be used again.

The amount of heat removed at the condenser is related to the state of the turbine exhaust, and hence, dependent on the plant capacity and efficiency, but the temperature rise of cooling water passing through the condenser will depend on its flow rate. A typical condenser-water flow rate for a 1000 MW unit is about 1500 ft^3/sec (675,000 gal/min) [2], and using 40% efficiency for a fossil unit, and 32% for a nuclear unit, this gives a temperature rise ranging from 12 ^oF for the fossil unit to 20 ^oF for the nuclear unit.

Biochemical processes, including the rate of oxygen use, increase with rising water temperature; however, the ability of water to hold

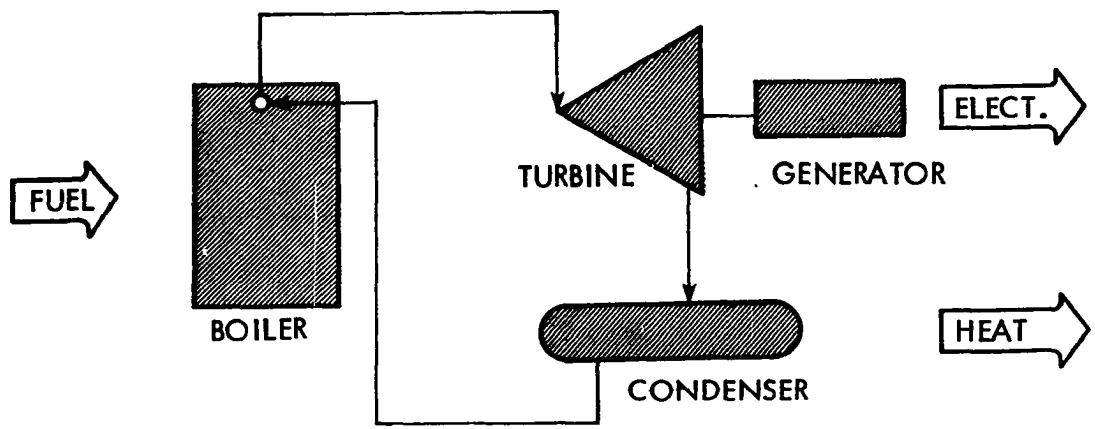

Fig. 1.1. Thermal plant cycle.

dissolved oxygen in solution decreases with increasing water temperature. Laboratory and field experiments have established lethal temperature limits and temperatures beyond which there is impairment of biological functions for fish and other components of the food chain. Indirect effects, which are more difficult to measure and evaluate, include the possibility of increased susceptibility to disease and increases in predators or less desirable species. There is general agreement that water temperature increases approaching the sublethal range of impaired biological activity should be avoided.

Another important side effect of the temperature rise is that, by diminishing the amount of oxygen in the water, it makes the water less capable of assimilating wastes. Toxic effects of chemical pollutants are also increased. The combined effects of the thermal discharge can thus cause significant deterioration of the stream water quality [6].

In an attempt to minimize these ill-effects and thereby provide maximum protection, regulatory agencies place strict controls on both maximum temperatures and allowable temperature rises, up to 5 ^{o}F, outside a certain zone called the "thermal mixing zone." The thermal mixing zone is the region in the immediate vicinity of the condenser discharge within which temperature excesses above the limits are allowed.

These temperature limits have a profound effect upon power plant siting and discharge design for if these requirements are not met, either an alternative means such as cooling towers must be employed, or the site of the power plant changed. That decision can only be taken after design for an optimal thermal discharge system has been made, based on the specifications of the cooling requirements for the power plant.

This requires knowledge of the temperature and velocity fields due to the discharge. Similarly, for ocean sewage outfalls, knowledge of the concentration and velocity fields due to the discharge is required in order to properly control the pollution problem. The present study deals with the prediction of these quantities through mathematical modeling.

Field studies and physical modeling (i.e., use of laboratory-sized models) are good ways of gaining that knowledge, but mathematical modeling has advantages in terms of economy and flexibility, hence aiding in the discharge design process. Mathematical modeling involves application of the fundamental equations of fluid dynamics and heat transfer, and making reasonable simplifying assumptions, to arrive at the differential equations governing the phenomena. These equations are then solved to obtain the results of interest, which must be compared with available measurements, to verify the modeling and solution method.

There are two approaches to mathematical modeling: (1) macro: involving a complete river or river system, lake or reservoir, estuary, or coastal area, and (2) micro: describing the distribution of heat in the immediate area of a thermal discharge. The latter approach, which is really all that is required from the mixing zone point of view, and also the more direct and economical one, is the approach taken in this investigation. In this approach, the flow is modeled as a turbulent buoyant jet or plume.

1.2. Status of Prediction Methods

The prediction of turbulent free shear flows, of which jet flow is probably the most important part, was for a long time most commonly done by integral methods, where the partial differential equations are integrated over the cross-section using assumptions such as the velocity and temperature (or concentration) profile shape and similarity, and arriving at a set of simpler, ordinary differential equations. Now, however, with the advent of faster and more economical digital computers, the differential methods have become the center of interest with most researchers. Here, the partial differential equations of the flow are solved directly using a finite-difference technique, with no assumptions of profile similarity being involved. A comparison of the Proceedings of the 1968 Stanford Conference on Computation of Turbulent Boundary Layers [7] and the 1972 Langley workshop [8] will provide an indication of the shift in emphasis towards differential methods. However, the methods most commonly used for plume prediction in waterways, oceans, and the atmosphere, still tend to be integral in nature [9-11]. Extensive work has been done by Abraham [12,13], Morton [14,15], Fan [16], Fan and Brooks [17], Hirst [10], and others. The integral method of Hirst is perhaps the most general. Differential methods would appear to have great potential usefulness in predicting the development of thermal plumes in lakes, rivers, oceans and the atmosphere since these methods allow arbitrary initial and boundary conditions, result in solutions for the local temperatures and velocities, and are not constrained to an assumed profile shape or family. However, examples of differential approaches in these

applications are scant. The Proceedings of the 1972 Langley Conference [8] contain a reasonably current study of presently known models and methods for the baseline case of the turbulent non-buoyant jet in co-flowing ambients. Other references, all dealing with non-buoyant jet calculations, are [18,19,20]. Trent and Welty [21,22] have presented a finite-difference method restricted to vertical plume flows. In the present study, a consistent analysis of several configurations is presented, using the differential approach.

1.3. Scope of Present Investigation

This investigation was carried out in an attempt to develop better methods for predicting the behavior of buoyant jets and plumes in response to the current interest and need for such prediction methods as, for example, in the design of power plant and ocean sewer outfalls. Although the research was originally directed toward thermal discharge applications in waterways, many of the results to date are applicable to atmospheric discharges also, and, without any modification of the computer program, even to ocean sewage outfall discharges. This will be explained more thoroughly later.

The approach has been to solve the boundary layer form of the governing differential equations by a finite-difference method utilizing a turbulence model to evaluate the turbulent diffusivities for heat and momentum.

The essential steps involved in the differential approach can be summarized as follows:

1. Develop the governing equations for the flow.
2. Establish appropriate initial and boundary conditions for the problem.
3. Non-dimensionalize the equations and initial and boundary conditions.
4. Cast the equations into finite-difference form.
5. Write the computer program.
6. Obtain the numerical results as computer output.

In Chapter 2, a summary of the basic assumptions involved and the flow configurations are shown. Chapter 3 is devoted to development of the present finite-difference analysis, starting with the governing differential equations of the flow in boundary layer form. The several steps in the differential approach as listed above are treated individually. This analysis used an explicit finite-difference scheme of the DuFort-Frankel type. The calculation procedure and the essential characteristics of the method are also presented. Chapter 4 examines the first application of the calculation procedure - the non-buoyant jet in a co-flowing or quiescent ambient. The several turbulence models considered and the results obtained are presented. Chapter 5 considers the buoyant vertical jet problem. Results for both homogeneous and stratified ambients are presented. In Chapter 6, the calculation method is extended to include curved trajectories as the buoyant jet discharged horizontally or inclined into a quiescent ambient, mixes with the ambient and rises due to buoyancy. Comparisons are made with experiment and with other methods, both integral and differential, wherever these have

been available, to establish the accuracy of the present analysis. Concluding remarks and suggestions for future work are made in Chapter 7.

2. PHYSICAL AND THEORETICAL CONSIDERATIONS

The basic problem is that of predicting the growth, properties, and trajectory of a round, heated turbulent jet or plume. Three flow categories will be considered: (1) the non-buoyant jet discharging into a co-flowing or quiescent ambient; (2) the vertically discharging buoyant jet or plume in a uniform or stratified ambient; and (3) the buoyant jet discharging horizontally or at an angle into a quiescent ambient under the simplifying assumption that the jet remains axisymmetric.

2.1. Background and Definitions

2.1.1. Flow configuration

Figure 2.1 shows the general flow configuration. On being discharged, the jet fluid mixes with the ambient. The mixing starts at the edges, and spreads both inward toward the jet centerline, and outward, causing the jet to grow. The axial distance to the point where mixing has reached the centerline is termed the starting length, and this flow regime is called the initial region, or zone of flow establishment. Here the flow is strongly influenced by the discharge conditions. After this point, the jet enters the main region or zone of established flow, where it continues to grow and the centerline velocity and temperature begin to decay, due to mixing with the slower-moving ambient.

When the jet momentum has been depleted to such an extent that the fluid is convected and diffused by the ambient currents and ambient turbulence, the jet is said to be in the far field region, or field zone. In this region, reduction of temperature is accomplished by passive

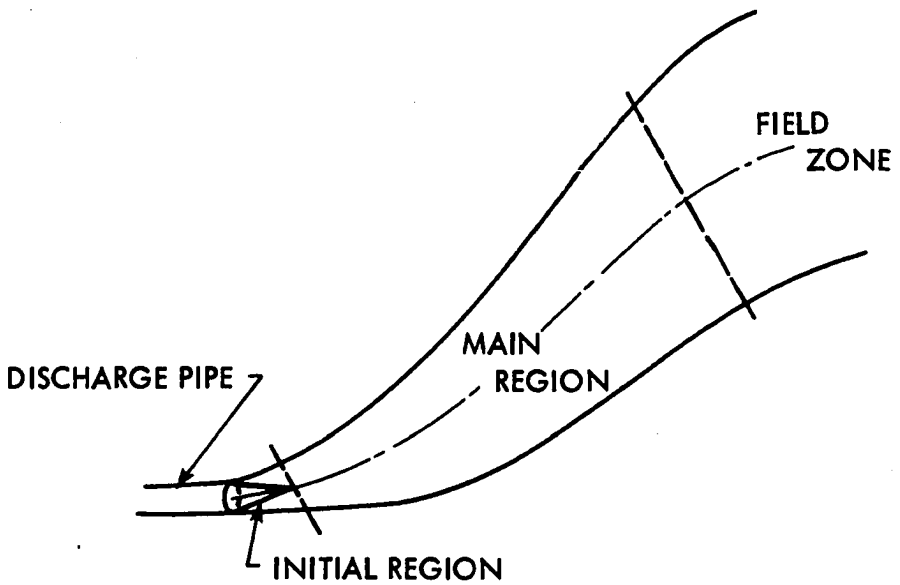

Fig. 2.1. Flow regimes for buoyant jets.

turbulent diffusion and surface heat losses. In the present analysis, emphasis is placed on the first two regimes, since it is here that the temperature excesses are significant from the point of view of thermal discharge design.

2.1.2. Ambient effects

The behavior of the jet is influenced by the initial conditions at diffuser exit, and by several ambient effects such as buoyancy, ambient density stratification, ambient currents, and turbulence levels. They are described briefly below.

Buoyancy: When the jet is produced as a heated discharge into a fluid of the same composition, it is warmer than the surrounding fluid, and hence, less dense. This difference in densities in the presence of the earth's gravitational field gives rise to an upward force known as buoyancy force, and this can have a pronounced effect on the jet behavior. For example, a buoyant jet discharging horizontally into a denser ambient will be deflected upwards, the amount of deflection depending on the degree of buoyancy under given flow conditions.

The terms jet and plume have different connotations, jet flow denoting a momentum dominated flow where buoyancy effects are considered negligible, and plume flow signifying a purely buoyant flow, with almost no momentum. Sometimes, however, the meanings do overlap, as when a flow, having both momentum and buoyancy, is called either a buoyant jet or forced plume, the terms being used interchangeably.

Where only general reference is intended, the words jet and plume will be used interchangeably in this work, (since no specific

characteristics are implied), allowing the terms to cover the whole gamut of flows ranging from pure jet to a pure plume flow.

Buoyancy effects also occur when sewage effluent is discharged through marine outfalls into the ocean since sewage effluent, being of nearly the same density as water, is less dense than sea water. This effect is examined in Chapters 5 and 6.

Ambient density stratification: Oceans, lakes, and the atmosphere are frequently stratified in density due to non-uniform temperature and/or salinity. Stable stratification, where ambient density decreases with increasing height, has the effect of gradually reducing the buoyancy force on a rising plume, until a region of zero buoyancy is reached where the plume motion upward will be only due to its vertical momentum. Further motion upward will result in negative buoyancy due to ambient density being lower than plume density and this will decelerate the plume until all upward motion is lost and the plume has reached its maximum height of rise. This effect is examined in Chapter 5.

Current effect: The natural environment is seldom stagnant, and free-stream velocity can affect the jet mixing, and also its trajectory in case of cross-flow. A limited investigation of this effect for co-flowing ambients will be given in Chapter 4.

Ambient turbulence: The natural ambient is nearly always in a state of turbulence. This can be tested by releasing a dye into a river or ocean and observing it diffuse. This turbulence is not of significant importance as compared to plume (or jet) generated turbulence, but as the ambient velocity grows in relation to jet velocity, this turbulence is no longer negligible. This will be seen in Chapter 4.

2.2. Basic Assumptions

The general assumptions underlying the analysis of this investigation are listed as follows:

1. The flow is steady, in the mean.
2. The fluid is assumed incompressible; density variations are included only in the buoyancy terms. This is commonly called the "Boussinesq approximation" [23].
3. The pressure variation is assumed to be purely hydrostatic.
4. Changes in density are assumed to be small enough so that a linear equation of state is valid.
5. The flow within the jet is assumed to be axisymmetric.
6. The governing equations can be reduced in accordance with boundary layer assumptions.
7. Viscous dissipation is neglected.
8. The ambient fluid is of infinite extent. How far this assumption can be applied to shallow water discharges will be examined in Chapters 5 and 6.

The flow was modeled as turbulent within the mixing zone from the start, and even though the Reynolds number was included in the calculations wherever it appeared, it was not considered as a significant parameter in the jet problem being investigated. According to Ricou and Spalding [24], the critical Reynolds number for the flow to be turbulent, $Re_{cr} = 2.5 \times 10^4$; Rawn, Bowerman and Brooks [25] mention that when discharge conditions corresponded to $Re_o = 5000 - 40{,}000$, the jet dilution was not dependent on Re_o. Hinze [26], in reviewing several experiments

with non-buoyant jets, observed a decreasing effect of Reynolds number, becoming negligible above 10^5; Cederwall [27] states that flow of an axisymmetric jet is instantaneously turbulent if $Re_o > 2 \times 10^3$, and according to the latest experimental work on buoyant vertical jets [28], by keeping $Re_o > 2500$, flow was always turbulent. In the present calculations Re_o was always greater than 10^5, even for the high buoyancy (low initial momentum) cases. Hence, the assumptions of turbulent mixing from the start and Re not being a significant parameter are justified.

However, in this investigation, laminar viscosity was not neglected. Many previous treatments for turbulent jets have neglected the laminar viscosity altogether. The effect of laminar viscosity is negligible in the main region, but not in the initial region.

3. ANALYSIS

In the present chapter, the finite-difference prediction method will be developed starting with the governing differential equations for the flow in boundary layer form. The several steps in this differential approach as listed in the introduction will be treated individually.

3.1. The Governing Equations

The development of the jet or plume as it moves through the ambient is governed by the conservation equations of mass, momentum and energy. In the general formulation, consideration will be given to an axisymmetric buoyant jet discharging at an angle θ_o to the horizontal, and since a jet with such a configuration will follow a curved path, a curvilinear co-ordinate system was used for analysis of the general problem. This coordinate system is shown in Fig. 3.1. The s-axis is located along the jet trajectory, while the y-axis is oriented normal to it. By trajectory here is meant a trace of the jet centerline. θ is the angle that the tangent to the trajectory at any point makes with the horizontal. The coordinate system is further described in Appendix B.

Curvilinear co-ordinates were first used by Tollmien [29] in relation to derivation of the Navier-Stokes' equations for laminar flow. Later, in 1938, Goldstein [30] presented the boundary layer equations for laminar, incompressible flow over a curved surface using curvilinear co-ordinates. Turbulent flow equations in curvilinear co-ordinates are found less frequently in the literature. Dvorak [31] and Rastogi and Whitelaw [32] treat the subject for some cases of curved flows. A more

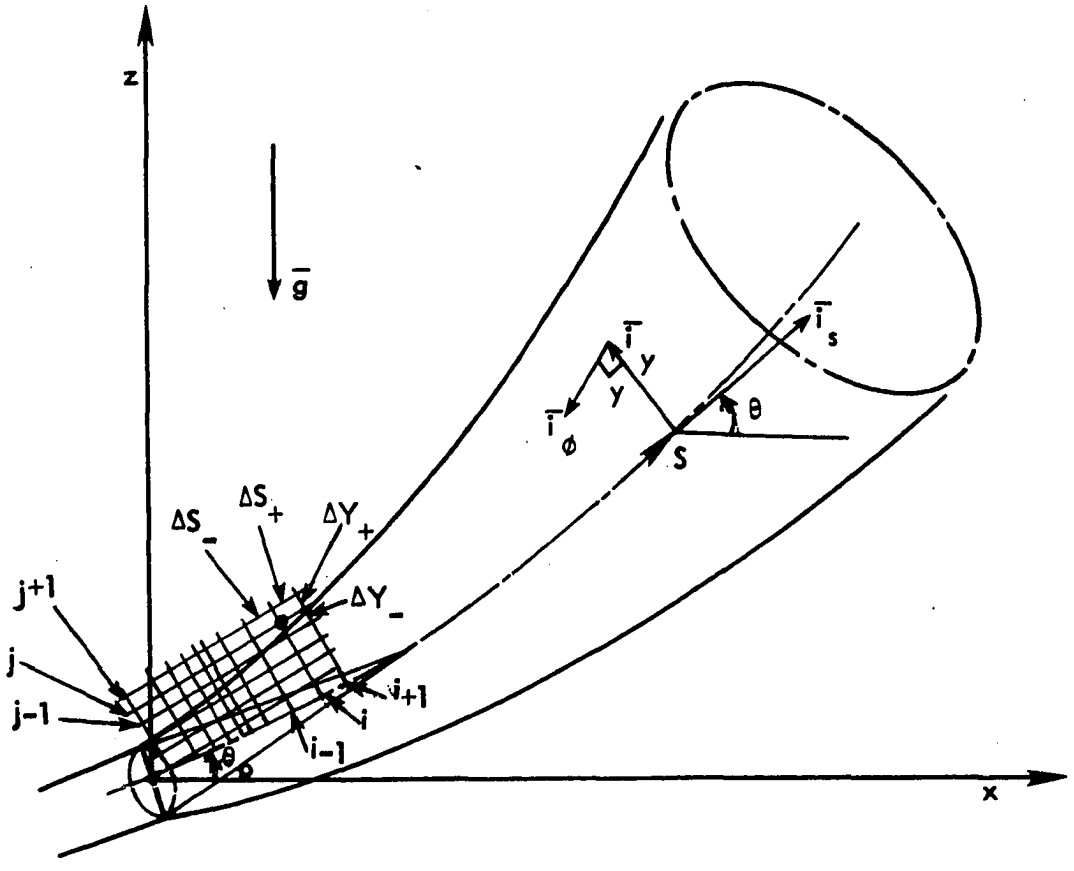

Fig. 3.1. Curvilinear coordinate system and finite-difference grid for buoyant jet analysis.

detailed and relevant treatment is found in Hirst [10] who presents a curvilinear co-ordinate approach in his integral analysis of turbulent jet flow. The present work is, however, to the author's knowledge, the first attempt at solving the partial differential equations for the jet flow in curvilinear co-ordinates using finite-differences.

Details of the development of the governing equations, employing the assumptions listed in Chapter 2, are given in Appendix B. The final form of the equations in curvilinear co-ordinates is as follows:

Continuity:

$$\frac{\partial}{\partial s}(uy) + \frac{\partial}{\partial y}(vy) = 0 \tag{3.1}$$

s-momentum:

$$u\frac{\partial u}{\partial s} + v\frac{\partial u}{\partial y} = \frac{1}{\rho y}\frac{\partial}{\partial y}(y\tau) + \frac{(\rho_\infty - \rho)}{\rho_o} g \sin\theta \tag{3.2}$$

y-momentum:

$$u^2\frac{d\theta}{ds} = \frac{(\rho_\infty - \rho)}{\rho_o} g \cos\theta \tag{3.3}$$

The terms $\frac{(\rho_\infty - \rho)}{\rho_o} g \sin\theta$ and $\frac{(\rho_\infty - \rho)}{\rho_o} g \cos\theta$ represent components of the buoyancy force which are generated due to density differences with the ambient.

Energy:

$$u\frac{\partial t}{\partial s} + v\frac{\partial t}{\partial y} = \frac{1}{\rho c_p y}\frac{\partial}{\partial y}(-yq) \tag{3.4}$$

A similar equation exists for salinity (species concentration). However, for illustrative purposes, the role of temperature, rather than species concentration, will be emphasized in this study.

The shear stress, τ, in Eq. (3.2), includes both the viscous and the apparent turbulent contributions, so that

$$\tau = \mu \frac{\partial u}{\partial y} - \rho \overline{u'v'} \tag{3.5}$$

Similarly, the heat flux, q, in the energy equation is due to both molecular and turbulent action. Thus,

$$q = -k \frac{\partial t}{\partial y} + \rho c_p \overline{v't'} \tag{3.6}$$

Equations (3.1) to (3.4) form a set of non-linear coupled differential equations with two independent variables. On first sight, there appear to be seven unknowns, namely, u, v, t, θ, τ, q, ρ. Actually, q and ρ are not additional unknowns. The turbulent heat flux is frequently related to the turbulent shear stress by a relation known as the Reynolds analogy between heat and momentum transfer, first proposed in 1874 by the British scientist Osborn Reynolds. It is a good approximation whenever the flow is turbulent, and can be applied to turbulent flow in boundary layers, pipes or ducts [33], as well as to turbulent free shear flow [34,35]. The details of this analogy as applied to the jet flow problem will be given below. Thus, since a relationship already exists between the molecular counterparts in the form of a laminar Prandtl number, the overall heat flux q can be expressed in terms of the overall shear stress through the Reynolds analogy. ρ is related to t by an algebraic equation of state (see Eq. (3.11) derived below).

However, as is usually the case in turbulent flow, the number of unknowns, now reduced to five, still exceeds the number of independent equations, namely, four, requiring an additional relationship to achieve "closure" of the mathematical formulation. This is provided by the turbulence model. Using the Boussinesq concept of eddy viscosity [26], τ can be modeled as

$$\tau = \rho \left(\nu + \nu_T\right) \frac{\partial u}{\partial y} = \rho n \frac{\partial u}{\partial y} \tag{3.7}$$

where ν_T is the eddy or turbulent viscosity, and n is the total or effective viscosity.

The eddy viscosity, ν_T, is generally much larger than the laminar viscosity ν. However, ν was retained in the analysis due to its importance in the initial region.

In the Reynolds analogy, it is assumed that the turbulent diffusivities for heat and momentum are related in a manner analogous to laminar flows. Thus,

$$Pr_T = \frac{\nu_T}{\alpha_T} \tag{3.8}$$

where Pr_T is the turbulent Prandtl number and α_T is the turbulent diffusivity for heat. This approach has worked reasonably well for wall boundary layers [36], [37], and tube flow [38], and will be seen to have equal success here. The heat flux, q, can then be written as

$$q = -\rho c_p \left(\alpha + \frac{\nu_T}{Pr_T}\right) \frac{\partial t}{\partial y} = -\rho c_p n_H \frac{\partial t}{\partial y} \tag{3.9}$$

where n_H is the effective thermal diffusivity.

Pr_T was kept equal to 0.7 in all calculations reported here. More details on turbulence modeling will be given in Chapters 4, 5, and 6.

The density, ρ, appearing in the convective or diffusive terms can be taken equal to the reference density, the fluid being assumed incompressible. However, in the buoyancy term, ρ is treated as a variable. This is the Boussinesq assumption that was listed under the assumptions in Chapter 2. A linear equation of state for ρ can be derived by expanding $\rho(t)$ in a Taylor series about the reference density ρ_{ref}:

$$\rho = \rho_{ref} + \left(\frac{\partial \rho}{\partial t}\right)_{p,ref} (t - t_{ref}) + \ldots$$

Or, neglecting higher order terms:

$$\rho = \rho_{ref} \left[1 - \beta(t - t_{ref})\right] \tag{3.10}$$

where $\beta = -\frac{1}{\rho_{ref}}\left(\frac{\partial \rho}{\partial t}\right)_p$ and is the isobaric volume expansivity of the fluid. Equation (3.10) can also be written as (see Appendix C):

$$\frac{\rho - \rho_\infty}{\rho_o} = \beta(t_\infty - t) \tag{3.11}$$

Equation (3.10) is valid for gases and most liquids. A higher order expression for the equation of state $\rho(t)$ may be utilized for fluids subject to large temperature differences. In general, ρ will be a function of both temperature and concentration. However, for the sake of analysis, temperature alone has been considered, and this can very easily be extended to include the salinity (concentration) effect.

3.2. Initial and Boundary Conditions

Equations (3.2) and (3.4) are classified as parabolic [39]. This gives rise to an initial value problem, where the calculation begins at the discharge point and is marched off in the streamwise direction, with the solution obtained being dependent on the solution at an upstream station. Thus, it is necessary to know the values of the variables at discharge to start the solution.

Equations (3.1) to (3.4) are first order with respect to s in three variables, hence three initial distributions are required. These are given as:

$$u(s_o,y) = f(y),\ t(s_o,y) = g(y),\ \theta(s_o) = \theta_o \tag{3.12}$$

As the solution advances, information relating to the values of the variables at the flow boundaries will also be needed in order to obtain a unique solution.

Equation (3.2) is second order with respect to y in u, requiring two boundary conditions for u. By the same reasoning, from Eqs. (3.4) and (3.1), two boundary conditions are required for t and one for v.

They are all specified as follows:

$$\begin{aligned} &\frac{\partial u}{\partial y}(s,0) = \frac{\partial t}{\partial y}(s,0) = 0,\ v(s,0) = 0 \\ &\lim_{y\to\infty} u(s,y) = u_\infty,\ \lim_{y\to\infty} t(s,y) = t_\infty \end{aligned} \tag{3.13}$$

The initial profiles can be obtained from experiments, empirical relations, approximate theories, or arbitrarily assumed. It is,

however, desirable that they should correspond to the real flow in certain gross features.

In most practical applications of the discharge problem, the initial velocity and temperature profiles are nearly uniform [1,28,40,41,42]. Hence, uniform profiles of velocity and temperature were used as initial conditions in all calculations of the present work. The numerical scheme can easily accommodate any other profile should that become necessary.

The initial v's which can be determined from the continuity equation (knowing the initial u's), were set equal to zero for convenience. This is compatible with problem specification since only uniform or fully developed turbulent initial velocity profiles have been used.

3.3. Non-dimensional Forms

Non-dimensionalization is an extremely useful tool in applying order-of-magnitude analyses to the Navier-Stokes equations in order to obtain a set of equations that are reduced in complexity, the degree of simplification depending on the nature of the flow phenomena and the accuracy desired in the analyses. As a computational step in the differential approach, however, it is not as essential. Two main reasons for its use in the present work are, first, that the solution, being in terms of non-dimensional parameters, would be of a more general nature, and second, that it is more convenient to use a simple form devoid of symbols and units.

The variables were non-dimensionalized as follows:

$$U = \frac{u}{u_o}, \quad V = \frac{v}{u_o}, \quad T = \frac{t - t_{\infty_o}}{t_o - t_{\infty_o}}, \quad S = \frac{su_o}{\nu}, \quad Y = \frac{yu_o}{\nu},$$

$$N = \frac{n}{\nu}, \quad N_H = \frac{n_H}{\nu} \tag{3.14}$$

In general, $t_{\infty_o} = t_\infty$ except when ambient is stratified and t_∞ is not constant. Thus, Eqs. (3.1) to (3.4) can be written in non-dimensional form after replacing density differences by equivalent temperature differences using the equation of state [Eq. (3.10), see also Appendix C] as:

Continuity:

$$\frac{\partial}{\partial S}(UY) + \frac{\partial}{\partial y}(VY) = 0 \tag{3.15}$$

s-momentum:

$$U\frac{\partial U}{\partial S} + V\frac{\partial U}{\partial Y} = \frac{1}{Y}\frac{\partial}{\partial y}\left(YN\frac{\partial U}{\partial Y}\right) + \frac{\sin\theta}{Re_o Fr_o}(T - T_\infty) \tag{3.16}$$

y-momentum:

$$U^2\frac{d\theta}{dS} = \frac{\cos\theta}{Re_o Fr_o}(T - T_\infty) \tag{3.17}$$

Energy:

$$U\frac{\partial T}{\partial S} + V\frac{\partial T}{\partial Y} = \frac{1}{Y}\frac{\partial}{\partial Y}\left(YN_H\frac{\partial T}{\partial Y}\right) \tag{3.18}$$

Re_o and Fr_o appear in the buoyancy term of the momentum equations as a result of non-dimensionalizing the variables.

The initial and boundary conditions transform as follows:

$$U(S_o,Y) = F(Y),\ T(S_o,Y) = G(Y) \tag{3.19}$$

$$\frac{\partial U}{\partial Y}(S,0) = \frac{\partial T}{\partial Y}(S,0) = 0,$$

$$\lim_{y\to\infty} U(S,Y) = U_\infty,\ \lim_{y\to\infty} T(S,Y) = T_\infty \tag{3.20}$$

If the initial profiles are assumed uniform, $F(Y) = G(Y) = 1.0$. In case of quiescent ambient, $U_\infty = 0$, and when the ambient is homogeneous, $T_\infty = 0$.

However, for stratified ambient cases,

$$T_\infty = \frac{-\lambda d_o}{Re_o\left(t_o - t_{\infty_o}\right)} Z \tag{3.21}$$

where λ is the ambient temperature stratification, usually specified in $^oC/m$ (or $^oF/ft$), and Z is the non-dimensional vertical height.

θ, being a dimensionless variable, remains unchanged during this entire step.

Details on how some of the non-dimensional forms are derived are given in Appendix C.

3.4. Finite-Difference Formulation

The set of equations (3.15) to (3.18) is to be solved over the region of interest, using a finite-difference method where the values of the dependent variables are calculated for the nodal points of a finite-difference grid. The solution method employed an explicit formulation of the DuFort-Frankel [43] type. Figure 3.1 shows the details of the

finite-difference grid used. The method is applicable for unequal grid spacings in both directions. However, for all computations in the present work, the ΔY spacings were kept equal, while ΔS was varied.

3.4.1. General

The aim in using a finite-difference method is to reduce a continuous system to a discrete or lumped parameter system which is suitable for high-speed computer solution. Thus, the variable is considered to exist only at discrete points of a grid instead of being continuous over the flow field, and the derivatives are therefore replaced by ratios of differences. This is usually accomplished by expanding the variables of the equations in Taylor series about appropriate grid points, and then truncating the resulting series, to obtain finite-difference approximations for the derivatives. Although finite-difference representations can be obtained in other ways [44], the use of Taylor series expansions gives a systematic and useful way of assessing the errors associated with the difference formulation.

The order of the terms neglected due to the truncation gives the order of the truncation error associated with the scheme. Order of, mathematically represented by the 0 notation, has been defined with reference to truncation errors in [45] as follows:

If s is any set and f, ϕ be real or complex functions defined on s, then the notation $f(s) = 0[\phi(s)], s \to 0$ means that a positive number K exists, such that $|f(s)| \leq K|\phi(s)|$ for $s \to 0$

To illustrate how derivatives are approximated, an example of a simple, forward-difference approximation for $\left(\frac{\partial U}{\partial S}\right)_{i,j}$ will be developed.

Taylor series expansion for $U(S+\Delta S,Y)$ about (S,Y) gives

$$U(S+\Delta S,Y) = U(S,Y) + \Delta S\frac{\partial U}{\partial S}(S,Y) + \frac{(\Delta S)^2}{2!}\frac{\partial^2 U}{\partial S^2}(S,Y)$$

$$+ \frac{(\Delta S)^3}{3!}\frac{\partial^3 U}{\partial S^3}(S,Y) + O[(\Delta S)^4]$$

Simple algebra yields

$$\frac{\partial U}{\partial S}(S,Y) + \frac{U(S+\Delta S,Y) - U(S,Y)}{\Delta S} - \frac{(\Delta S)}{2!}\frac{\partial^2 U}{\partial Y^2}(S,Y)$$

$$+ \frac{(\Delta S)^2}{3!}\frac{\partial^3 U}{\partial S^3}(S,Y) + O[(\Delta S)^3]$$

or

$$\left(\frac{\partial U}{\partial S}\right)_{i,j} = \frac{U_{i+1,j} - U_{i,j}}{\Delta S} + O[\Delta S].$$

The truncation error is of the order of ΔS, hence this is a first-order approximation. More details on truncation error will be found in the next section. The partial differential equations are thus transformed into a set of algebraic equations, which are then solved step by step to give a solution that exists at a finite number of discrete grid points. Both explicit and implicit methods can be developed by expanding the Taylor series about different grid points and using various combinations of these.

Most finite difference schemes applied to the jet flow problem have been implicit in nature [8,19]. Where explicit methods have been used, they have employed a co-ordinate transformation which places restrictions on the accuracy and generality of the method [8,46]. The latter reference is restricted to laminar jet flow calculations only. Explicit

methods possess the advantage that the values of the unknowns at each downstream station are evaluated directly or explicitly. Implicit schemes, in general, involve the solution of a system of simultaneous equations for the variables, thus requiring greater algebraic complexity and hence increased computation time for each step, but they are usually unrestricted by stability considerations for commonly used forms and allow for larger streamwise steps than permitted by conventional explicit methods. Interestingly, however, the DuFort-Frankel method is less restricted by stability considerations as compared to conventional explicit methods. This can be shown by application of the Von Neumann condition [47], and was also seen to be true in the actual calculations where considerably larger step sizes could be taken using this method. This increased stability is obtained because the value of a dependent variable at (i,j) is replaced by its average at (i+1,j) and (i-1,j) when the variable at (i,j) appears in a derivative term.

The DuFort-Frankel (henceforth referred to as D-F) scheme has been used successfully for predicting flow in wall boundary-layers [36,37] and tubes [38]. In the present study, the scheme was developed for application to jet flow. Examples of how derivatives are approximated using this scheme on a uniform grid are given in Section 3.4.3.

3.4.2. The difference equations

The DuFort-Frankel forms of Eqs. (3.14) to (3.17) are:

$$\frac{Y_{j+1} + Y_j}{4(\Delta S_+ + \Delta S_-)} \left[U_{i+1,j+1} + U_{i+1,j} - U_{i-1,j+1} - U_{i-1,j} \right]$$

$$+ \frac{\left(Y_{j+1} V_{i+1,j+1} - Y_j V_{i+1,j} \right)}{\Delta Y_+} = 0 \qquad (3.22)$$

$$\frac{U_{i,j}}{(\Delta S_+ + \Delta S_-)} \left(U_{i+1,j} - U_{i-1,j} \right) + \frac{V_{i,j}}{(\Delta Y_+ + \Delta Y_-)}$$

$$\times \left(U_{i,j+1} - U_{i,j-1} \right) = \frac{2}{Y_j (\Delta Y_+ + \Delta Y_-)}$$

$$\times \left\{ \left[\frac{\left(Y_{j+1} + Y_j \right)\left(N_{i,j} + N_{i,j+1} \right)}{4} \right.\right.$$

$$\left.\left. \times \frac{\left(U_{i,j+1} - 0.5 \left[U_{i+1,j} + U_{i-1,j} \right] \right)}{\Delta Y_+} \right]$$

$$- \left[\frac{\left(Y_j + Y_{j-1} \right)\left(N_{i,j} + N_{i,j-1} \right)}{4} \right.$$

$$\left. \left. \times \frac{\left(0.5 \left[U_{i+1,j} + U_{i-1,j} \right] - U_{i,j-1} \right)}{\Delta Y_-} \right] \right\}$$

$$+ \frac{\left(T_{i,j} - T_{\infty_i} \right)}{Re_o \, Fr_o} \sin \theta_i \qquad (3.23)$$

$$\frac{(U_{i,j})^2}{(\Delta S_+ + \Delta S_-)}(\theta_{i+1} - \theta_{i-1}) = \frac{(T_{i,j} - T_{\infty_i})}{Re_o Fr_o}\cos\theta_i \tag{3.24}$$

$$\frac{U_{i,j}}{(\Delta S_+ + \Delta S_-)}(T_{i+j,j} - T_{i-1,j})$$

$$+ \frac{V_{i,j}}{(\Delta Y_+ + \Delta Y_-)}(T_{i,j+1} - T_{i,j-1})$$

$$= \frac{2}{Y_j(\Delta Y_+ + \Delta Y_-)}\left\{\left[\frac{(Y_{j+1} + Y_j)(N_{H_{i,j+1}} + N_{H_{i,j}})}{4}\right.\right.$$

$$\left.\times \frac{(T_{i,j+1} - 0.5[T_{i+1,j} + T_{i-1,j}])}{\Delta Y_+}\right]$$

$$-\left[\frac{(Y_j + Y_{j-1})(N_{H_{i,j}} + N_{H_{i,j-1}})}{4}\right.$$

$$\left.\left.\times \frac{(0.5[T_{i+1,j} + T_{i-1,j}] - T_{i,j-1})}{\Delta Y_-}\right]\right\} \tag{3.25}$$

The finite-difference equations have been written in a form applicable for uneven grid spacing in both streamwise and cross-stream directions, even though ΔY, the cross-stream grid, was kept constant in the calculations.

The centerline derivative boundary condition, Eq. (3.20), was implemented using Taylor series expansions for the velocity and temperature about the centerline as follows:

$$U_{i+1,2} = U_{i+1,1} + \left(\frac{\partial U_{i+1}}{\partial Y}\right)_1 \Delta Y + \left(\frac{\partial^2 U}{\partial Y^2}\right)_1 \frac{(\Delta Y)^2}{2!} + O(\Delta Y)^3 \quad (3.26)$$

$$U_{i+1,3} = U_{i+1,1} + \left(\frac{\partial U_{i+1}}{\partial Y}\right)_1 (2\Delta Y) + \left(\frac{\partial^2 U}{\partial Y^2}\right)_1 \frac{(2\Delta Y)^2}{2!}$$

$$+ O(\Delta Y)^3 \quad (3.27)$$

Multiplying both sides of Eq. (3,26) by 4 and then subtracting Eq. (3.27) from it yields, after setting $\left(\frac{\partial U_{i+1}}{\partial Y}\right)_1 = 0$:

$$4U_{i+1,2} - U_{i+1,3} = 3U_{i+1,1} + O(\Delta Y)^3$$

Using a second order approximation to the zero derivative, therefore, gives

$$U_{i+1,1} = \frac{4U_{i+1,2} - U_{i+1,3}}{3} \quad (3.28)$$

Similarily,

$$T_{i+1,1} = \frac{4T_{i+1,2} - T_{i+1,3}}{3}$$

Another way of implementing the centerline boundary condition [48] is to obtain a special form of Eqs. (3.16) and (3.17) by letting $Y \to 0$ and then applying L'Hospital's rule to the right hand side of the equations. These equations are then differenced and the symmetry condition $U_{i+1,2} = U_{i+1,0}$ where the subscript 0 refers to the first grid on the other side of the centerline, is incorporated.

3.4.3. Consistency, stability, convergence

Consistency and stability are both major concerns arising in the use of finite difference methods, hence a discussion of these aspects and how they relate to convergence of the solution is in order at this time.

To satisfy the consistency condition, the finite-difference representation should approach the partial differential equations being approximated, as the mesh size is shrunk. The stability condition, on the other hand, requires that round off errors, or errors from any source, do not grow as the solution is advanced. (Round-off errors are introduced when the discrete equations are not solved exactly).

Consistency is generally studied by expanding the dependent variables in Taylor series and observing the difference between the partial differential equations and the finite-difference representation. This difference is due to the neglected terms and is known as the truncation error associated with the difference scheme. A consistent scheme is defined as one in which this error vanishes as the mesh size approaches zero. Generally, the smaller the truncation error, the faster the convergence of the numerical solution to the true one [49]. Using derivatives of U in the Y direction as examples, the truncation errors can be examined.

In the standard explicit method,

$$\frac{\partial U}{\partial Y} = \frac{U_{i,j+1} - U_{i,j}}{\Delta Y} - \frac{\partial^2 U}{\partial Y^2}\,\frac{\Delta Y}{2!} - \frac{\partial^3 U}{\partial Y^3}\,\frac{(\Delta Y)^2}{3!} \cdots$$

The truncation error for this formulation is $O(\Delta Y)$.

In the D-F scheme,

$$\frac{\partial U}{\partial Y} = \frac{U_{i,j+1} - U_{i,j-1}}{\Delta Y} - \frac{\partial^3 U}{\partial Y^3}\frac{(\Delta Y)^2}{3!} - \frac{\partial^5 U}{\partial Y^5}\frac{(\Delta Y)^4}{5!} \cdots$$

and the truncation error is seen to be $O[(\Delta Y)^2]$.

It is necessary that any truncation error be at most $O(\Delta Y)$, or $O(\Delta S)$ in case of streamwise differences, to satisfy consistency. This is true for all derivatives approximated by the present method, but one term deserves closer attention. The second-derivative term in the normal direction is written for constant mesh size, as:

$$\frac{\partial^2 U}{\partial Y^2} = \frac{U_{i,j+1} + U_{i,j-1} - U_{i+1,j} - U_{i-1,j}}{(\Delta Y)^2} + \frac{\partial^2 U}{\partial S^2}\left(\frac{\Delta S}{\Delta Y}\right)^2$$

$$- \frac{\partial^4 U}{\partial Y^4}\frac{(\Delta Y)^2}{12} \qquad (3.29)$$

[It is worthy of note that for a standard explicit method, the numerator would be of the form $(U_{i,j+1} + U_{i,j-1} - 2U_{i,j})$. By comparing the two forms, the essential feature of the D-F scheme can be revealed.] The truncation error in Eq. (3.29) is:

$$O\left[\left(\frac{\Delta S}{\Delta Y}\right)^2\right] + O\left[(\Delta Y)^2\right]$$

Thus, the formulation is mathematically consistent only if ΔS goes to zero faster than ΔY, and this has been the main criticism leveled against the D-F formulation. Fortunately, the entire term consists of

$\frac{\partial^2 U}{\partial S^2}\left(\frac{\Delta S}{\Delta Y}\right)^2$ and for boundary layer flows, $\frac{\partial^2 U}{\partial S^2}$ is negligibly small as compared to other terms in the equation. Thus, even for $\left(\frac{\Delta S}{\Delta Y}\right) \simeq 1$, Eq. (3.29) would be expected to be a good approximation, even for finite ΔS and ΔY. A complete consistency analysis for the difference Eqs. (3.22) to (3.25) is carried out in Appendix D.

Stability is a very important consideration, since even the best finite-difference scheme in terms of truncation error can be unstable and hence give a solution which is entirely different from that of the partial differential equations, rendering the results useless. A brief discussion of the stability considerations for the present D-F formulation follows.

For the simple diffusion equation, this scheme is unrestrictedly stable [43], [49]. In its application to prediction of wall boundary layer flows [36] and tube flows [38], it was found to always be stable. Naturally, therefore, no stability constraint for the method was known or believed to exist. But when this method was applied to the jet calculations reported in this work, constraints on the allowable streamwise stepsize were revealed. A careful application of the Von Neumann [47] stability analysis by the author to Eqs. (3.22), (3.23), and (3.25) resulted in the following stability constraint:

$$\Delta S_+ \leq \min_{j=2,NYJ} \left[\frac{U_{i,j} \Delta Y}{\left| V_{i,j} + \frac{FUNC}{2\Delta Y} \right|} \right] \tag{3.30}$$

where NYJ = max (NY,NYT) and

$$FUNC = \max \left[\left(N_{i,j-1} - N_{i,j+1} \right), \left(N_{H_{i,j-1}} - N_{H_{i,j+1}} \right) \right]$$

This is derived in Appendix E. No general theory is available for proving stability and convergence in the case of non-linear equations with variable coefficients such as is the case here, and a common practice is to investigate the 'local' stability whereby the coefficients are considered constant or error-free in a small neighborhood of each grid point [50]. The stability criteria developed thereby is for 'local' stability but if the requirement is checked at each grid point, then it is reasoned that an instability could not originate.

The analysis is thus a heuristic extension of the rather general theory of Von Neumann applicable to linear problems with constant coefficients. Even so, in the actual testing ground of numerical computations, the stability criterion obtained in this way proved to be the most effective in eliminating the stability problem.

This restriction is not severe, and except very close to nozzle exit it is really very generous as compared to that for the ordinary explicit method (See Appendix F). A streamwise stepsize ΔS_+ of about 8-10% of the width of the mixing zone in the main region was found to give good results for the co-flowing stream calculations, and for quiescent ambient cases up to 6% of the mixing zone was used without stability problems. This is several times larger than would be possible using the

ordinary explicit scheme where, in addition to the viscosity difference, the value of the viscosity itself appears in the denominator [44] (see also Appendix F). A small free-stream velocity (3-5% of jet velocity) was specified for the quiescent ambient cases in order to increase allowable stepsize. (The accuracy of the solution was found to be unaffected by this procedure).

3.5. Method of Solution

A skeleton flow chart illustrating the order of calculation is shown in Fig. 3.2.

Equation (3.23) can be solved directly for $U_{i+1,j}$ if all the U's are known at the i and i-1 levels and the V's, T's and θ known at the i level. As the D-F scheme requires information from two previous streamwise stations, namely, i and i-1, a modification of the ordinary explicit method described in [51], which requires information from only one previous station, was used to start the solution. Details of this explicit scheme are given in Appendix F. Equation (3.23) is then solved for $U_{i+1,j}$ for all j values in the mixing zone, starting with the point adjacent to the jet centerline and working outward to the edge of the jet or plume, using the boundary conditions specified by Eq. (3.28) at the jet centerline. The outer boundary is located when $(U_{i+1,1} - U_{i+1,j})/(U_{i+1,1} - U_{\infty_{i+1}})$ is not less than a specified value, in this case, 0.99. In section 3.2., the free stream boundary condition for u was applied at $y \to \infty$, but for practical purposes, the above criterion for locating the edge is sufficiently accurate. With the $U_{i+1,j}$'s determined, Eq. (3.22)

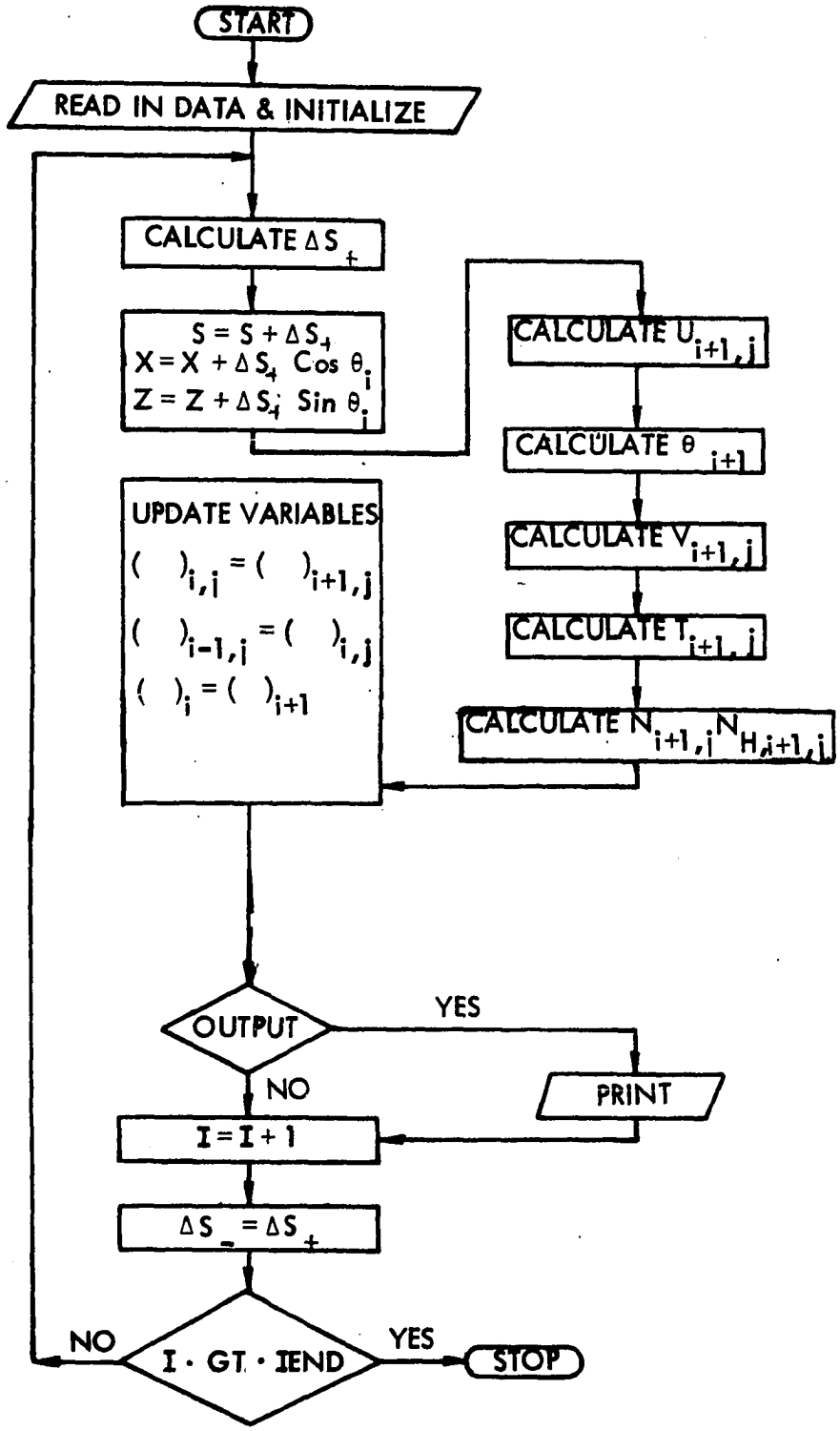

Fig. 3.2. Skeleton flow chart for the general calculation method.

can be solved for $V_{i+1,j+1}$, starting from the point adjacent to the jet centerline and working outward, using the specified boundary value of the normal component of velocity at the jet centerline. θ_{i+1} is then determined for the general problem of the buoyant curved jet by solving Eq. (3.24), and $T_{i+1,j}$'s are determined as explained earlier for U's, by solving Eq. (3.25), i.e., the finite-difference form of the energy equation.

It is worth noting that the normal momentum equation appearing in the form shown as Eq. (3.24), shows a constant value of θ across the cross-section, hence evaluating it at the centerline would mean using $(U_{i,1})$ and $(T_{i,1})$. But a better and more realistic estimate of θ at station i+1 can be made if Eq. (3.24) is representative of the entire flow cross-section at i. Hence, Eq. (3.24) was integrated over the cross-section using the U and T values generated by the s-momentum and energy equations. Thus, no profile assumptions were made as is the case with integral methods. This will be clarified further in the curved jet analysis of Chapter 6. In the first two applications of this analysis, as described in Chapters 4 and 5, the normal momentum equation did not appear, and was, therefore, not used.

According to Fig. 3.2, the effective viscosity and conductivity are evaluated next. This is the place in the program where the different models for the turbulence are examined. More details on turbulence models will be presented in Chapters 4, 5, and 6.

Finally, the variables are all updated to prepare for the next computational step, i.e., all variables at i+1 become quantities at i, and those at i become quantities at i-1. The solution is thus stepped off until all the desired flow region has been calculated.

An increasing streamwise step size was incorporated into the program. It should be emphasized that each variable is calculated explicitly at each location, no iterations or simultaneous solutions being required.

An interesting aspect of the solution procedure, namely, the generation of the plume trajectory, will be briefly described. Once the forward streamwise step ΔS_+ is calculated, its horizontal and vertical components, in order, are determined as follows:

$$\Delta X_+ = \Delta S_+ \cos \theta_i$$
$$\Delta Z_+ = \Delta S_+ \sin \theta_i$$

Then the cumulative distance travelled by the jet, and its co-ordinates, are generated by the summations:

$$\begin{aligned} S_{i+1} &= S_i + \Delta S_+ \\ X_{i+1} &= X_i + \Delta S_+ \cos \theta_i \\ Z_{i+1} &= Z_i + \Delta S_+ \sin \theta_i \end{aligned} \tag{3.31}$$

Although various numbers of radial grid points were used in studying the convergence properties of the method, most calculations were made by dividing the discharge radius into 20 ΔY increments.

The method is fast, and most of the computations reported here have required less than two minutes and none more than 2 1/2 minutes of computation time on the IBM 360/65, which is a relatively slow machine.

More details on the peculiarities of the calculation method and additional features that were incorporated into the computer code as the method was put to greater use, will be given in succeeding chapters.

The computer program used for calculating the buoyant curved jet configuration is listed for the reader's convenience in Appendix A. Different models can be examined by altering one subroutine. This code, written in FORTRAN IV, was prepared for execution at the Iowa State University Computation Center.

3.6. Results

Results from this method have been compared to experiment, and to other methods, both integral and differential (where these have been available) to demonstrate the capability of the calculation scheme and modeling that have been employed. These will be seen in detail in the succeeding chapters where the horizontal non-buoyant jet, the vertical plume with buoyancy, and the buoyant curved jet are all examined individually.

4. THE NON-BUOYANT JET IN A CO-FLOWING OR QUIESCENT AMBIENT

In this chapter, the calculation scheme described earlier is applied to the base-line case of the turbulent non-buoyant jet. This case is important because it provides a suitable test configuration for a verification study of the computational technique developed for the jet flow calculations, and as a first step in evaluating the different models for the turbulent transport process.

Heated non-buoyant jets are not common in practical applications, but they do represent the limiting case for the horizontally discharging jet at very large Froude numbers. The multiport diffuser pipe discharging power plant cooling water is one application where sufficiently large Froude numbers are expected to occur that buoyancy effects can be neglected. Based on the numbers given in [2], Fr_o for such flows could be as high as 3000 or even higher, and the analysis of a round jet would be valid as long as these jets did not interfere.

4.1. Introduction

Non-buoyant jets have been studied extensively during the past 40-50 years as a classic example of non-isotropic free turbulence. The problem of turbulent jet mixing of an incompressible fluid with an ambient at rest was first analyzed successfully by Tollmien in 1926 [52]. He considered a point source and hence the solution does not hold for a finite opening. Kuethe [53], in 1935, extended Tollmien's results to the case of a two-dimensional jet issuing into a medium not at rest, and also worked out an approximate method for the computation of the

velocity profile in the initial part of a round jet issuing into medium at rest. Squire and Trouncer [54], in 1944, extended Kuethe's results to the case of a round jet issuing into a uniform stream by assuming certain velocity profiles across the jet. Other investigations followed. Good reviews of analytical work done in this area can be found in Pai [55], Hinze [26], and Abramovich [56].

Experimental efforts of most prominence have been the work of Albertson et al. [57] for simple momentum jets, and those of Forstall and Shapiro [58], and Landis and Shapiro [59], for jets in co-flowing ambients. All the analytical approaches mentioned have been based upon approximate methods of analysis using integral methods with different modifications. The most recent in this class of methods is the work of Hirst [10]. However, as has been mentioned in Chapter 1, in order to predict the flow properties with precision throughout the flow field, to allow arbitrary initial and boundary conditions, and to permit non-similarity in the flow behavior, one would have to turn to more refined methods.

In several types of turbulent flow calculations, such as prediction of wall boundary layers and confined flows, differential methods have emerged as the most successful solution methods capable of providing such details of the flow as the velocity and temperature distributions [37,38,60]. In 1970, W. C. Reynolds [61], while commenting on the 1968 Stanford Conference [7] where integral methods were yet dominant in computation of turbulent flows, remarked that, "while there were a number of successful and attractive integral methods tested at the conference, one had to be impressed with the generality and speed of computations

based on the partial differential equations. These schemes can be extended to new situations much more readily than integral methods. While integral methods are indeed useful in certain special cases, there is a definite interest in use of partial differential equation schemes."

The accuracy and generality of these methods depend upon developing or identifying appropriate models for the turbulent transport mechanism. This has been done with reasonably good success in the case of wall boundary layers, but for turbulent jet flows a simple, general transport model capable of accurately predicting the full range of flows from discharge to the fully established flow regime has eluded researchers to date [8,35]. Here "simple model" is defined as one which does not require the simultaneous solution of any auxiliary partial differential equations through the problem domain in order to evaluate the turbulent shear stress. The main motivation for turning to more complex models is to achieve greater generality in being able to accurately predict a wider range of flows with the same model.

Although the need for jet and plume predictions which account for buoyancy, cross-flow, and surface interaction effects is clear, it also appears desirable to consider the merits of several turbulence models for the "base-line" case of the heated nonbuoyant ($Fr_o \simeq \infty$), axisymmetric, turbulent jet discharging into a quiescent or co-flowing stream before considering additional complicating effects. The proceedings of the Langley Conference [8] contain a reasonably current study of presently known models and methods applicable to this "base-line" flow. Other related publications are [18-20]. One of the best performers at the conference was the kϵ2 model proposed by Launder et al. [62]. This

is a two equation model of turbulence requiring the simultaneous solution of two auxiliary partial differential equations, thereby increasing the computation time over that required by simple models. However, it was demonstrated that no one model, simple or complex, gave consistently accurate predictions for the two different velocity ratios represented by Test Cases 9 and 20.

In the present chapter, predictions from several turbulence models are compared and a new eddy viscosity model presented which accounts for ambient turbulence effects, and results in improved predictions for a wide range of velocity ratios, including the important case of jet into still ambient flows. The explicit, non-iterative finite-difference scheme previously used for wall boundary layers [36] and confined flows [38] was developed to solve the conservation equations for jet flows and is shown to work well for the entire range of flows investigated.

4.2. The Governing Equations

The flow configuration, with finite-difference grid superimposed on the flow field, is indicated in Fig. 4.1.

For a straight-line trajectory, no curvature effects exist and hence, under boundary layer assumptions, the y-momentum equation, Eq. (3.3), vanishes. Also, in the absence of buoyancy effects, the buoyancy term drops out from the momentum equation, causing it to be uncoupled from the energy equation (note that the energy equation remains coupled to the momentum equation, however).

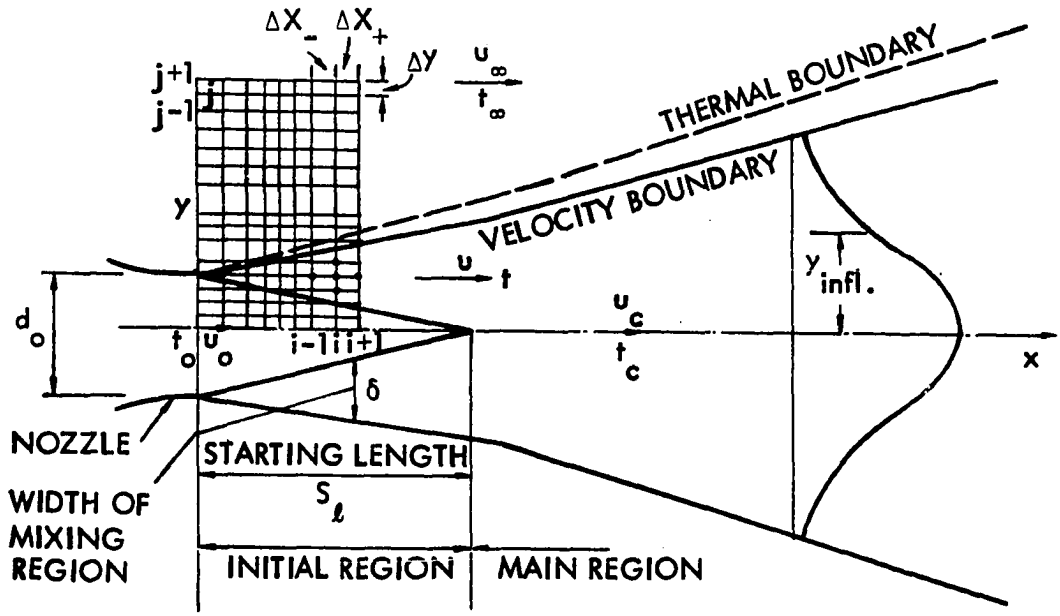

Fig. 4.1. Jet configuration.

The resulting set of equations can be written as follows:

Continuity:

$$\frac{\partial}{\partial s}(uy) + \frac{\partial}{\partial y}(vy) = 0 \tag{4.1}$$

Axial momentum:

$$u\frac{\partial u}{\partial s} + v\frac{\partial u}{\partial y} = \frac{1}{\rho y}\frac{\partial}{\partial y}(y\tau) \tag{4.2}$$

Energy:

$$u\frac{\partial t}{\partial s} + v\frac{\partial t}{\partial y} = \frac{1}{\rho c_p y}\frac{\partial}{\partial y}(-yq) \tag{4.3}$$

Here, $s = x$, since for a horizontal configuration, the streamwise coordinate coincides with the horizontal. τ and q are as defined in Chapter 3.

The initial and boundary conditions are the same as specified in Chapter 3, except that here $\theta_o = 0^o$ and is, in fact, not required since θ is not an unknown, the trajectory being a straight line.

4.3. Finite-Difference Formulation

Since a detailed analysis has been presented in Chapter 3, only the essential features will be shown here.

Equations (4.1) to (4.3), normalized by introducing the non-dimensional variables presented in Chapter 3, can be written as:

$$\frac{\partial}{\partial S}(UY) + \frac{\partial}{\partial Y}(VY) = 0 \tag{4.4}$$

$$U\frac{\partial U}{\partial S} + V\frac{\partial U}{\partial Y} = \frac{1}{Y}\frac{\partial}{\partial Y}\left(YN\frac{\partial U}{\partial Y}\right) \tag{4.5}$$

$$U\frac{\partial T}{\partial S} + V\frac{\partial T}{\partial Y} = \frac{1}{Y}\frac{\partial}{\partial Y}\left(YN_H\frac{\partial T}{\partial Y}\right) \tag{4.6}$$

The boundary and initial conditions transform in a similar manner.

Examples of how derivatives are approximated and the truncation errors involved have been given earlier and will not be repeated here.

The DuFort-Frankel (D-F) scheme has been described in Chapter 3, and the continuity and energy equations in difference form are identical to Eqs. (3.22) and (3.25). The momentum equation can be written as:

$$\frac{U_{i,j}}{(\Delta S_+ + \Delta S_-)}\left(U_{i+1,j} - U_{i-1,j}\right) + \frac{V_{i,j}}{(\Delta Y_+ + \Delta Y_-)}\left(U_{i,j+1} - U_{i,j-1}\right)$$

$$= \frac{2}{Y_j(\Delta Y_+ + \Delta Y_-)}\left\{\left[\frac{(Y_{j+1} + Y_j)(N_{i,j} + N_{i,j+1})}{4}\right.\right.$$

$$\left.\times\frac{\left[U_{i,j+1} - 0.5(U_{i+1,j} + U_{i-1,j})\right]}{\Delta Y_+}\right] - \left[\frac{(Y_j + Y_{j-1})(N_{i,j} + N_{i,j-1})}{4}\right.$$

$$\left.\left.\times\frac{\left[0.5(U_{i+1,j} + U_{i-1,j}) - U_{i,j-1}\right]}{\Delta Y_-}\right]\right\} \tag{4.7}$$

4.4. Transport Models and Results

As a first step towards applying the numerical scheme for the turbulent jet flow problem, Prandtl's mixing length hypothesis for the turbulent exchange was incorporated to achieve closure.

This suggests using the following formulation for the Reynolds' stress term in the momentum equation:

$$- \rho\overline{u'v'} = \rho \ell^2 \left|\frac{\partial u}{\partial y}\right| \frac{\partial u}{\partial y}$$

so that the eddy viscosity μ_T assumes the form

$$\mu_T = \ell^2 \left|\frac{\partial u}{\partial y}\right| \tag{4.8}$$

The quantity ℓ is the so-called "mixing length," determined by the geometry of the flow system, typically as a fraction of the local width of the mixing region for free shear flow.

Here, $\ell = 0.0762\,\delta$ was used, where δ is the width of the mixing zone in the initial region and the jet velocity radius in the main region of the flow. This model will be labeled Model A for future reference.

As was mentioned earlier, in Chapter 3, it will be understood everywhere that the eddy diffusivity for heat, α_T, is related to μ_T by the turbulent Prandtl number. Experimental evidence for the use of $Pr_T = 0.7$ for non-buoyant jets is provided by the results in [58,59]. However, to maintain the generality of the prediction technique, the value was kept the same for the succeeding configurations as well.

Starting length predictions using the mixing length model were very good over a wide range of velocity ratios. These predictions are shown in Fig. 4.2 along with the experimental results of Albertson et al. [57], Landis and Shapiro [59], Forstall and Shapiro [58], the analytical predictions of Hirst [10], and the empirical correlations of Forstall [58] and Abramovich [56]. Albertson based his similarity solution [57]

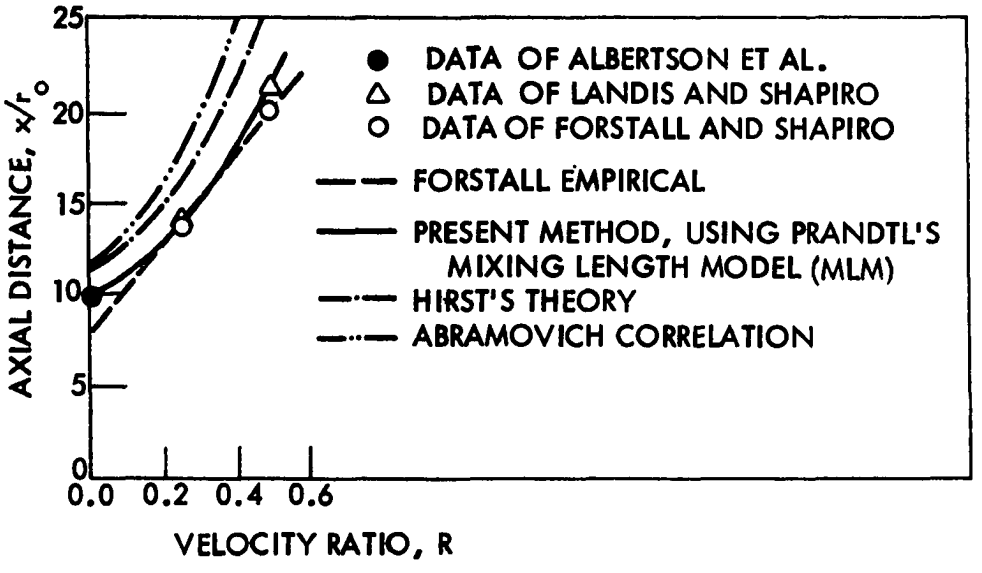

Fig. 4.2. MLM in initial region - starting length variation with velocity ratio.

on a starting length equal to 12.4 radii; however, he actually measured a starting length of less than 10 radii, as shown in Fig. 4.2. In the main region, however, success is not so clearly apparent. The broken lines in Fig. 4.3 show the results of using Eq. (4.8) in the main region for velocity ratio R = 0.25.

One major disadvantage typically attributed to mixing length models, the prediction of zero viscosity on the jet centerline, was overcome when the model was refined on the assumption that main mixing eddies extend to a scale on the order of the transverse distance from the jet centerline to the inflexion point (y_{infl}) of the velocity profile where mixing is expected to be the greatest. A constant value of the turbulent viscosity, equal to the value at the inflexion point, was then used from the centerline to the inflexion point. Mathematically, this is expressed as:

$$\begin{aligned} \nu_T &= \ell^2 \left|\frac{\partial u}{\partial y}\right| \quad y > y_{infl} \\ &= \ell^2 \left|\frac{\partial u}{\partial y}\right|_{y_{infl}} \quad 0 \leq y \leq y_{infl} \end{aligned} \tag{4.9}$$

The solid lines in Fig. 4.3 represent the predictions of the mixing length model using this refinement according to $\ell = 0.236\ y_{infl}$. This model is referred to in the figures as the modified mixing length model and for future reference it will be called Model B. The modification is seen to lead to better agreement, overall, with the experimental data of Landis and Shapiro [59]. However, the decay of centerline values is still left underpredicted in the main region, especially at larger axial distances. Also shown in Fig. 4.3 are the predictions of Hirst [10] using an integral method.

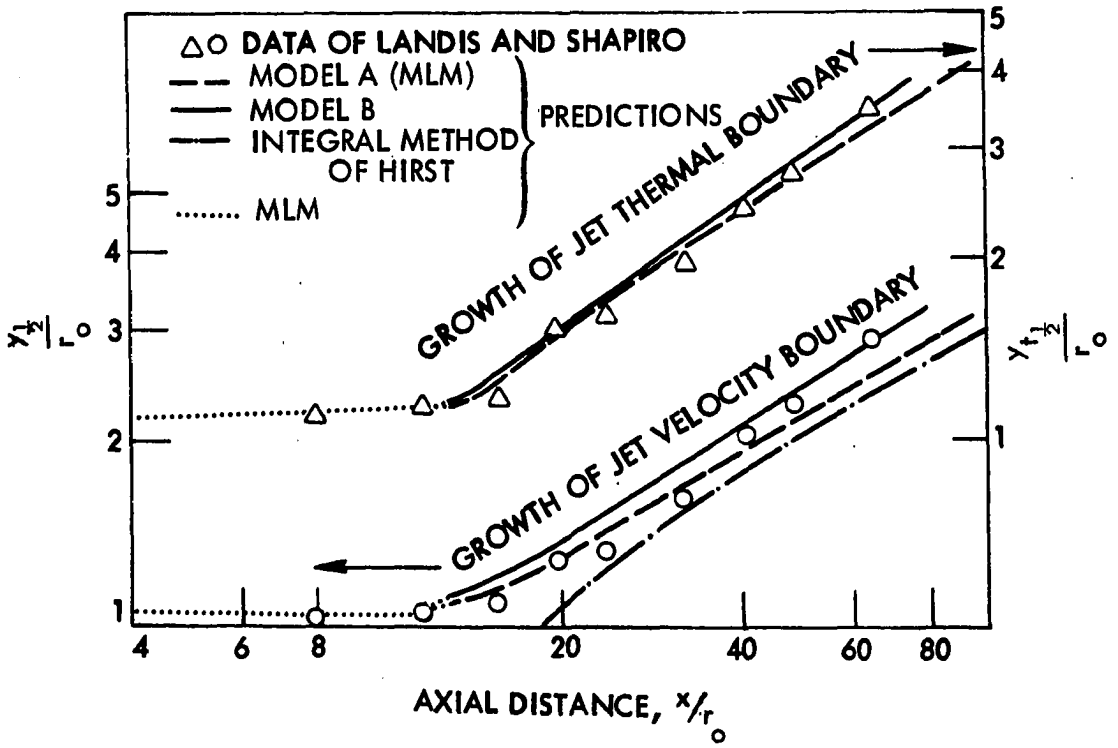

Fig. 4.3a. MLM and modified MLM in main region - growth of half-radius for R=0.25.

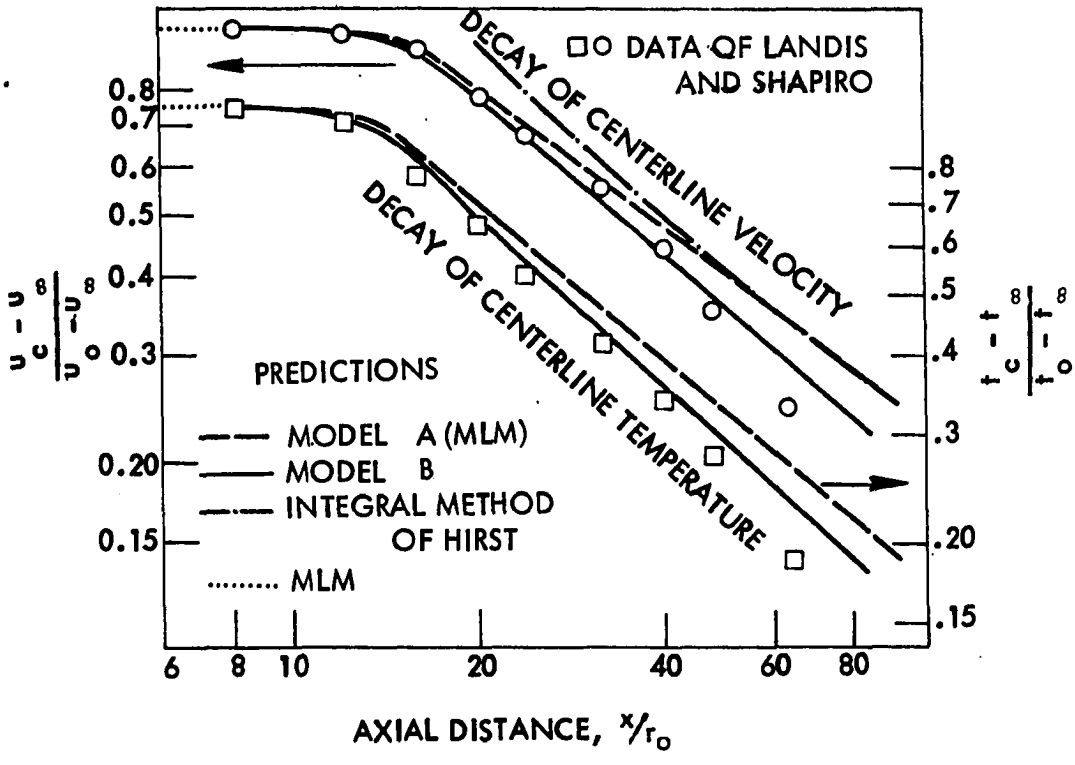

Fig. 4.3b. MLM and modified MLM in main region - decay of centerline values for R=0.25.

The next model examined was the eddy viscosity model proposed by Schetz [18] of the form

$$\mu_T = \frac{2K_1}{r_o} \int_0^\infty |u_e - u| y dy \tag{4.10}$$

where Eq. (4.10) relates the turbulent viscosity to the mass flow defect (or excess) per unit width in the mixing region. Here, $K_1 = 0.018$.

Schetz arrived at this model as an axisymmetric equivalent, starting with the generalized form of Clauser's planar model for the outer region of a turbulent boundary layer. Predictions using this model, Model C, for $R = 0.25$ are shown by broken lines in Fig. 4.4. As noted by Schetz [63], the centerline decay values are seen to be overpredicted for this velocity ratio. The Schetz model assumes a constant value for the turbulent viscosity across the mixing layer, but measurements indicate [26] that it in fact varies and has an intermittent character near the outer edge of the mixing layer. Hence, in an attempt to account for these observed intermittency effects, it was decided to modify Model C to the form

$$\mu_T = \frac{2K_2\gamma}{r_o} \int_{y_c}^\infty |u_e - u| y dy \tag{4.11}$$

where γ is equal to an intermittency function and $K_2 = 0.012$. An expression was developed by the authors for γ as follows:

$$\gamma = 1.0 \qquad 0 \le \frac{y}{y_{1/2}} \le 0.8$$

$$\gamma = (0.5)^z \qquad \frac{y}{y_{1/2}} > 0.8 \text{ where } z = \left(\frac{y}{y_{1/2}} - 0.8\right)^{2.5} \tag{4.12}$$

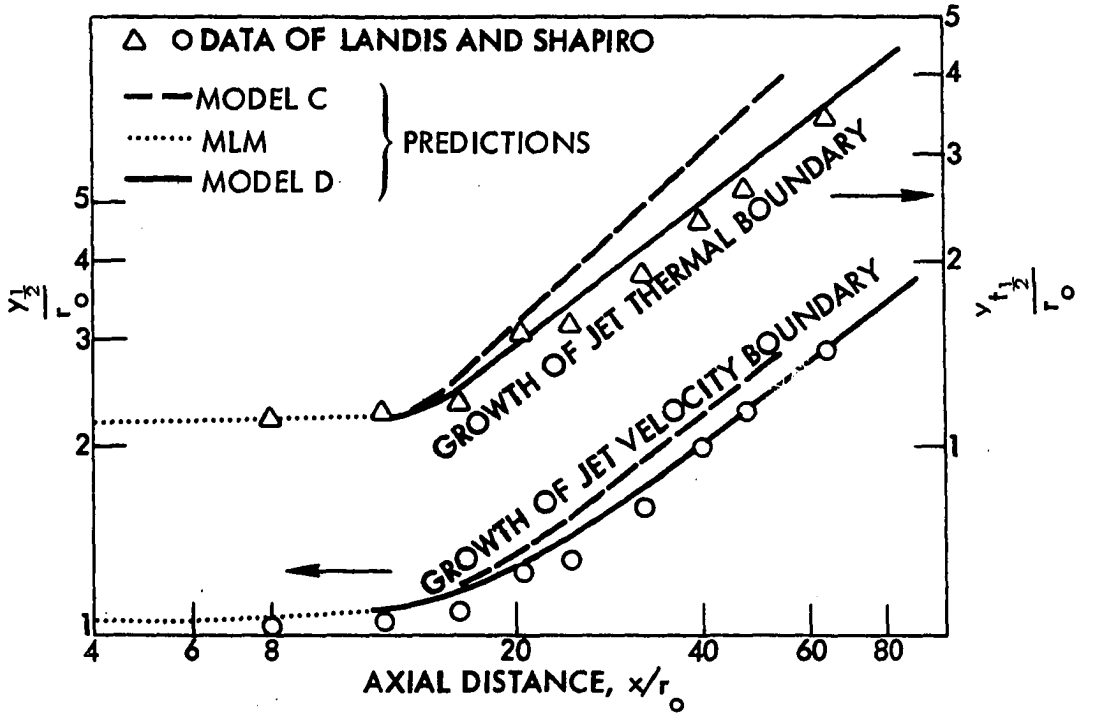

Fig. 4.4a. Schetz and modified Schetz models - growth of half-radius for R=0.25.

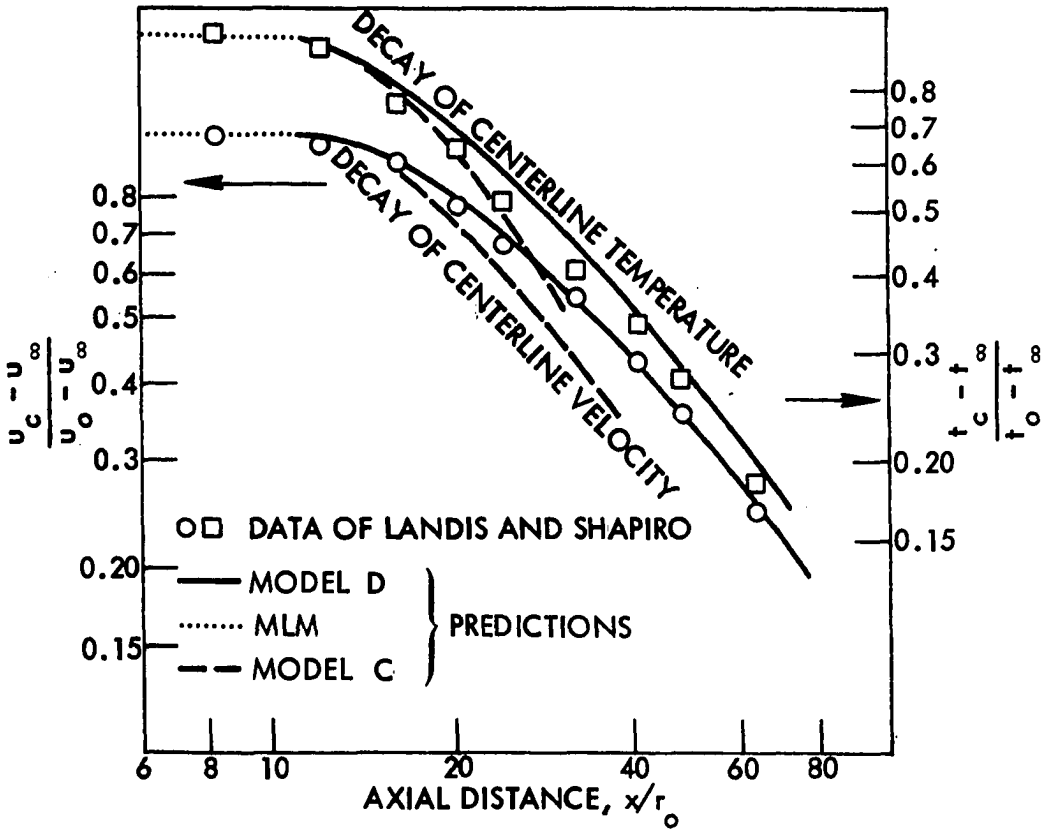

Fig. 4.4b. Schetz and modified Schetz models - decay of centerline values for R=0.25.

This gives a distribution for γ which agrees well with the experimentally determined curve in [64]. Predictions were greatly improved for this velocity ratio and are shown as the solid line in Fig. 4.4. Another modification of Eq. (4.10) can be found in Ref [65].

However, for R = 0.5, the modified Schetz model, or Model D, did not do as well (Fig. 4.5). This effect seemed to plague all models that were brought out in the Langley workshop [8] as well, where, if predictions agreed well for R = 0.25, Test Case 9, then the agreement was poor for R = 0.48, Test Case 20. However, the results of Test Case 20 are in good agreement with the Forstall and Shapiro [58] measurements at a velocity ratio of 0.5 in the main region, suggesting that the difference in velocity ratio is the most significant difference in the main region between Langley Cases 9 and 20. An observation in the same Proceedings that "the deviation of predictions from experiment for higher velocity ratios can be attributed to the increased influence of free-stream turbulence on mixing rate at higher velocity ratios" serves to corroborate this notion.

To account for this behavior, a velocity ratio function was developed with the idea that there must be a free stream turbulence level effect since the mixing of a jet with an ambient in motion would be influenced by the eddy motion characteristic of this flowing ambient, and this effect would assume greater importance in the mixing as the stream velocity grew in relation to the jet velocity. Starting with the hypothesis that the first order effect of the "free stream" turbulence on turbulent mixing characteristics of a stream might be more likely to scale

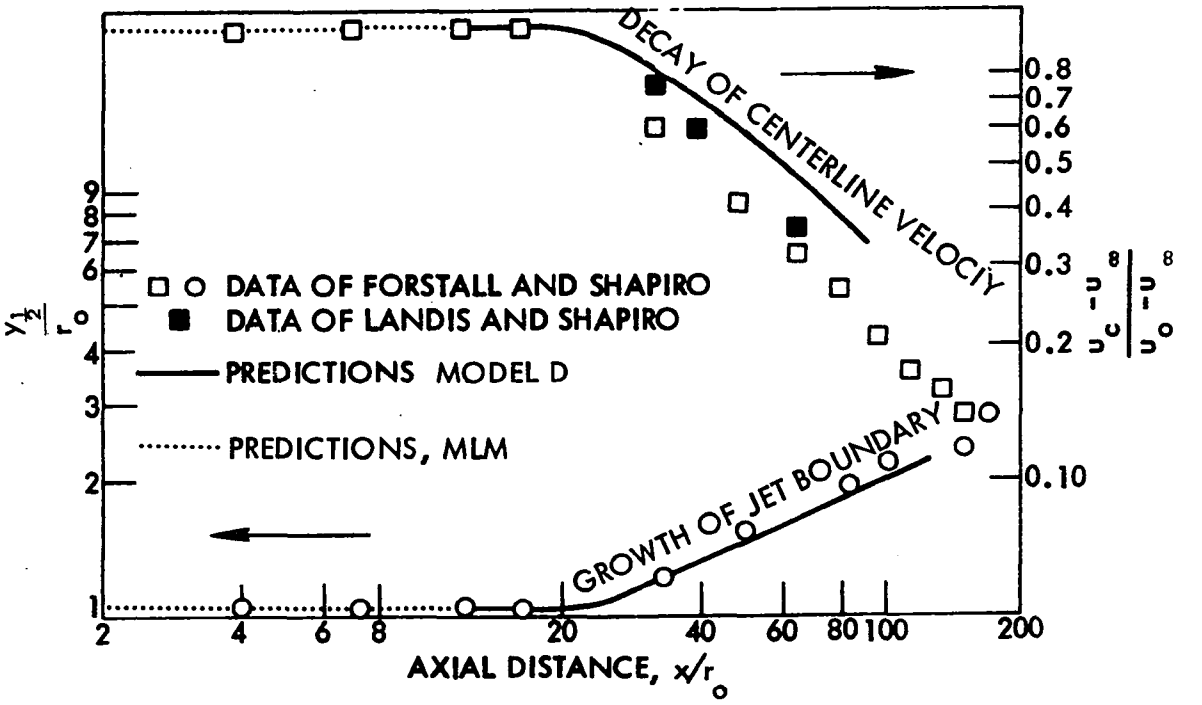

Fig. 4.5. Modified Schetz model for R=0.5.

with the stream kinetic energy than any other simple parameter, the following form for F was developed:

$$F = \text{CONST}\ (1 + 2.13R^2) \tag{4.13}$$

Finally, after localizing the concept of mass flow defect as proposed in the Schetz model, a new variable viscosity model, Model E, of the form

$$\mu_T = \frac{2F}{r_o} \int_y^\infty |u_e - u| y dy \tag{4.14}$$

with CONST = 0.015 in Eq. (4.13) for F, was proposed. Here, the viscosity at a given distance y from the center of the jet is proportional to the mass flow defect (or excess) per unit width in the mixing region from that point to the outer edge of the mixing layer. The general trend of the resulting viscosity variation is qualitatively similar to that provided by the use of the intermittency factor, but here the model would permit variations in response to local variations in velocity profile shape.

Predictions of this proposed model, Model E, used in the main region for a wide range of velocity ratios are shown in Fig. 4.6 along with the data of Landis and Shapiro [59], Forstall and Shapiro [58], Albertson et al. [57], and Trupel (cited in [56]). The predictions, which extend up to 100 diameters downstream of the nozzle exit, are seen to agree well with experiments over the entire range of velocity ratios considered, including the case of the jet discharging into a still ambient.

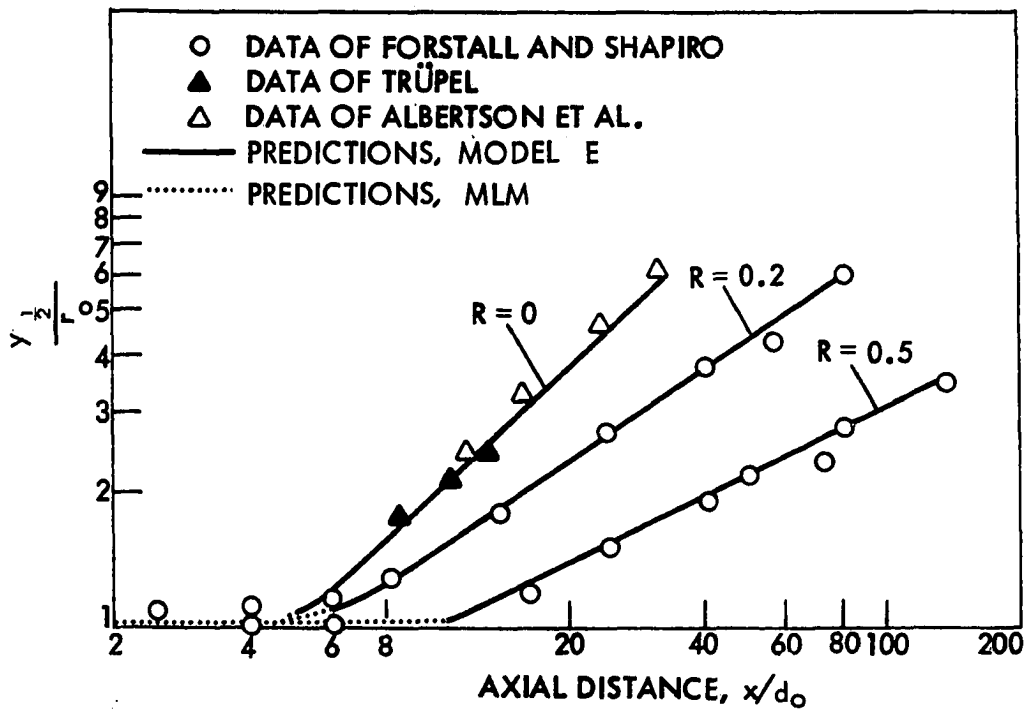

Fig. 4.6a. Proposed model (Model E) for different velocity ratios - growth of half-radius.

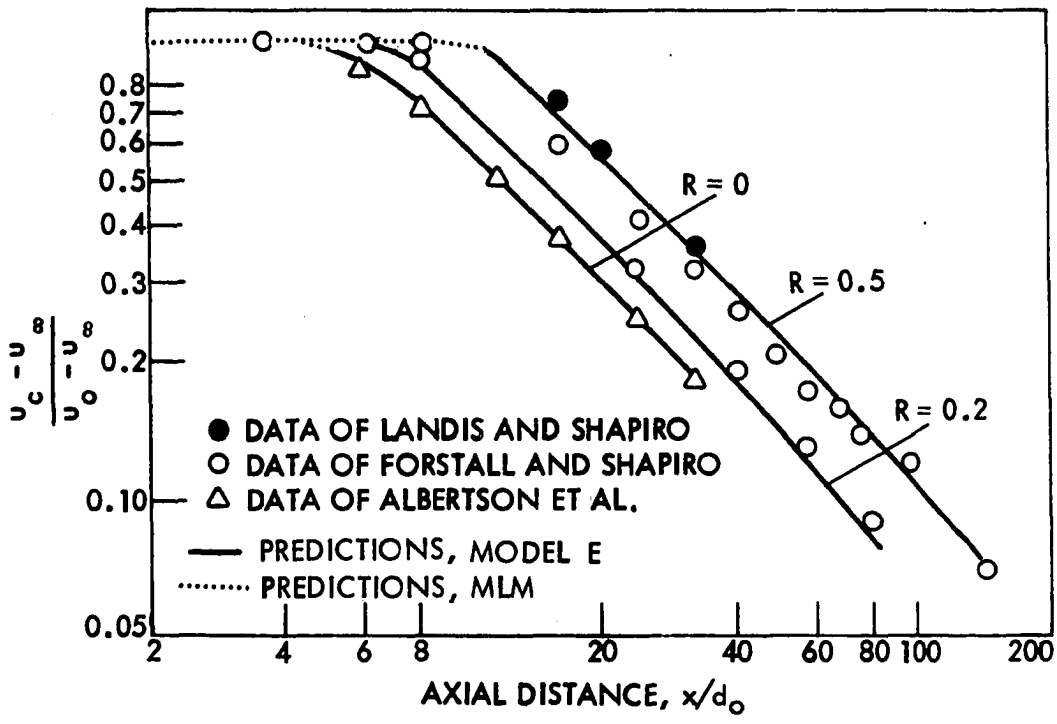

Fig. 4.6b. Proposed model (Model E) for different velocity ratios - decay of centerline velocity.

It is quite satisfying to see that the velocity ratio squared term in F appears to account for the effect of velocity ratio for the cases considered. The effect is a large one since F increases by about 53% over the range of cases illustrated in Figs. 4.6a and 4.6b.

All predictions of the present method for a jet discharging into quiescent surroundings were made for R = 0.03. The use of smaller velocity ratios resulted in no significant changes in the predictions, but since the stability criterion for the starting method [36,51] dictated very small starting step sizes, R = 0.03 was used for reasons of economy.

For further comparisons, the data of Test Cases 9 and 20 from the Langley workshop [8] are shown in Figs. 4.7 and 4.8 with predictions using some of the models considered in the Langley workshop, as well as the present model. For Test Case 9 (Fig. 4.7), the predictions of the Harsha turbulent kinetic energy model are shown only in the initial region. In the main region, the line was so close to that of Model E that it is not shown. Overall, the proposed simple model is seen to perform as well as even the more complex models considered in Figs. 4.7 and 4.8. Also, from these two figures, it can be learned that, though the flow appears simple, there is a wide spread in the predicted values, indicating that the status of predictions for this class of flow is not as good as for wall boundary layers.

All predictions of the present method shown in Figs. 4.3 to 4.8 used initial profiles at the end of the initial region which were provided by Prandtl's mixing length model (Model A). The predictions in Fig. 4.8 could have been further improved if the velocity ratio function F was incorporated into Model A as well.

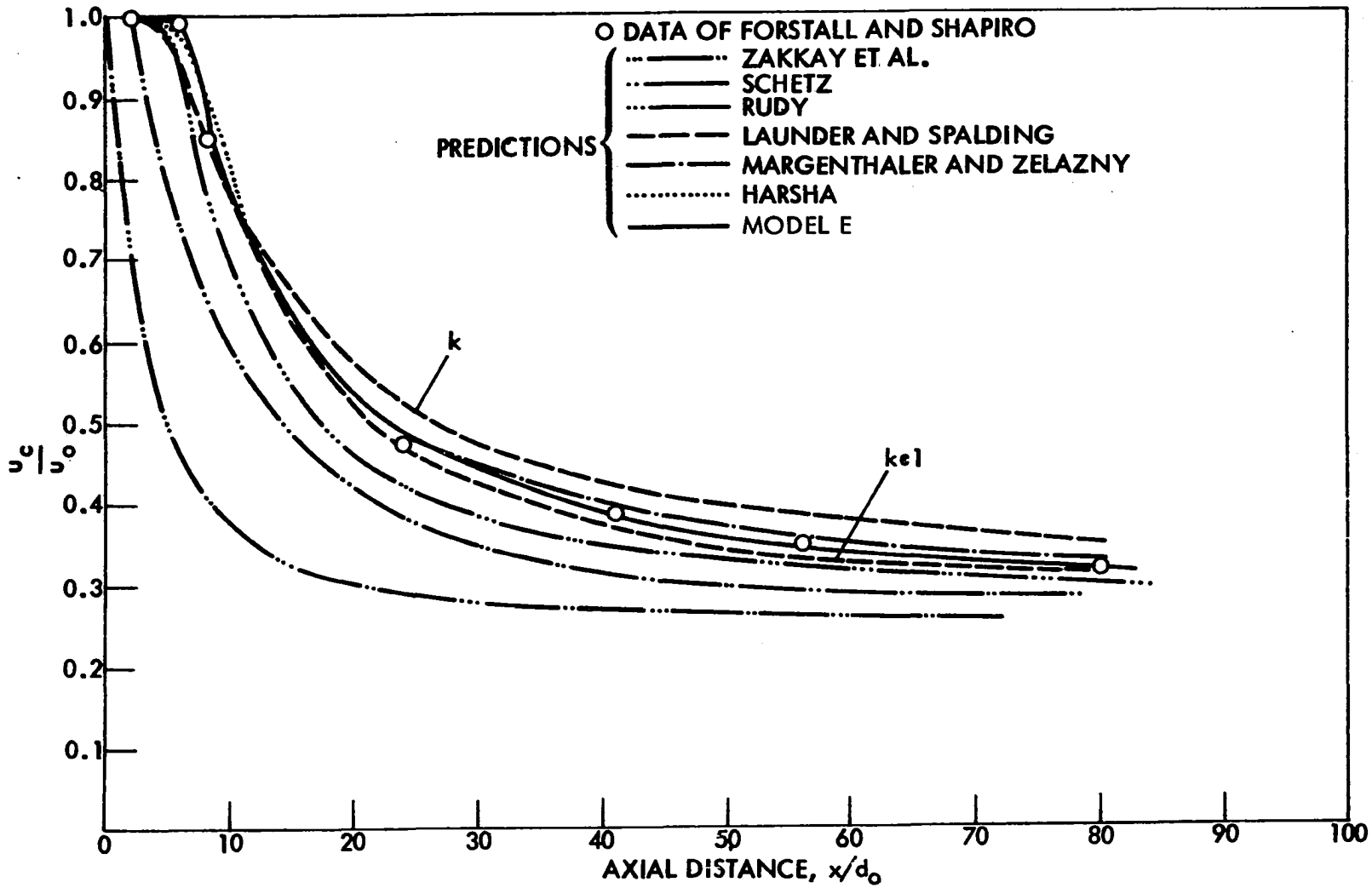

Fig. 4.7. Model E for Langley Test Case 9, R=0.25 - comparisons with experiment and other models.

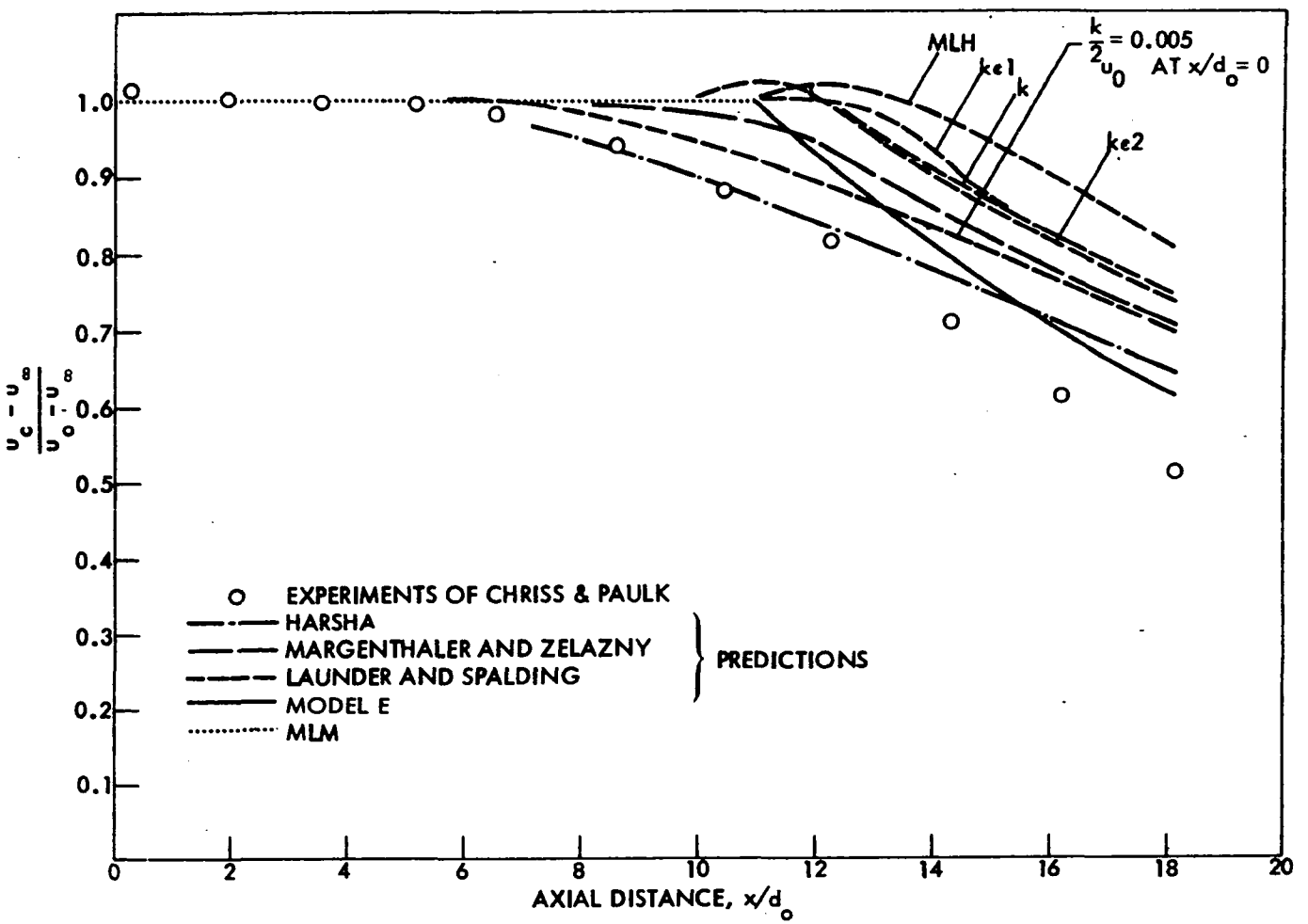

Fig. 4.8. Model E for Langley Test Case 20, R=0.48 - comparisons with experiment and other models.

When the modified Schetz model and the proposed model were used from the injection point, starting with slug profiles of velocity and temperature, they gave good agreement with data; however, the constant had to be changed in order to achieve reasonable predictions in the initial region.

An additional shortcoming associated with Model C which rendered it unsuitable for use in the initial region was that the viscosity predicted by the model appeared overly sensitive to the definition of the mixing zone, the starting length prediction changing by a factor of 3 (unless the constant was adjusted to compensate) if the width of the mixing zone was arbitrarily increased by one grid point.

All of the models evaluated in this work were found to predict velocity and temperature profiles which, when non-dimensionalized, agreed fairly well with measurements. However, the predictions of the Schetz constant viscosity model tend to fall out of the experimental band close to the edge of the jet. See Fig. 4.9.

It is worth emphasizing at this point that the proposed model is very successful in the non-buoyant jet case, but it is not meant to be an ultimate model. Rather, this development is meant to show the viability of simple models for such a configuration, and the desirability of recognizing and incorporating certain important features, such as ambient turbulence effect, into the model. The velocity ratio function could equally well be applied to Model D, or Prandtl's constant viscosity model (labeled Model F) of the form:

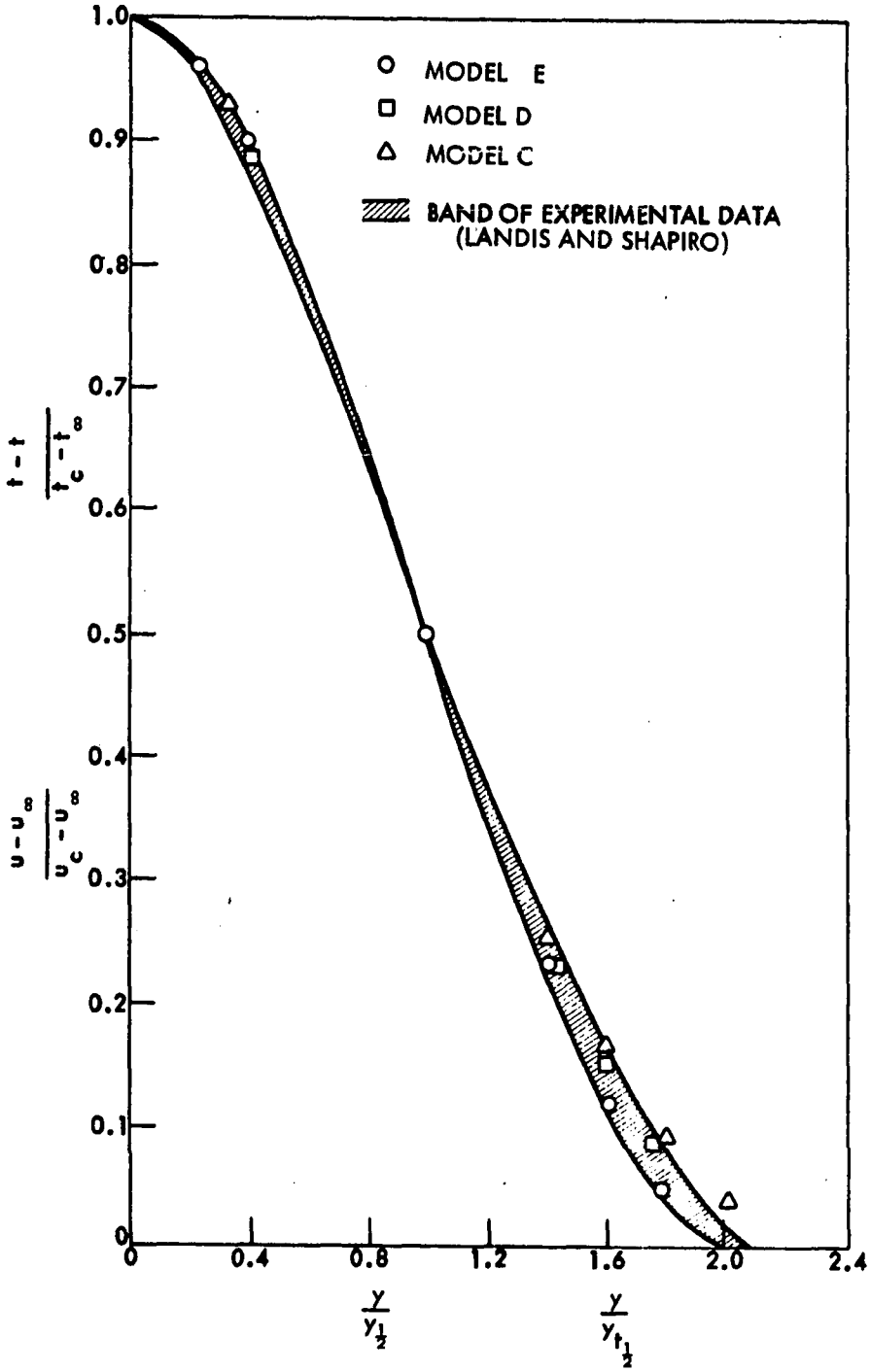

Fig. 4.9. Fully normalized profiles of velocity and temperature at $x/r_o = 20$, $R = 0.25$.

$$\nu_T = K_3 \, y_{1/2} \left(u_{max} - u_{min}\right)$$

where $K_3 = 0.0246$ (4.15)

To demonstrate this point, Fig. 4.10 shows the good agreement between experimental data and the predicted centerline decay values for different velocity ratios using Model F modified to

$$\nu_T = F \, y_{1/2} \left(u_{max} - u_{min}\right) \tag{4.16}$$

where F is given by Eq. (4.13) and CONST = 0.0246.

Assumptions of a linear variation of mixing zone with x and profile similarity, which have been used in the development of some models (e.g., Cohen [66]), were carefully avoided here since it was planned to use the analysis for more complex flows (of which some have been reported in Chapters 5 and 6) where these assumptions would not be valid.

4.5. Some Numerical Aspects

The stability criterion in the final form, Eq. (3.30) shown in Chapter 3, had not been developed at this point of the study. Carefully selecting the step size and using Eq. (4.17)

$$\left| \frac{V_{i,j} \, \Delta S_+}{U_{i,j} \, \Delta Y} \right| < 1 \tag{4.17}$$

as a rough upper bound along with a safety factor, succeeded in eliminating the instability problem for most of the calculations reported.

However, going to velocity ratios that approached zero, typically 0.03 or 0.05, caused a peculiar trend of instability to be observed where

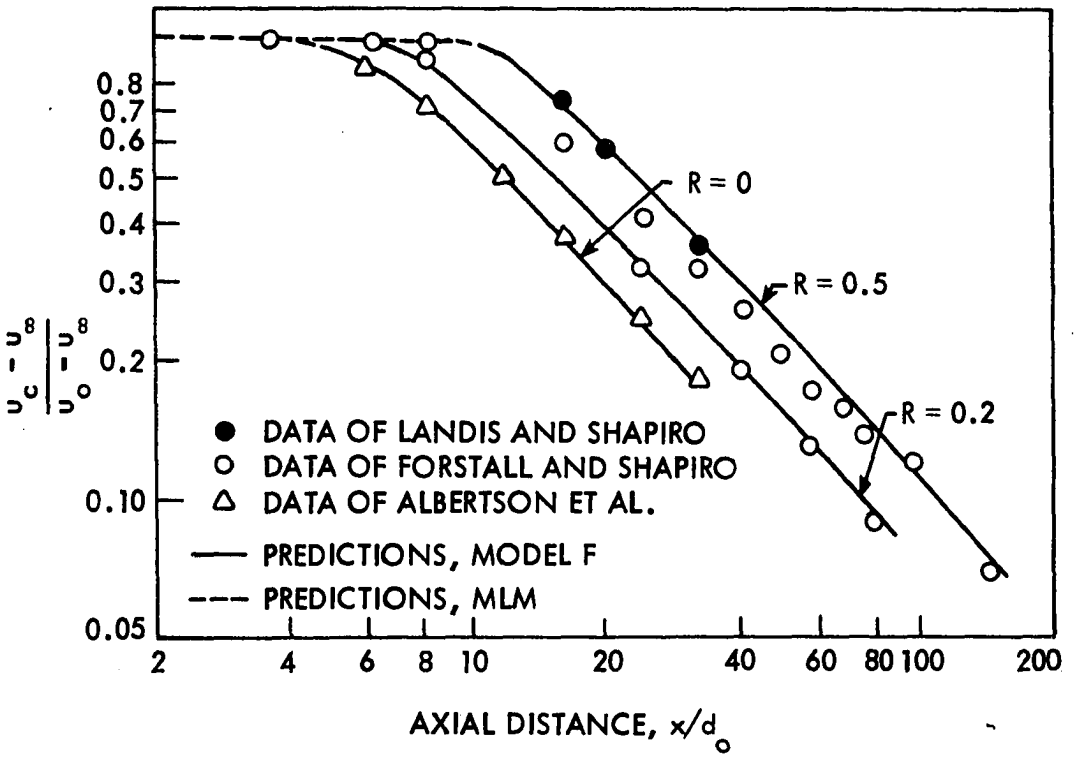

Fig. 4.10. Model F for different velocity ratios - decay of centerline velocity.

the transverse velocity started growing near the outer edge of the jet and then grew rapidly out of control, eventually swamping the solution. No remedy seemed available until it was recognized as a phenomenon where the effective viscosity was small compared to the product of the lateral velocity flux and the lateral grid spacing. Recourse was taken to a "high-lateral flux modification," introduced as a novelty of numerical analysis by Patankar and Spalding [67] in the new version of their computation procedure. This was adapted for the present program as described below.

The qualitative description of the high lateral flux condition in the previous paragraph was given mathematical form, following the substance of Eq. (6.2-31) in [67] as:

$$\left(N_{i,j} + N_{i,j+1}\right) = \frac{1}{2}\left[AL1 + \left|V_{i,j}\,\Delta Y\right| + \left|AL1 - \left|V_{i,j}\,\Delta Y\right|\right|\right]$$

$$\left(N_{i,j} + N_{i,j-1}\right) = \frac{1}{2}\left[AL2 + \left|V_{i,j}\,\Delta Y\right| + \left|AL2 - \left|V_{i,j}\,\Delta Y\right|\right|\right]$$

$$\text{where } AL1 = \left(N_{i,j} + N_{i,j+1}\right) \text{ and } AL2 = \left(N_{i,j} + N_{i,j-1}\right) \qquad (4.18)$$

Equation (4.18) implies the following:

(I) If $AL1 > \left|V_{i,j}\,\Delta Y\right|$

Then, $\left(N_{i,j} + N_{i,j+1}\right) = \frac{1}{2}\left[AL1 + \left|V_{i,j}\,\Delta Y\right| + AL1 - \left|V_{i,j}\,\Delta Y\right|\right]$

$= AL1.$

(II) If $\left|V_{i,j}\,\Delta Y\right| > AL1$

Then, $\left(N_{i,j} + N_{i,j+1}\right) = \frac{1}{2}\left[AL1 + \left|V_{i,j}\,\Delta Y\right| + \left|V_{i,j}\,\Delta Y\right| - AL1\right]$

$= \left|V_{i,j}\,\Delta Y\right|$

This modification had the effect of eliminating the high lateral flux problem. Later on, further evidence for the necessity of this formulation was obtained by a stability analysis of the momentum equation using Karplus' electric analogue method [68].

In answer to a possible question that this represents only a patching operation, Patankar and Spalding say that most of the available procedures, perhaps all of them, need doctoring in this or a similar way. In addition, it is worth noting that the fact that this modification was found to be necessary for an implicit method is evidence that this is not a defect peculiar with the explicit method.

This modification was thenceforth retained as a special feature of the computer program which would enable it to handle all such cases of high lateral velocities.

As mentioned in Chapter 3, step sizes roughly 8-10% of the mixing width (δ) in the main region could be taken without occurrence of instability for all except the $R \to 0$ cases.

The results described in the previous section were obtained as output from the IBM 360/65 computer. The program was designed to use a growing step size in the downstream direction, so that the calculation becomes more economical with increasing streamwise distance. However, it was not necessary to go beyond 100 diameters for any case reported in this chapter.

4.6. Concluding Remarks

The highlights of the study presented in this chapter can be summarized as follows:

1. A fast and effective explicit finite-difference method has been developed for the simultaneous solution in the physical plane of the conservation equations for both free and co-axial jet flows. The method can be used with a variety of models for the turbulent viscosity and provides a useful tool for evaluating transport models.

2. Prandtl's mixing length model (Model A) worked well in the initial region and gave very accurate predictions for the starting length over a wide range of velocity ratios. Not much can be said as to the superiority of one model over another in the initial region, since a variety of initial conditions can occur, making it difficult to draw general conclusions. However, a model least sensitive to different starting assumptions would appear to have an edge as a reasonable starting model. The mixing length formulation seems to satisfy this need. This enhances our confidence in the applicability of the model for calculations in the design of the discharge system for a power plant.

3. Agreement between predictions and experiment was not good for the mixing length model in the main region. Modifying it so that the turbulent viscosity did not approach zero at the jet centerline improved predictions in the main region. Using y_{infl} as the characteristic length also contributed to improved agreement with experimental data, but no suitable cross-section length scale was found which led to truly good agreement for the decay of centerline values. On the other hand, even this mixing length model fared better than the predictions of the integral method of Hirst [10] for the experimental data considered.

4. A modification (Model D) to the constant viscosity model of the form suggested by Schetz (Model C), which employed an intermittency

function as a multiplying factor, was found to lead to significantly better agreement with experimental data for one velocity ratio but not for another.

5. A new variable viscosity model (Model E) was proposed for the turbulent jet which appeared to account satisfactorily for the effect of velocity ratio on the turbulent mixing as evidenced by the consistently good agreement between predictions and measurements over a wide range of velocity ratios, including the important case of the jet discharging into a quiescent ambient. In the limited comparisons that were possible for the class of flow being considered, the simple proposed model (with ambient turbulence effect included) appeared to perform as well as even the more complex models of turbulence.

6. The presence of a wide variety of approaches to achieve turbulence closure is in itself an evidence of their approximate nature, and until a more fundamental understanding of the mixing phenomenon is achieved, the superiority of one model over another will always be debatable and case-dependent, irrespective of the complexities involved in the modeling.

5. THE BUOYANT VERTICAL JET OR PLUME IN A UNIFORM OR STRATIFIED AMBIENT

5.1. Introduction

The practical applications of this configuration include the discharge of thermal or sewage effluent into the ocean and also the discharge of effluent from chimneys and cooling towers into a still atmosphere.

Until recently, experimental data for the buoyant vertical jet in uniform ambient was scant, the only ones that were known being the limited measurements of Abraham [69], the data of Frankel and Cumming [70], and the results of Rouse et al. [71] for pure buoyant plumes above a point heat source. Recently, however, some very excellent sources became available. They are the measurements of Pryputniewicz [28], and Ryskiewich and Hafetz [72] for a wide range of initial conditions, and including the effects of the free surface, for the vertically discharged buoyant jet. A concise presentation of the results of [28] can be found in [73].

Theoretical analysis in terms of approximate methods for prediction of vertical buoyant jets and plumes in uniform ambients dates back to Schmidt's work in 1941 [74], which considered the mechanics of convective plumes (pure buoyancy cases, no initial momentum). Rouse et al. [71] carried out similar work in 1952. They arrived at a theoretical solution for a source of pure buoyancy using an integral method, and compared their assumed Gaussian profiles to their own measured profiles.

The approach of both these investigators involved a solution to the integral conservation equations of vertical momentum, mechanical energy,

and energy, assuming a form for the velocity and density difference profiles, and assuming that the shear stress integral in the mechanical energy equation was similar and known. Morton et al. [15] also used the integral method, but they dropped the mechanical energy equation and used instead the integral form of mass conservation. This required the use of an entrainment function instead of the shear stress integral.

Morton [14] extended the analysis of [15] to include the effect of initial momentum. The analysis of Morton served as the forerunner for later, more general formulations such as those of Fan [16], Fan and Brooks [17], and Hirst [10].

Numerical treatment of the partial-differential equations governing the vertical plume flow in uniform ambient by finite-difference methods has been restricted to the work of Trent [75], Trent and Welty [21], and Oosthuizen [76]. Trent and Welty have solved the two-dimensional vorticity transport equations without boundary layer assumptions using an iterative scheme. They compare their results for deep-water discharge to their similarity solutions based on Abraham's theory. Oosthuizen uses a simple implicit finite-difference scheme to solve the boundary layer form of the governing equations. However, his analysis is restricted to low Re_o flows, so that he makes laminar calculations up to an experimentally determined distance x_{trans} after which he shifts to turbulent calculations.

The discharge of a vertical plume into a stably stratified ambient, where the density of the receiving medium decreases with increasing height, has also been studied by several investigators. For this case, the jet will only reach a certain height, determined by two parameters:

the initial buoyancy of the plume relative to its initial momentum, and the degree of ambient stratification. Later, these parameters will be expressed as dimensionless groups.

Experimental height of rise data have been given by Hart [77], Crawford and Leonard [78], Abraham and Eysink [79], Fox [80], and others. Theoretical approaches have all been integral in nature and can be found in Hart [77], who modifies Abraham's equations for jets in a homogeneous ambient to predict height of rise, Morton et al. [15], and later Morton [14], Priestley and Ball [81], Fan [16], Fan and Brooks [17], Fox [80], Hirst [9], and others. Sneck and Brown performed experiments to represent plume rise from large-diameter sources such as cooling towers, and the results of their experiments are presented in [82] along with the theory of Fox.

A valuable reference for the stratified ambient case is [9], where Hirst presents the results of his integral method using a generalized entrainment function which is an extension of Fox's variable entrainment function, and presents the experimental results of several investigators for height of rise, in a tabular form.

No differential approaches to predict height of rise have been seen for the stratified ambient case discussed above. For more information on buoyant jet theory, the reader can refer to the works of Abraham [12], Baumgartner and Trent [1], and Hirst [10], which present very good reviews on the subject.

The results to be presented in this chapter were obtained using the same numerical method that worked well for the non-buoyant jet analysis. The formulation is basically the same as for the non-buoyant jet, except

that a buoyancy term is included in the momentum equation. Also, in the case of stratified ambient, the ambient temperature varies, providing a variable boundary condition.

This is believed to be the first time that a finite-difference method has been used with success to solve the boundary layer form of the governing equations for this class of jet flow. The merits in using explicit methods have been briefly mentioned in Chapter 3. Again an eddy viscosity approach to turbulence modeling will be seen to be successful.

Comparisons have been made for zero buoyancy height with the results in [82], and for zero momentum height, with the experimental results of several investigators in [9].

5.2. Flow Configuration

Figure 5.1a shows the configuration of a jet issuing into a uniform ambient. The jet is accelerated by buoyancy, causing the centerline velocity at discharge to start increasing. This makes the precise determination of the location where the velocity starts to decay, more difficult. The starting length, S_ℓ, is therefore based on temperature (or concentration) rather than velocity for buoyant flows. In a uniform ambient, the jet will rise indefinitely, unless interrupted by a free-surface (in case of submerged ocean outfall) because, regardless of the reduction in buoyancy by mixing, the jet is always somewhat buoyant with respect to the environment.

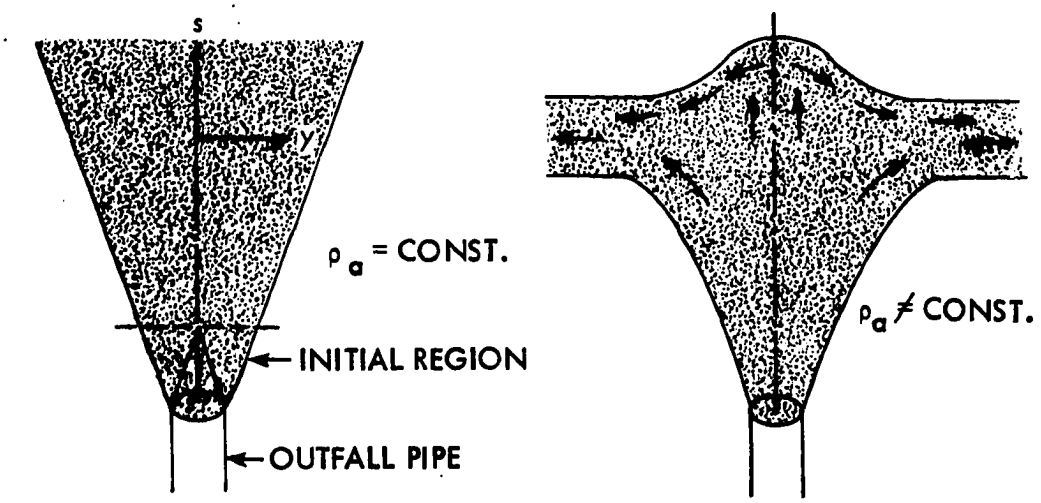

(a) VERTICAL PLUME IN UNIFORM AMBIENT

(b) VERTICAL PLUME IN STRATIFIED AMBIENT

Fig. 5.1. Flow configurations.

In Fig. 5.1b the jet can be seen discharging into a stably stratified ambient. Thermal stratification is the usual occurrence [77], and the one that is shown in the figure. This plume will not rise indefinitely. Initially, the main loss of buoyancy will be due to entrainment of dense ambient fluid as the jet moves upward. In addition, the density of the ambient fluid decreases with elevation. Hence, as the plume ascends, due to both of these effects, the density difference relative to the local ambient steadily decreases, eventually reducing to zero. At this stage, there is no accelerating force, and the flow continues upward by virtue of the vertical momentum it possesses, only to encounter negative buoyancy forces (due to local ambient fluid being lighter than jet fluid) that eventually cause total loss of upward momentum. At this level of maximum rise, the plume fluid is denser than the local surroundings and consequently will cascade downward around the upward flow, to ultimately spread laterally at a level of neutral buoyancy.

Both the height at which buoyancy first goes to zero, called the zero buoyancy height, Z_B, and the height at which momentum reduces to zero, called the zero momentum height, Z_M, are important unknowns to be determined by the prediction method.

The zero momentum height is very important from the point of view of thermal discharge design since it determines whether the plume will reach and spread out on the water surface or stay submerged and spread out below the water surface (in case of ocean outfalls). The discharge system can be designed to achieve either of these conditions depending upon the requirements of the water quality standards. For atmospheric discharges, the most adverse conditions for plume rise and dispersion

are a ground based atmospheric inversion accompanied by no crosswind, and ground based inversions usually occur with still air [82]. Thus, if the height of rise of a plume can be predicted under these limiting conditions, a conservative estimate of the plume's performance under general field conditions can be made.

The zero buoyancy height, where $(\rho - \rho_\infty)$ is first diminished to zero, is significant since the behavior of the plume changes markedly after this height. First, the plume centerline temperature (or concentration) is usually observed to increase slightly after this height. Also, soon after Z_B, the plume ceases to entrain any more ambient fluid. In fact there is negative entrainment as the plume begins to spread out horizontally.

5.3. The Governing Equations

The equations listed below are a degenerate form of those presented in Chapter 3 for $\theta_o = 90^o$. Since the plume trajectory will follow a straight line, θ remains constant = 90^o, and the y-momentum equation is absent. The resulting set of equations is the same as Eqs. (4.1) to (4.3), except that the s-momentum equation now has a buoyancy term.

$$\frac{\partial}{\partial s}(uy) + \frac{\partial}{\partial y}(vy) = 0 \tag{5.1}$$

$$u \frac{\partial u}{\partial s} + v \frac{\partial u}{\partial y} = \frac{1}{py} \frac{\partial}{\partial y} (y\tau) + \frac{(\rho_\infty - \rho)}{\rho_o} g \tag{5.2}$$

$$u \frac{\partial t}{\partial s} + v \frac{\partial t}{\partial y} = \frac{1}{\rho c_p y} \frac{\partial}{\partial y} (- yq) \tag{5.3}$$

Here, s = z, since for a vertical configuration the streamwise coordinate coincides with the vertical.

The boundary conditions are given by Eq. (3.13) and the initial conditions by Eq. (3.12).

The variable boundary condition describing ambient stratification is explained in the next section.

5.4. Non-dimensionalization

The dimensionless variables are given by Eq. (3.14), and the normalized equations in terms of these variables can be written as:

$$\frac{\partial}{\partial S}(UY) + \frac{\partial}{\partial Y}(VY) = 0 \tag{5.4}$$

$$U\frac{\partial U}{\partial S} + V\frac{\partial U}{\partial Y} = \frac{1}{Y}\frac{\partial}{\partial Y}\left(YN\frac{\partial U}{\partial Y}\right) + \frac{(T - T_\infty)}{Re_o\, Fr_o} \tag{5.5}$$

$$U\frac{\partial T}{\partial S} + V\frac{\partial T}{\partial Y} = \frac{1}{Y}\frac{\partial}{\partial Y}\left(YN_H\frac{\partial T}{\partial Y}\right). \tag{5.6}$$

As mentioned earlier, the general behavior of the buoyant vertical jet in an ambient of variable density will depend on the initial relative buoyancy of the plume, and the degree of ambient stratification.

Buoyancy is represented by a non-dimensional parameter called the Froude number, Fr. It expresses the ratio of the inertia to buoyancy forces, so that a high Fr means that the effects of buoyancy will be small and vice versa.

Mathematically,

$$Fr = \frac{u^2}{2g\delta \frac{(\rho_\infty - \rho)}{\rho_o}} \tag{5.7}$$

The initial Froude number, therefore, would be represented by

$$Fr_o = \frac{u_o^2}{gd_o \frac{(\rho_\infty - \rho_o)}{\rho_o}} .$$

The ambient stratification is commonly specified either of two ways:

i) as λ, the degree of stratification, expressed in $^oC/m$ (or $^oF/ft$), in which case the non-dimensional form is as shown in Chapter 3.

ii) as $\bar{T}$, a non-dimensional stratification parameter. Mathematically, this is defined as

$$\bar{T} = \frac{(\rho_\infty - \rho_o)}{-r_o \frac{d\rho_\infty}{dz}} \tag{5.8}$$

This was implemented in terms of temperature as follows (valid for both gases and liquids):

The equation of state is,

$$\rho = \rho_{ref} \left[1 - \beta(t - t_{ref})\right] \tag{5.9}$$

Differentiating both sides with respect to z yields,

$$\frac{d\rho}{dz} = -\beta \rho_{ref} \frac{dt}{dz} \tag{5.10}$$

Also, from Eq. (5.9),

$$\frac{(\rho - \rho_{ref})}{\rho_{ref}} = - \beta(t - t_{ref})$$

or, for $\rho_{ref} = \rho_o$,

$$\frac{(\rho_\infty - \rho_o)}{\rho_o} = - \beta\ (t_\infty - t_o)$$

which yields

$$(\rho_\infty - \rho_o) = \beta\ \rho_o(t_o - t_{\infty o}) \tag{5.11}$$

Substituting Eqs. (5.10) and (5.11) into Eq. (5.9) yields

$$\overline{T} = \frac{(t_o - t_\infty)}{r_o \frac{dt_\infty}{dz}} \tag{5.12}$$

where $\frac{dt_\infty}{dz} = |\lambda|$, the degree of stratification.

5.5. The Difference Formulation

The difference forms of the continuity and energy equations are the same as Eqs. (3.22) and (3.25). The momentum equation can be written in difference form as follows:

$$\frac{U_{i,j}}{(\Delta S_+ + \Delta S_-)}\left(U_{i+1,j} - U_{i-1,j}\right) + \frac{V_{i,j}}{(\Delta Y_+ + \Delta Y_-)} \times \left(U_{i,j+1} - U_{i,j-1}\right)$$

$$= \frac{2}{Y_j(\Delta Y_+ + \Delta Y_-)} \times \left\{\left[\frac{\left(Y_{j+1} + Y_j\right)\left(N_{i,j} + N_{i,j+1}\right)}{4} \times \frac{\left(U_{i,j+1} - 0.5\left[U_{i+1,j} + U_{i-1,j}\right]\right)}{\Delta Y_+}\right]\right.$$

$$- \left[\frac{(Y_j + Y_{j-1})(N_{i,j} + N_{i,j-1})}{4} \times \frac{(0{\cdot}5[U_{i+1,j} + U_{i-1,j}] - U_{i,j-1})}{\Delta Y} \right] \Bigg\}$$

$$+ (T_{i,j} - T_{\infty i}) \Big/ (Re_o Fr_o) \qquad (5.13)$$

The initial and boundary conditions transform as explained in Chapter 3.

5.6. Transport Models and Results

5.6.1. Uniform ambient

In the initial region, the simple mixing length formulation (Model A) that was seen to be successful as the starting model in the non-buoyant jet analysis, was used here also, with the constant in the mixing length left unchanged. Thus,

$$\nu_T = \ell^2 \left| \frac{\partial u}{\partial y} \right| \qquad (5.14)$$

where $\ell = 0.0762\delta$ as before.

Starting length predictions using this model were very consistent when compared with the analytical results of Abraham [12] and Hirst [83]. See Fig. 5.2.

In the main region of flow, the modified mixing length model (Model B) of the previous chapter, was found not to be readily applicable to the buoyant jet case. This was because occasional slight distortions in the velocity profile rendered it impossible to predict the location of the inflexion point accurately. These distortions are very slight and do not constitute an instability, but they are enough to render the criterion for locating the inflection point ineffective, especially since

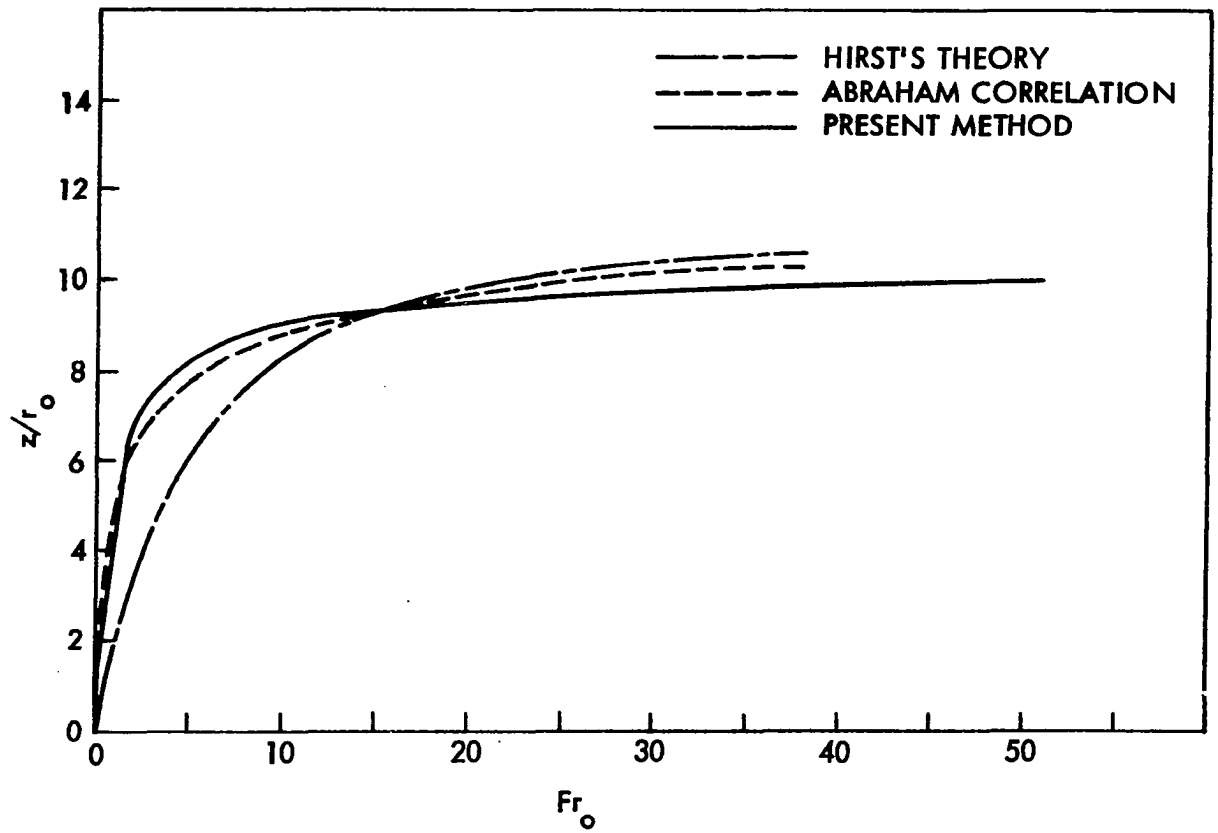

Fig. 5.2. Predictions in initial region - starting length variation with Froude number.

large variations in y_{infl} can cause large variations in the predicted mixing.

Models C and D of the previous chapter (Schetz and Modified Schetz Models, respectively) were incorporated with the constant modified for the quiescent ambient according to Eq. (4.13) and the results were not satisfactory. A comparison using Model D with the numerical solution of Trent and Welty (21) and their similarity solution, for $Fr_o = 106$ is shown in Fig. 5.5. Agreement is not very good. It was expected that Model E, based on the same mass defect concept, wouldn't fare much better. (The ambient turbulence effect given by Eq. (4.13) automatically drops out of consideration since R = 0 for an ambient at rest.)

Attention was therefore directed to Prandtl's constant viscosity model (Model F) of the form [this is the same as Eq. (4.15)]:

$$\nu_T = K_3 y_{1/2} \left(u_{max} - u_{min}\right) \tag{5.15}$$

where $K_3 = 0.0246$

Predictions using this model show much better agreement with other methods (see Figs. 5.3, 5.4, 5.5). For all figures in this chapter, "present method" will imply the use of this model in the main region.

Perhaps the most meaningful test of the model would be provided by comparing the resulting predictions with experimental data. Accordingly, comparisons will be made with the experimental measurements of Pryputniewicz [28], [73], and Ryskiewich and Hafetz [72] on buoyant vertical plumes.

Figure 5.6 shows the general pattern of growth and decay of the predicted centerline values for Froude numbers from 1 to 1000. This

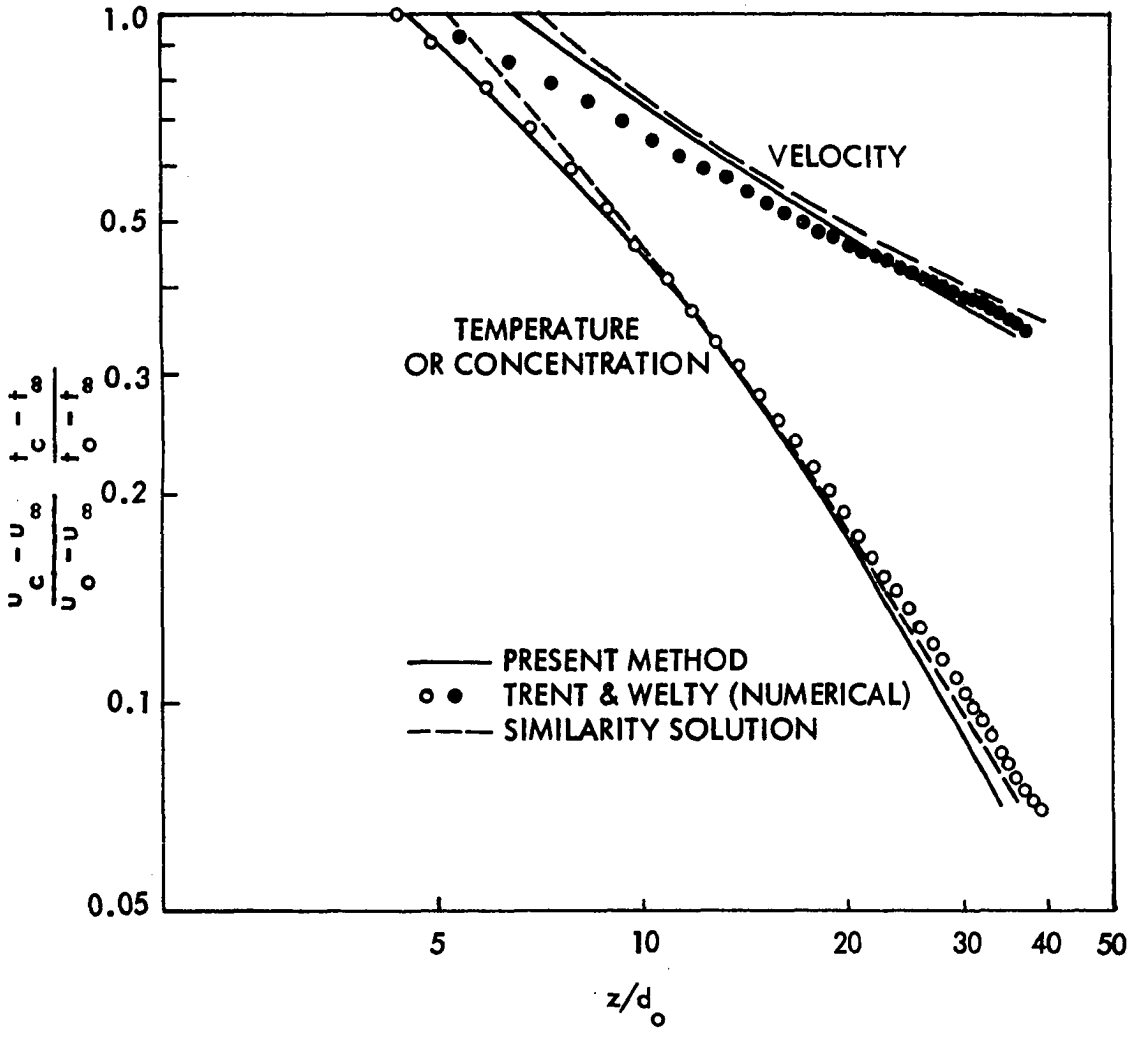

Fig. 5.3. Decay of centerline values for Fr_o=35; buoyant vertical jet in uniform ambient.

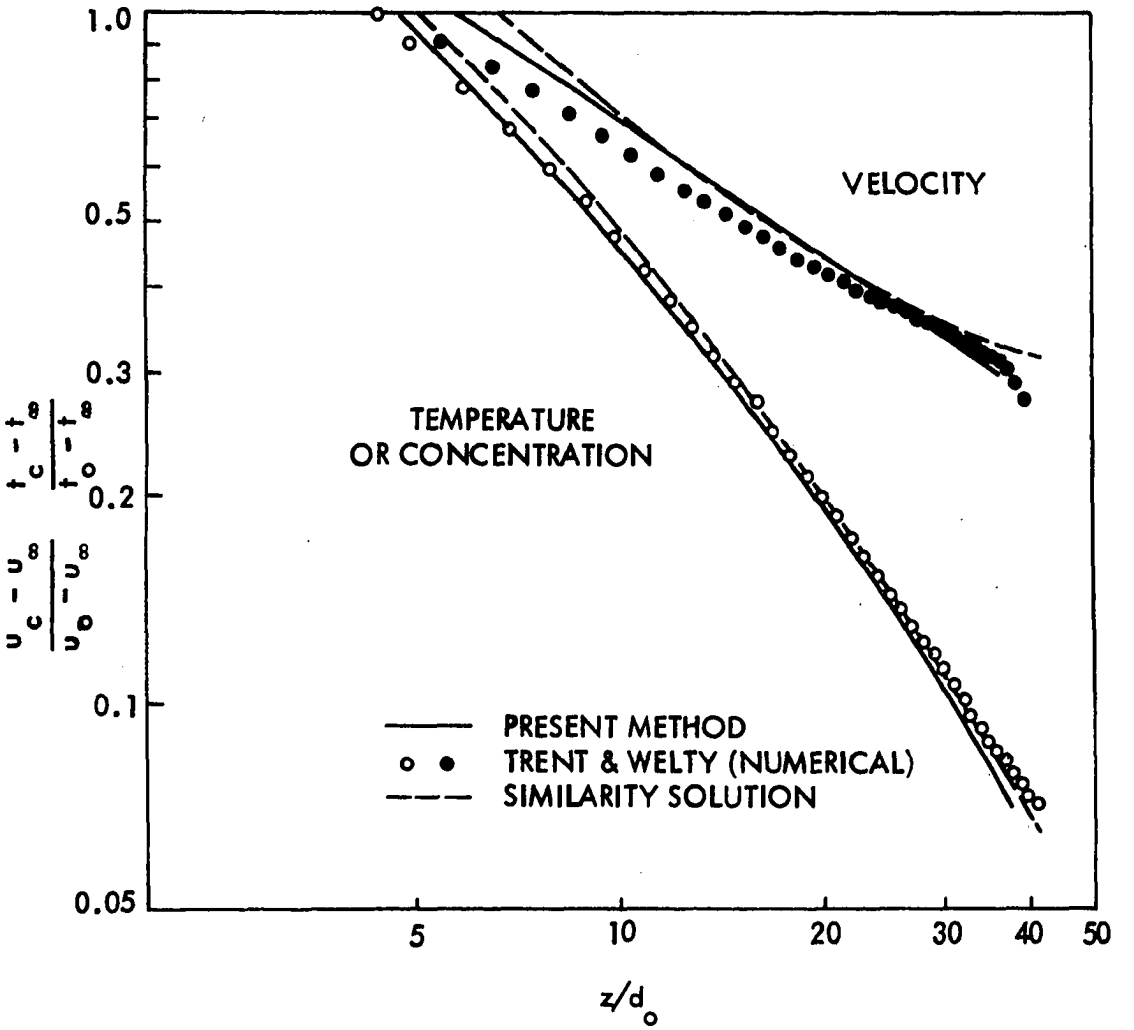

Fig. 5.4. Decay of centerline values for Fr_o=52; buoyant vertical jet in uniform ambient.

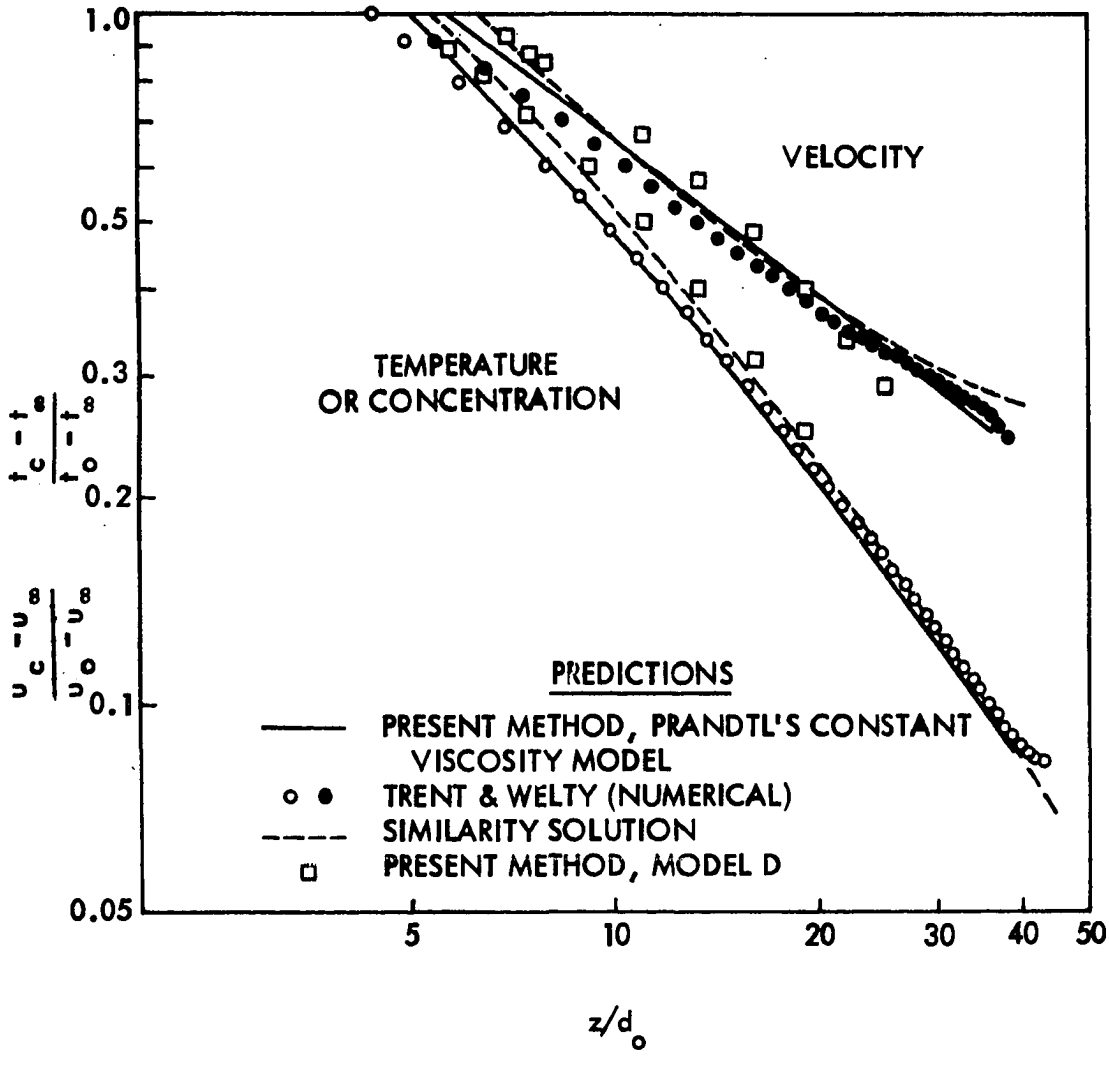

Fig. 5.5. Decay of centerline values for Fr_o=106; buoyant vertical jet in uniform ambient.

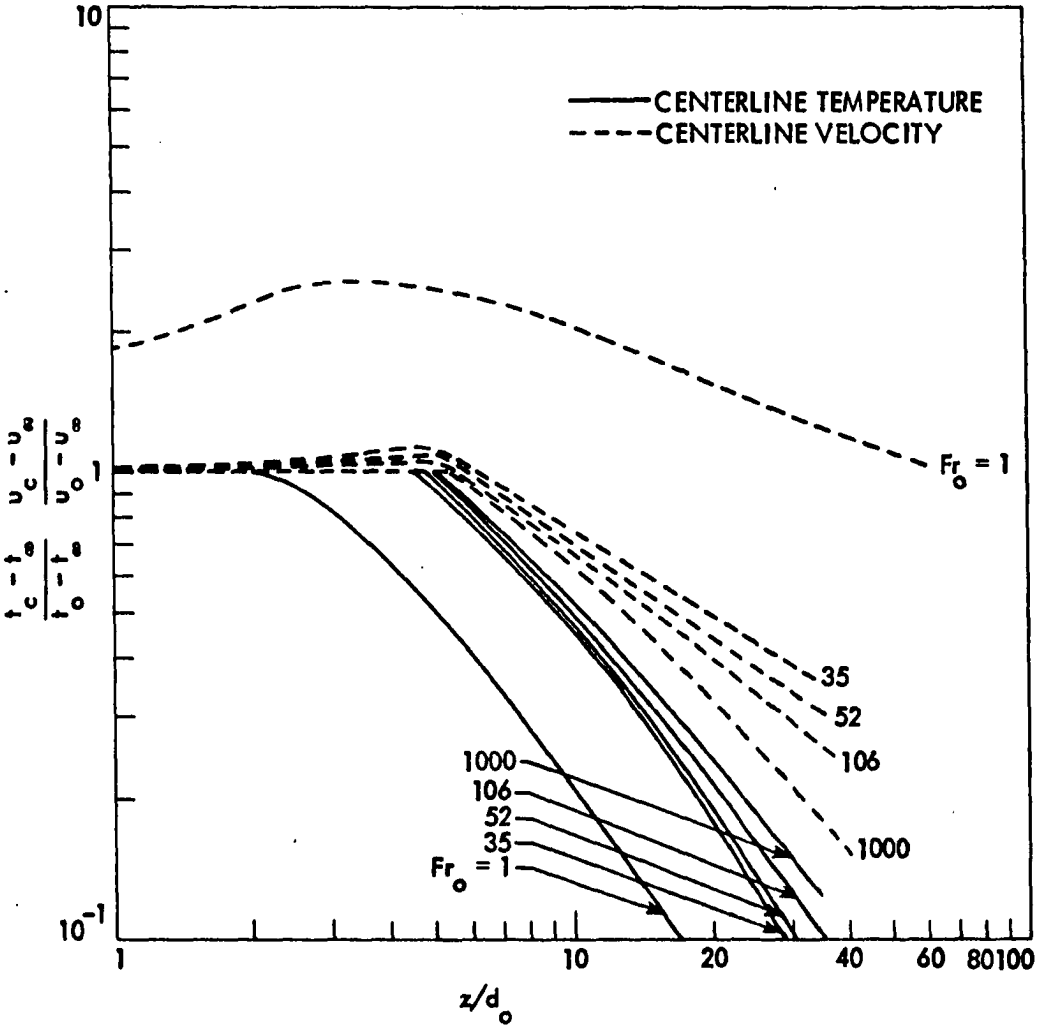

Fig. 5.6. Predicted effect of Fr_o on decay of centerline velocity and temperature; vertical buoyant jet or plume in uniform ambient.

represents approximately the whole gamut of flows ranging from high buoyancy ($Fr_o \to 0$) on one end to high initial momentum ($Fr_o \to \infty$) on the other. Since the jet is accelerated due to buoyancy the centerline velocity initially increases over its discharge value. For $Fr_o = 1$, the high-buoyancy case, this increase is seen to be almost 250%. The seemingly strange behavior of starting length seen in Abraham [69], i.e. concentration starting length decreasing with decreasing Fr_o, while velocity starting length (if based on centerline velocity beginning to decay below its discharge value) increasing, can be explained from Fig. 5.6. Buoyancy causes jet velocity to increase steadily beyond its discharge value, and so when mixing has reached the centerline and centerline concentration beings to decay, the centerline velocity is still above its starting value. And, with decreasing Froude number, this buoyancy force is greater relative to the jet inertia, causing greater acceleration of the jet, hence a greater velocity increase, requiring a larger distance for the velocity to return to the discharge value. However, if velocity starting length is based on the distance to where velocity starts decaying from its maximum value, it is not much different from the concentration value. This also clarifies Abraham's statement [69] that "experiments show the difference between s_ℓ (velocity) and s_ℓ (concentration) to be of the order $1\text{-}2d_o$."

Figures 5.7 to 5.10 compare the predictions of the present method with experiment. In Fig. 5.7, predicted centerline decay values of velocity and concentration for $Fr_o = 1$ are compared with the experimentally confirmed slopes of Rouse et al. [71] for $Fr_o \to 0$. Agreement is excellent. Figures 5.8 and 5.9 show centerline temperature comparisons

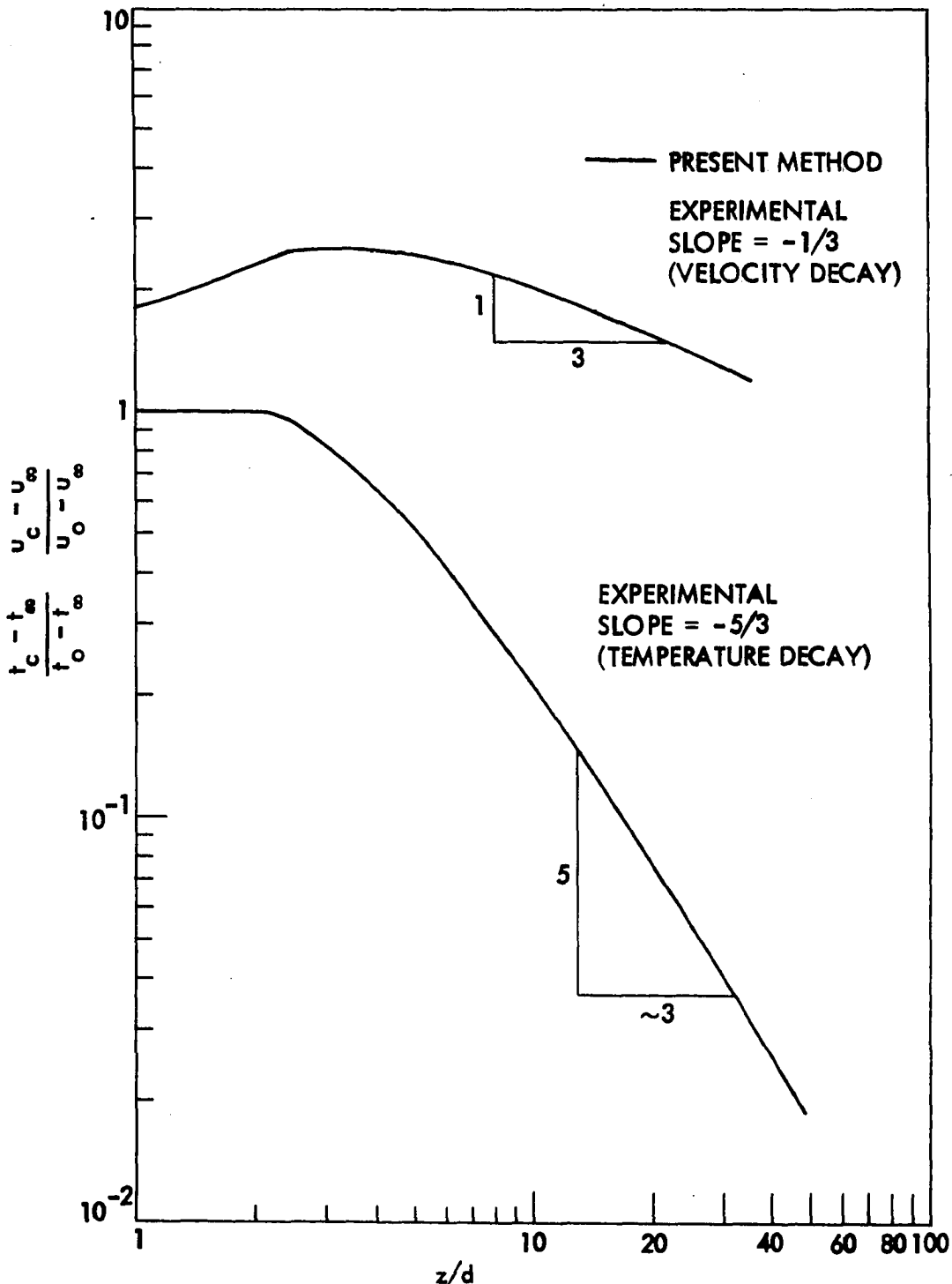

Fig. 5.7. Comparison of predicted slope of centerline decay with experimentally confirmed slope [Rouse et al.]; vertical buoyant plume, $Fr_o = 1$, uniform ambient.

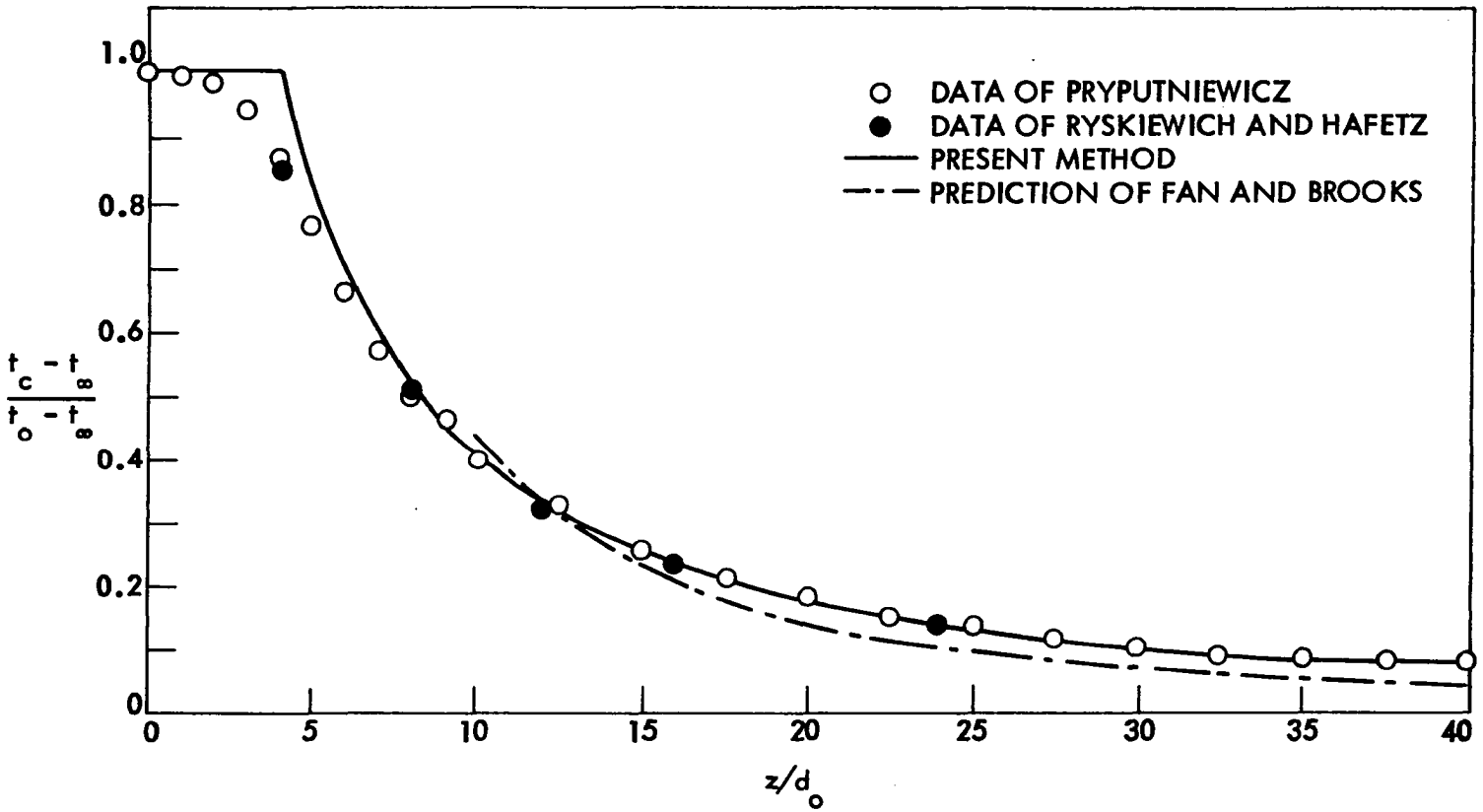

Fig. 5.8. Centerline temperature comparisons for $Fr_o = 16$; buoyant vertical jet in uniform ambient.

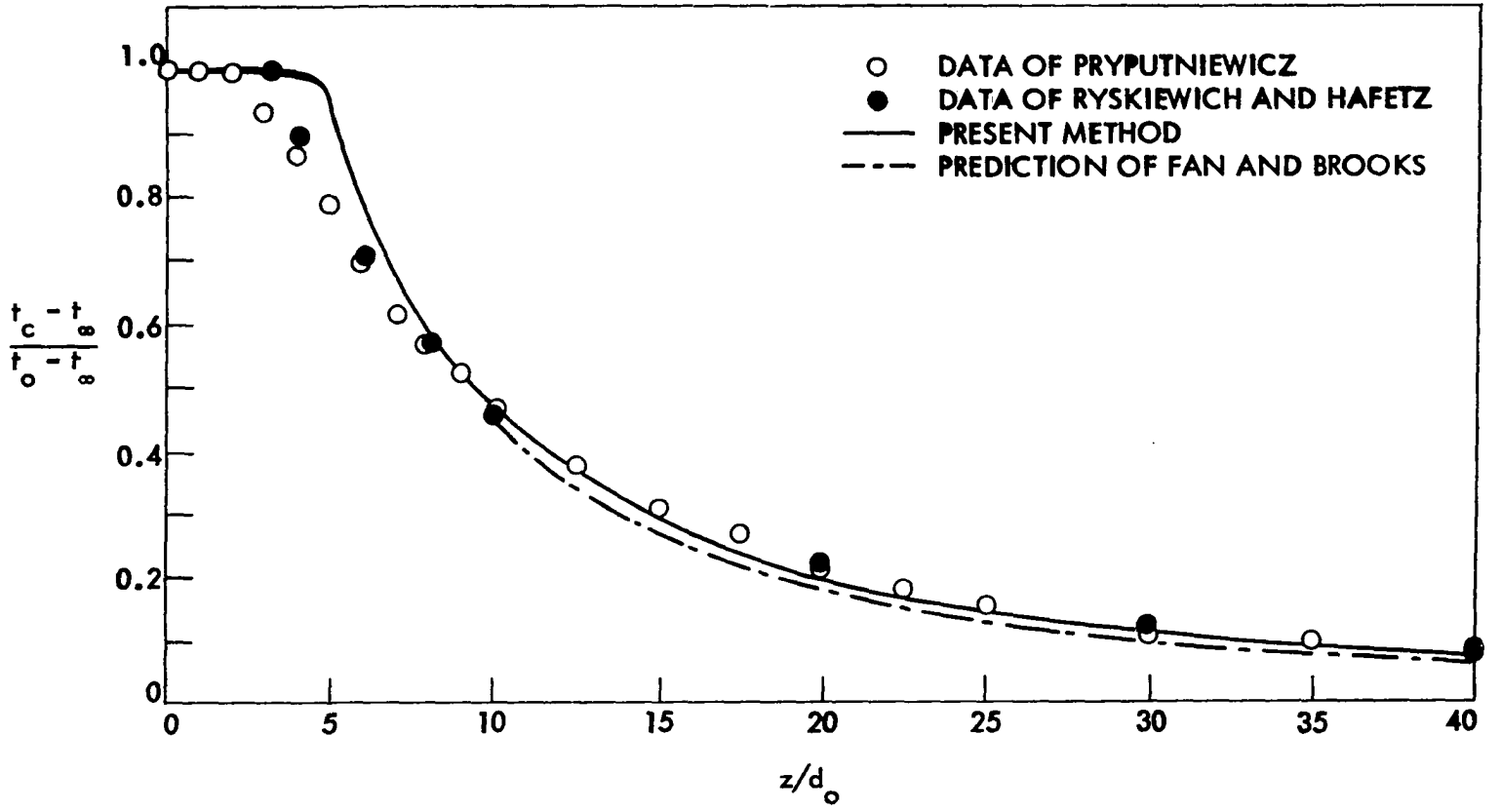

Fig. 5.9. Centerline temperature comparisons for $Fr_o = 64$; buoyant vertical jet in uniform ambient.

using the present method with the experimental data of [28] and [72] for Fr_o = 16 and 64, respectively. Agreement is very good. The predictions of Fan and Brooks in [16] are also included for added comparison. Figures 5.10a to 5.10e indicate more comparisons for Fr_o = 1,4,256,625, and 2500. There is a slight tendency to underpredict the $Fr_o \to 0$ case and overpredict the $Fr_o \to \infty$ case, suggesting that buoyancy may serve to increase the effective viscosity slightly. Also, the data of Pryputniewicz [28] seem to indicate shorter starting lengths, especially at higher Froude numbers. Overall, however, agreement is excellent, and the model used is seen to be quite good despite its simplicity. Reference to Launder and Spalding [35] and other works indicated that even the more complicated models of turbulence needed additional terms to account for buoyancy effects. Hence, some attempts were made in the present work to incorporate such an effect in the transport model in terms of an inverted Froude number [3]. The small effects for this configuration, however, were not seen to be significant enough to justify complicating the model and thereby increasing the computation time involved. A more exhaustive investigation into this might include a consideration of the effects of the Richardson number (Ri). However, comparisons should be made with additional experimental data before the slight discrepancy between predictions and experiment is attributed solely to the effects of buoyancy (Ri) on the turbulent viscosity for this configuration.

Before the experimental data of [28] and [72] became available, the most detailed results were those of Frankel and Cumming [70]. Abraham [13] and later Pryputniewicz [28] seem to discount the validity of these

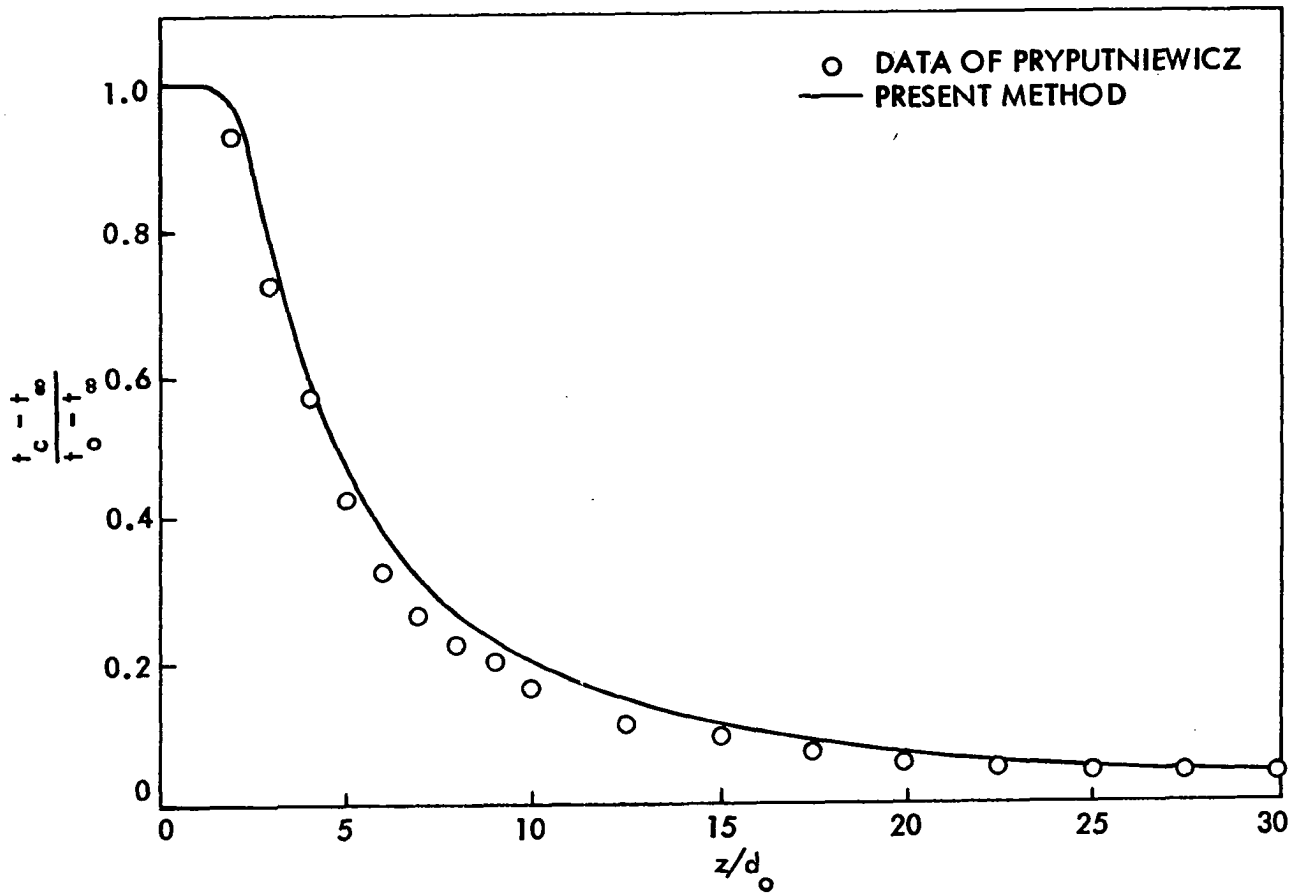

Fig. 5.10a. Predicted and experimental decay of centerline temperature for $Fr_o = 1.0$; buoyant vertical jet in uniform ambient.

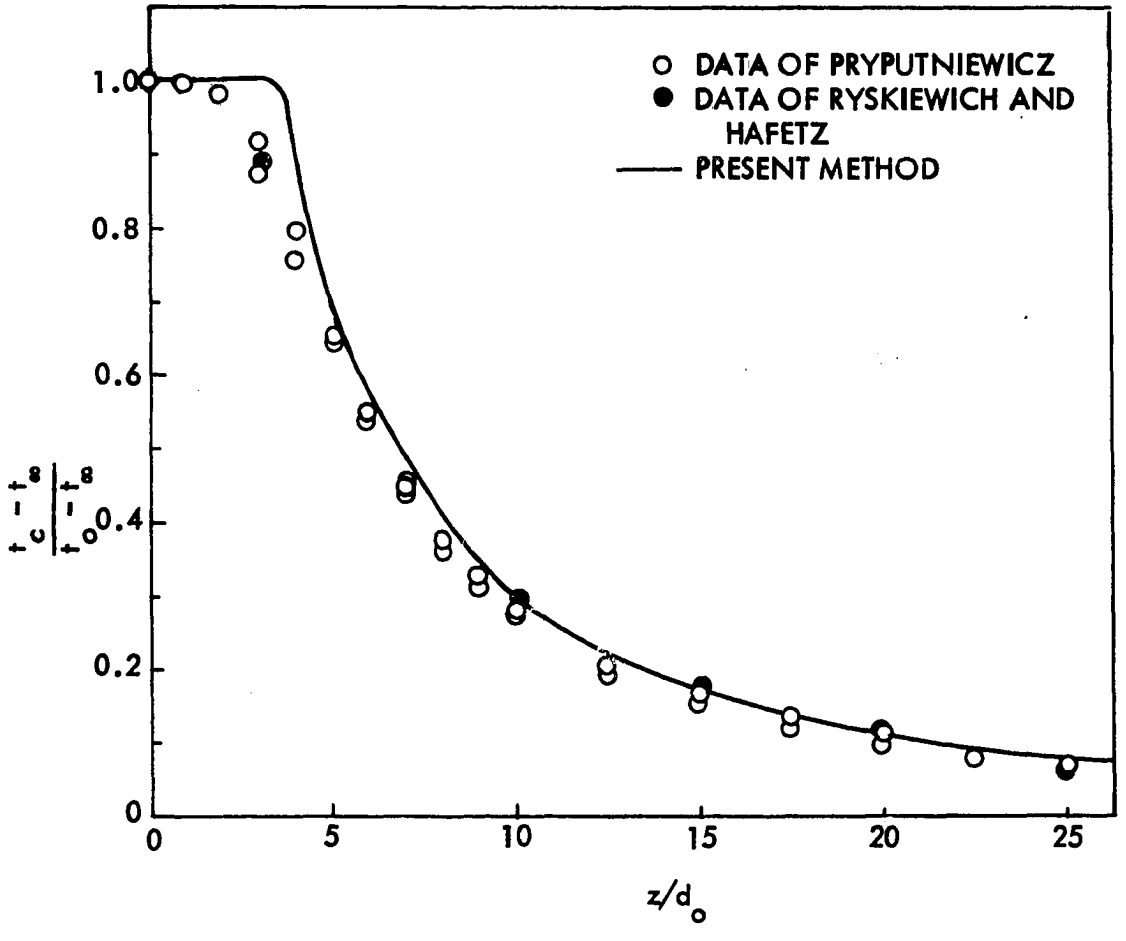

Fig. 5.10b. Predicted and experimental decay of centerline temperature for $Fr_o = 4.0$; buoyant vertical jet in uniform ambient.

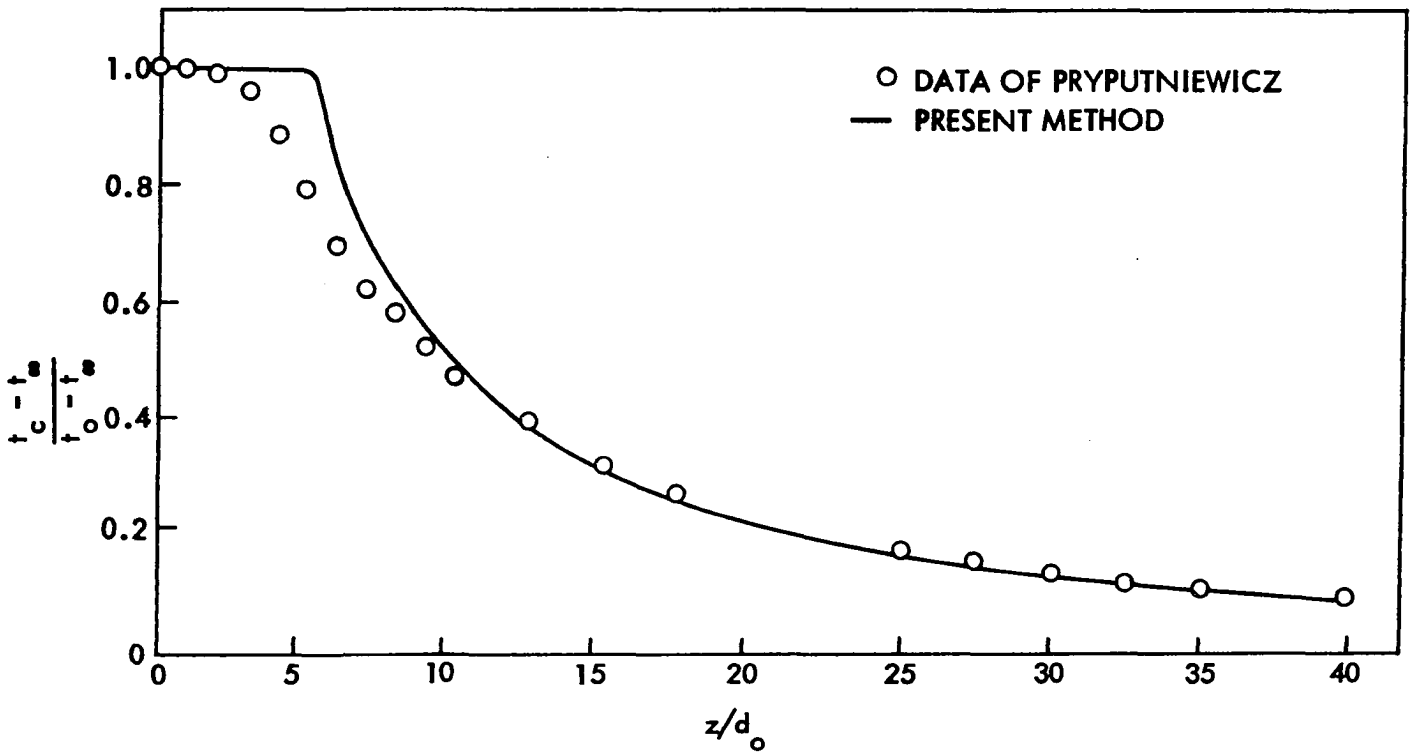

Fig. 5.10c. Predicted and experimental decay of centerline temperature for Fr_o = 256; buoyant vertical jet in uniform ambient.

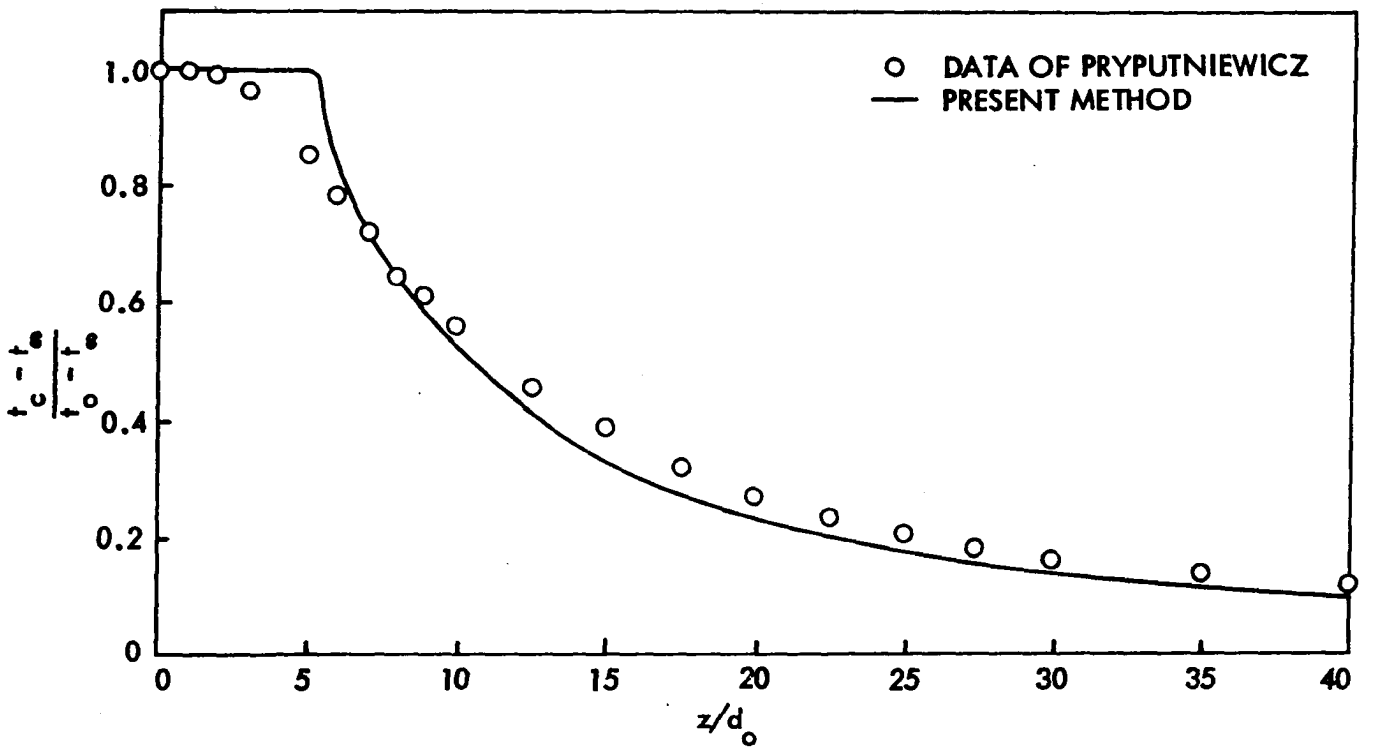

Fig. 5.10d. Predicted and experimental decay of centerline temperature for Fr_o = 625; buoyant vertical jet in uniform ambient.

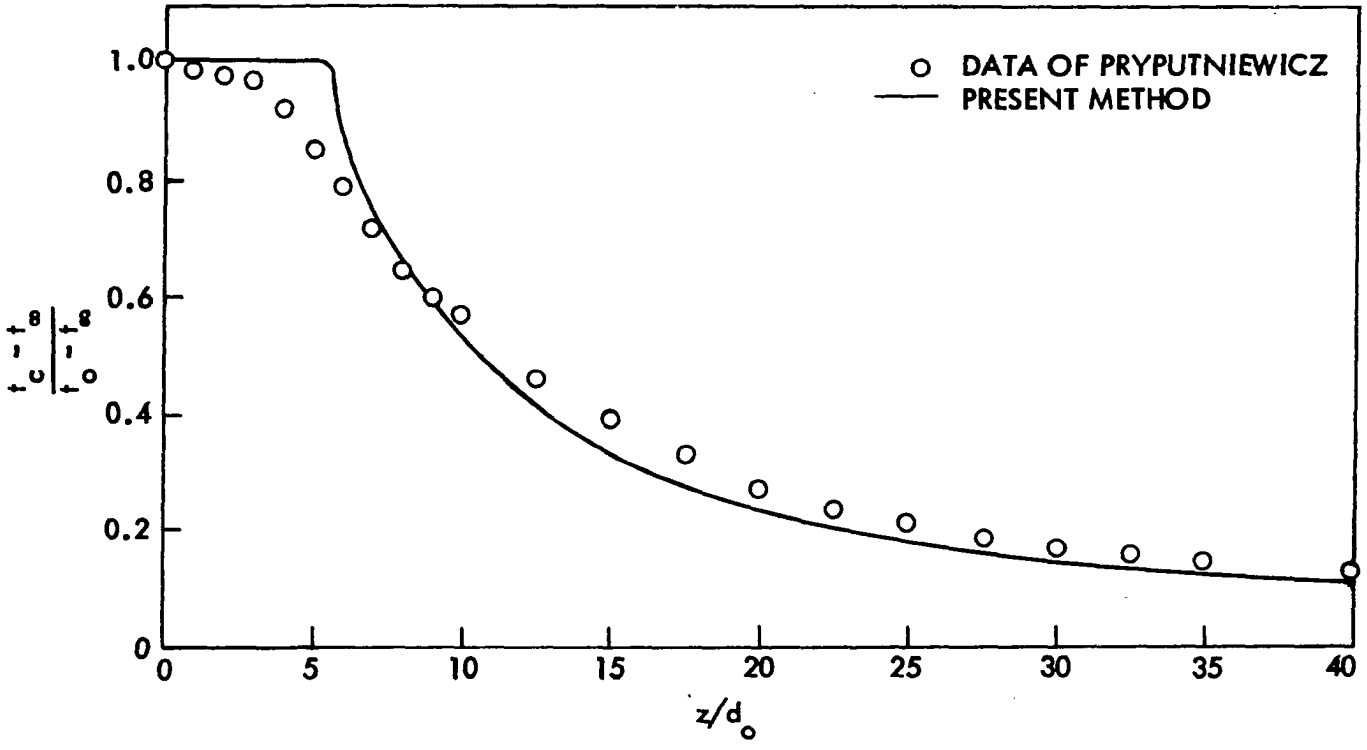

Fig. 5.10e. Predicted and experimental decay of centerline temperature for Fr_o = 2500; buoyant vertical jet in uniform ambient.

data since they were not obtained under steady state conditions.

According to Briggs [84], for two buoyant plumes to be similar, their Froude numbers must be the same. Re_o is assumed high enough not to affect the similarity, and the flow is considered turbulent from the start (see Chapter 2). Froude's similarity law is also mentioned in Hart [77] who, in fact, designed his model experiments to represent the prototype, according to this law. Pryputniewicz [28] experimented with different parameters, keeping Fr_o the same, and found the law to be valid. Figure 5.11 shows the result when the present formulation was applied to confirm this law. The results are seen to be excellent.

In Figs. 5.12 and 5.13, centerline plume temperature is compared to the theoretical predictions of Pryputniewicz [28] and Trent [75]. The former has used a degenerate form of Hirst's integral equations in the main region and Robidue's results [85] in the initial region as the starting point, while the latter has employed a finite-difference method. Experimental data is included as a basis for comparison. Overall, the results of the present method are seen to agree most favorably with experiments over the range of Froude numbers presented, and the results of Pryputniewicz based on Hirst's method seem to be better than those of Trent.

It is interesting to note that the experimental results in Figs. 5.12 and 5.13 were for discharge depths of $H/d_o = 40$ and 80, respectively. The predictions are good for both cases. This brings the question as to how far the present analysis would be valid in case of relatively shallow discharge where surface effects come into play. The effect of water surface is essentially to retard reduction of the plume temperature in

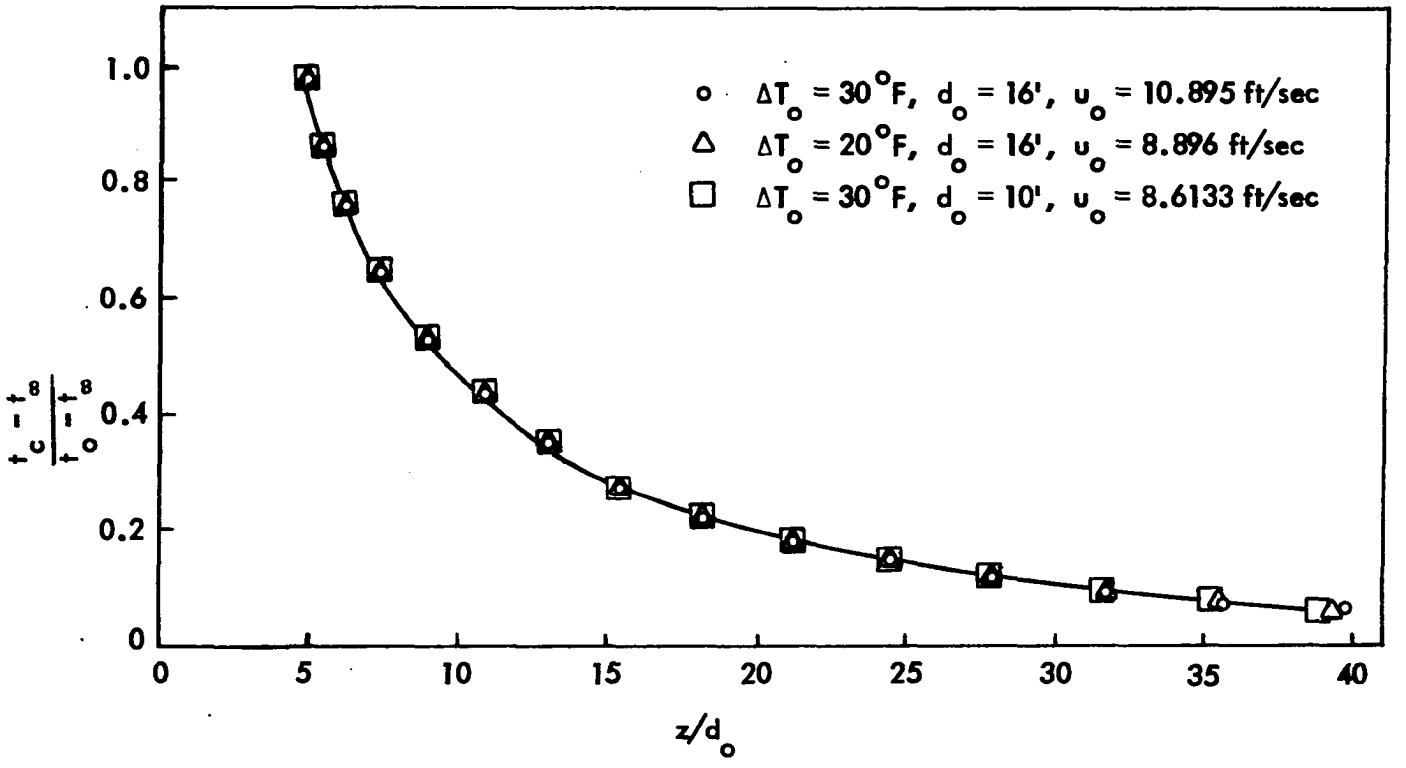

Fig. 5.11. Froude's similarity law at $Fr_o = 64$; buoyant vertical jet in uniform ambient.

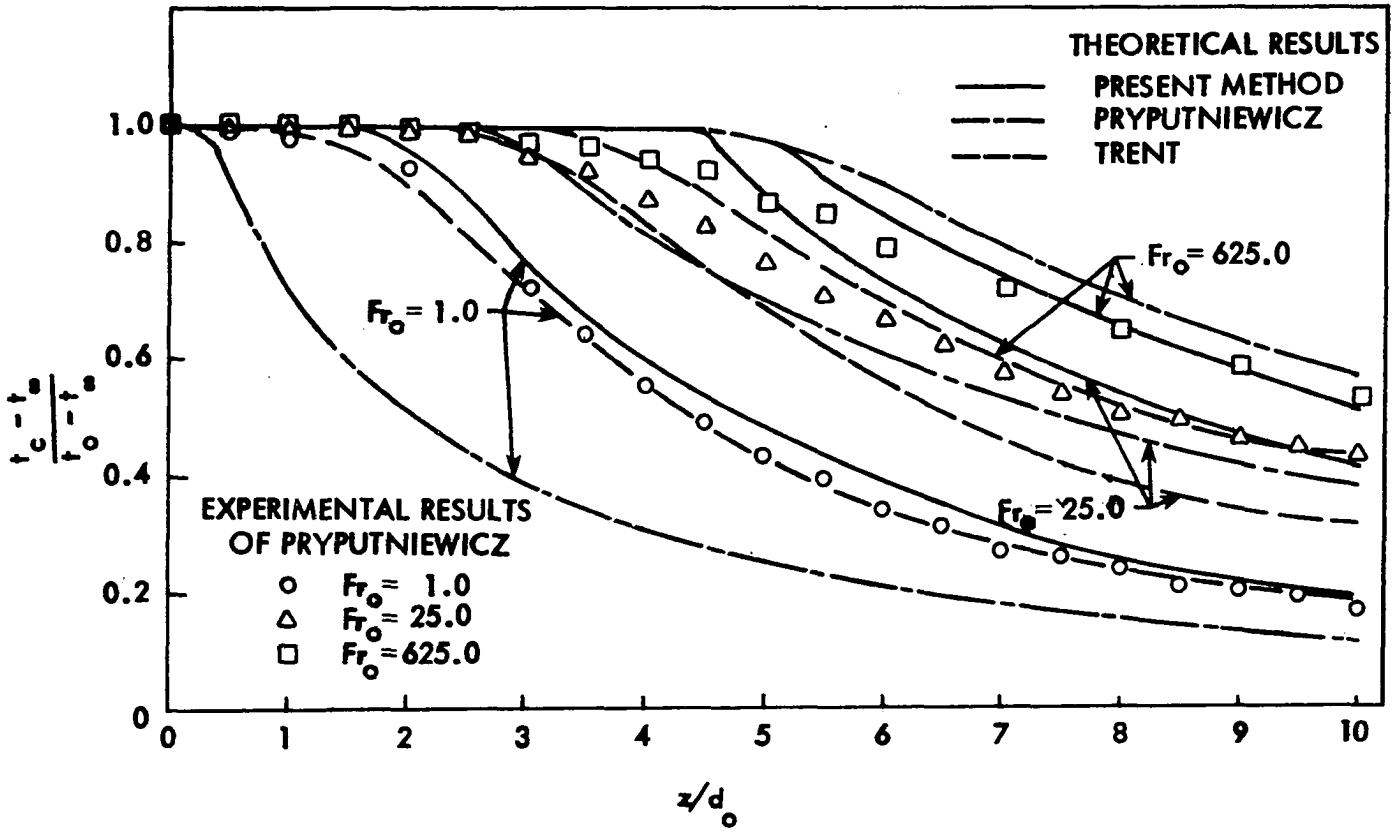

Fig. 5.12. Comparisons with experimental and theoretical results; buoyant vertical jet in uniform ambient.

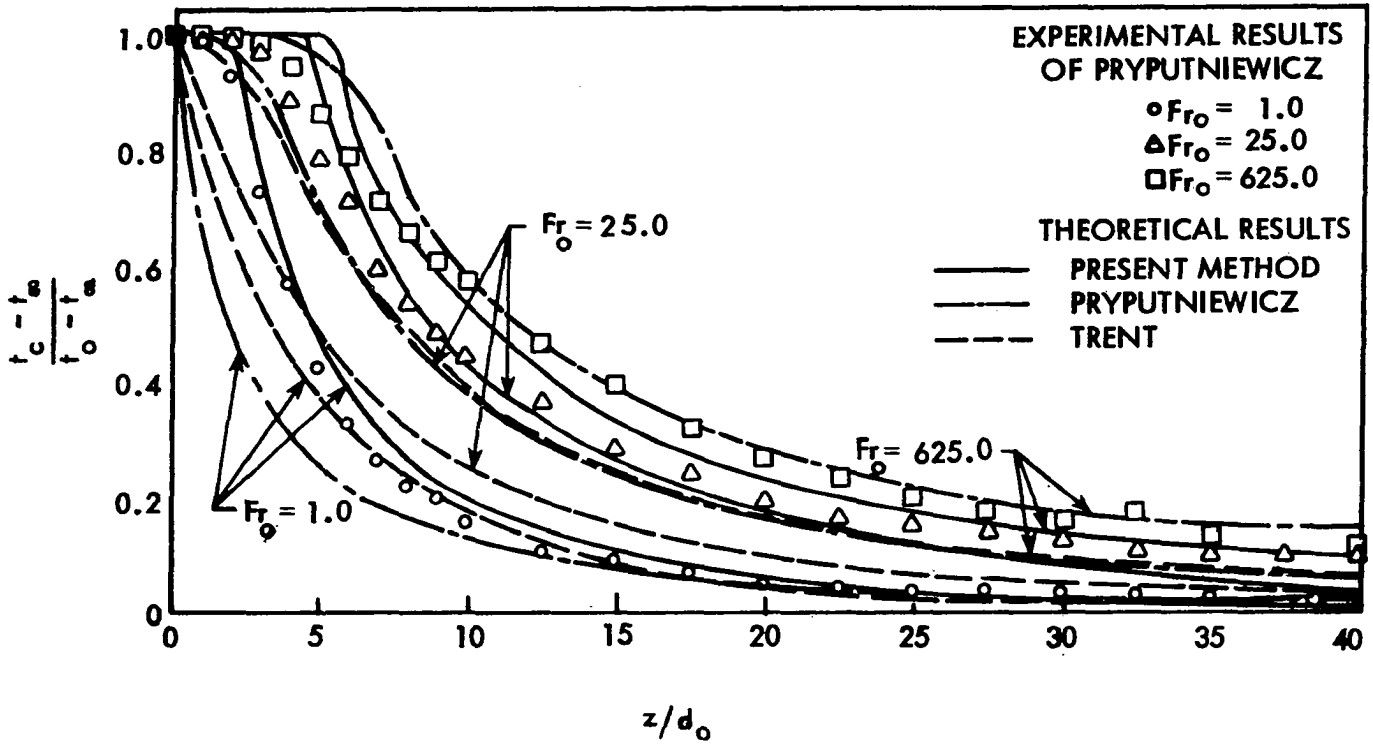

Fig. 5.13. Comparisons with experimental and theoretical results; buoyant vertical jet in uniform ambient.

the vicinity of the surface [72]. Robidue in his report [85] introduced the concept of an "effective depth." The effective depth was defined as that height above the jet discharge beyond which the plume experiences no further entrainment and continues to the surface with its temperature unaffected. Thus, the jet behaves as a free jet within this depth. Pryputniewicz [28], and Ryskiewich and Hafetz [72] experimentally examine the effect of discharge depth on centerline temperature decay. The conclusion from the former is that the rate of centerline decay is relatively independent of the discharge depth for Fr_o below 256. According to the latter, the same conclusion holds for Fr_o as high as 900. In their experiments, which were carried out for flows with discharge depths ranging from H/d_o = 10 to 80, and for a wide range of Fr_o, the effective depth was found to be 92-93.5% of total depth for Fr_o as high as 900, i.e. the results are relatively independent of discharge depth up to that value of discharge Froude number. This provides an idea of the range of Fr_o values over which the present method can be used to predict shallow water discharges.

In a typical ocean outfall configuration for a 1000 MW unit (nuclear or fossil), the discharge Froude number would range between 50 and 100, well within the range of applicability of the present analysis. These values are based on the numbers given in [2].

In general, the present analysis can also be used to give an estimate of excess temperature at the surface by calculating as usual up to effective depth, and allowing the plume excess temperature to remain constant above that height. By excess temperature here is meant

the difference between maximum (or centerline) plume temperature and the local surrounding temperature.

5.6.2. Stratified ambient

The same turbulence modeling was employed for the stratified ambient analysis as well. The zero buoyancy height was predicted for several cases. These are shown compared to predictions based on the theory of Fox [82] in Fig. 5.14. It is worthy of note that the Fox theory agrees well with the experiments of Sneck and Brown [82] in air for modest z_M/r_o, but for liquids, Fox's experiments and those of Abraham provide evidence of its applicability for high z_M/r_o only. In addition, the parameters in Fig. 5.14 were derived by Sneck and Brown based on the formulation for Froude number as

$$Fr = \frac{u_o^2}{\Delta g r_o} \qquad \text{where} \qquad \Delta = \frac{\Delta t_o}{T_{o,a}}$$

For air, since $\frac{\Delta t_o}{T_{o,a}} \approx \frac{\Delta \rho_o}{\rho_o}$, this is equivalent to the conventional definition, i.e. $Fr_o = \frac{u_o^2}{2gr_o\left(\frac{\Delta \rho_o}{\rho_o}\right)}$. However, for water, $\frac{\Delta t_o}{T_{o,a}} \neq \frac{\Delta \rho_o}{\rho_o}$, and this difference reduces in significance at high discharge Froude numbers where $\frac{\Delta \rho_o}{\rho_o}$ is very small, i.e. when z_M/r_o is high.

With this background, it is easy to see why when a case with water was tried corresponding to $\frac{r_o G}{\Delta g} = 0.4 \times 10^{-1}$ and $G\left(\frac{u_o^2}{\Delta g}\right) = 0.1$, the predicted z_B/r_o was almost twice that obtained from Fig. 5.14.

Table 5.1 presents the predicted results for maximum height of rise compared to the experimental data of several investigators cited in [9]. Agreement is seen to be favorable. The discrepancy between the Fox

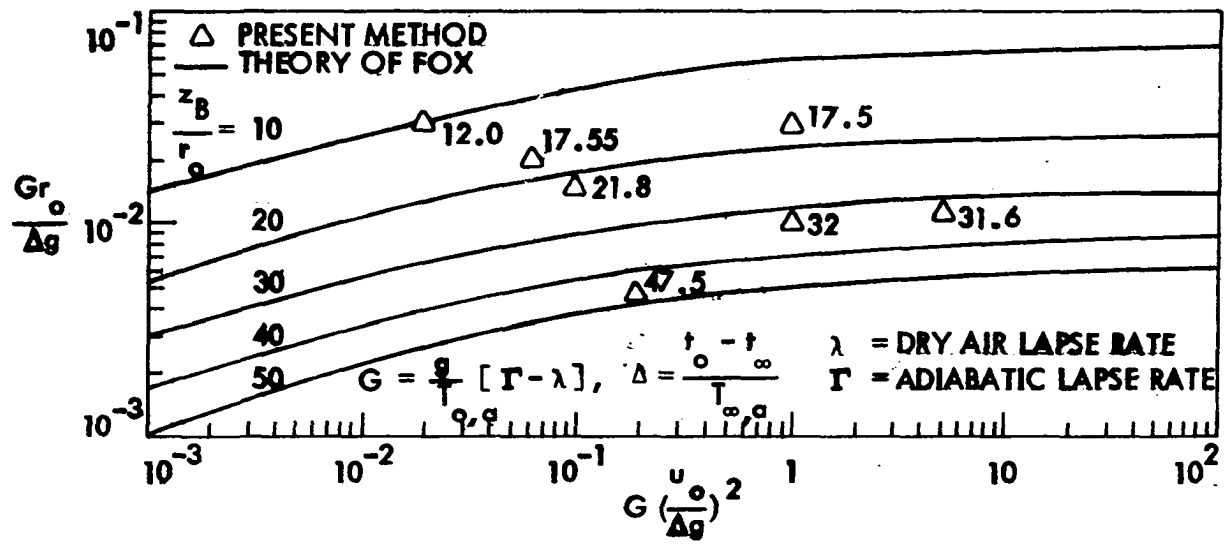

Fig. 5.14. Zero buoyancy plume height; vertical plume in stratified ambient.

Table 5.1. Maximum height of rise for vertical plumes into stratified ambients.

No.	Discharge Froude Number, Fr_o	Stratification Parameter, $\bar{T}$		z_M/r_o Measured	z_M/r_o Predicted: Present Method	z_M/r_o Predicted: Fox Theory
1	54.5	83		61	61.2	35
2	50.5	141	Abraham &	74	72.7	50
3	69	94	Eysink	64	65	44
4	605	134		68	72.5	49
5	324	205	Fan	86	105	72
6	63	1586	Fox	104	115	--

Table 5.2. Maximum height of rise for vertical plumes into stratified ambients.

No.	Discharge Froude Number Fr_o	Stratification Parameter, $\bar{T}$	z_M/r_o Predicted: Fox Theory	z_M/r_o Predicted: Present Method
1	17.199	33.3	33.3	36.6
2	0.344	33.3	18.0	18.0

theory and experiment for modest z_M/r_o (the results of Abraham and Eysink) is difficult to explain but could be attributed to the reasons cited earlier. Time and resources have not to date permitted extension of these calculations for higher values of Fr_o. However, it is felt that the calculations described in this chapter cover the Fr_o range of most practical interest. It is to be noted that the predictions of Fox are seen to agree closely with his own experiments for high Froude number jet flows [80]. Also, there is good agreement between the experiments in [82] in air for modest z_M/r_o, and the Fox theory. This is also corroborated in Table 5.2, where results of the present analysis for air at modest z_M/r_o compare well with the predictions of Fox.

Further comparisons of maximum height of rise are indicated in Fig. 5.15, where the predictions of the present method and those of Hirst [9] are plotted against experiment. Hirst has made a more extensive comparison with experiment than indicated in Fig. 5.15, and only the region of overlap with the range of z_M/r_o contained in Table 5.1 has been included in Fig. 5.15.

Figure 5.16 shows results of a sensitivity analysis to see if assuming an edge velocity = 5% of jet velocity for quiescent ambients causes deviation in the results. To this end, the analysis was carried out individually for U_{edge} = 7%, 5%, 3%, and 1%. The effect is seen to be minimal, and extrapolating to give the values of z_M/r_o and z_B/r_o corresponding to $U_{edge} = 0$, showed a deviation of less than 2%, which is very small.

It is understandable that boundary layer assumptions and assumptions of similarity (common to integral methods) would be of questionable

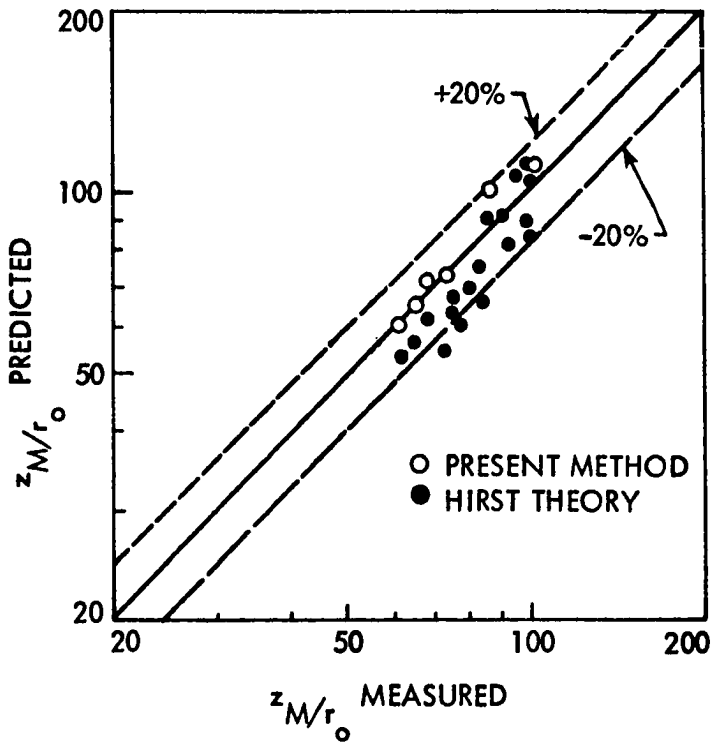

Fig. 5.15. Maximum height of rise for vertical plumes discharged to stratified ambients.

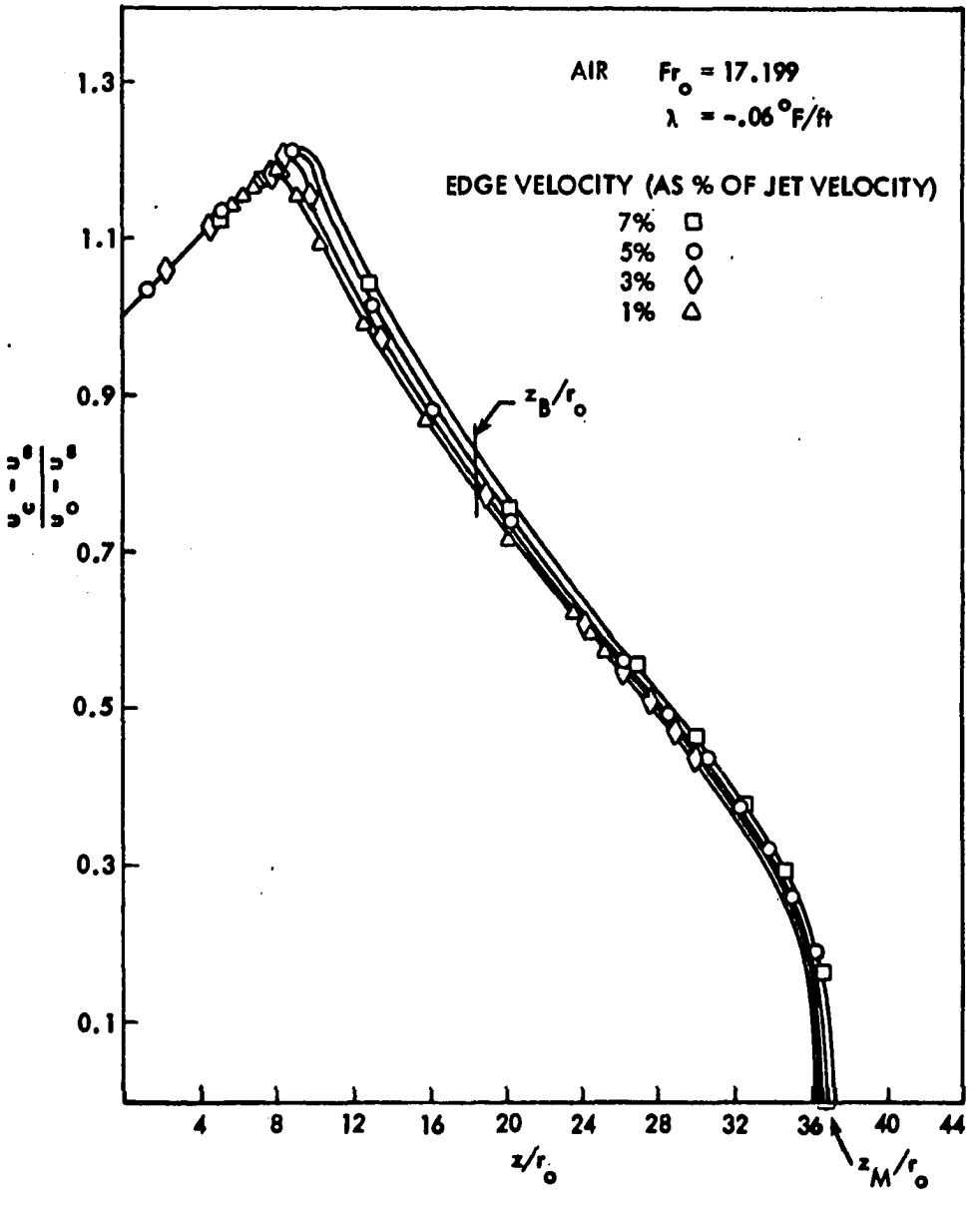

Fig. 5.16. Predicted centerline velocity decay, zero buoyancy height, and zero momentum height for several values of prescribed edge velocity; buoyant vertical jet into stratified ambient.

validity in the region of negative buoyancy for the stratified ambient problem. In the differential approach, it is expected that a transverse momentum equation would be needed to get more accurate predictions of the flow field here. Interestingly, however, the present analysis was carried to zero momentum height using boundary layer assumptions, with good results. The computer printout also showed the transverse velocity to be in the outward direction, which corresponds to the negative entrainment hypothesis. One reason for the success of the present analysis in this region of flow might be that the bulk of the spreading occurs after the fluid has reached the ceiling height, z_M, and then flows down around the upflow in a cascade, to settle and spread at a lower level of neutral buoyancy [80,82].

5.7. Some Numerical Aspects

The formulation was basically the same as for the non-buoyant jet (see Chapter 4), but the following differences deserve specific mention:

i. The momentum equation now had a buoyancy term and was therefore coupled to the energy equation. The velocity profile was therefore not independent of the temperature solution.

ii. In the case of stratification, the ambient temperature varied, providing a variable boundary condition.

iii. Most of the cases in Chapter 4 involved both jet and ambient moving in the same direction. Here, all calculations were for ambient

at rest, hence the solution could easily become unstable, unless a stability criterion was carefully derived and some novel techniques applied to keep the calculation scheme economical to use. Thus, attention was focused on refining both the method and stability criterion to allow the solution to proceed without oscillations and with optimum step-size.

At first, application of the D-F method to this problem produced oscillations in both temperature and velocity profiles shortly after starting length. These oscillations started at the edge, began spreading inward, and went rapidly out of control. When the calculation was allowed to continue, this was followed by a separate oscillation phenomenon originating close to the plume centerline and spreading outward.

The mild stability restriction observed when the D-F scheme is applied to laminar boundary layer flow [44,86] i.e.

$$\left| \frac{\Delta S_+ V_{i,j}}{\Delta Y\, U_{i,j}} \right| \leq 1 \qquad (5.16)$$

was found to be quite ineffective for the problem being investigated. The check was made more severe as follows:

$$\left| \frac{\Delta S_+ V_{i,j}}{\Delta Y\, U_{i,j}} \right| \leq 0.5$$

Oscillations were reduced somewhat, but still remained troublesome.

The "high-lateral-flux" modification of Chapter 4 was first removed from the UVEL subroutine, and then put back again, together with a

similar modification in the TEMP subroutine. The effect, if any, was not observable. The cause seemed to be elsewhere.

When these operations were supplemented by a restriction on stepsize growth, oscillations sometimes appeared to diminish, and at other times remained unaffected. The investment in reduced stepsize by the addition of this operation did not appear very rewarding.

Other adjustments, including the stability analysis of Karplus [68] which requires all coefficients in the difference equation when written in a certain way, to be positive, were incorporated in turn, but the oscillations remained.

A more thorough look at the Von Neumann stability analysis seemed indicated. This was done, and a new stability restriction incorporating the lateral difference in effective viscosity was derived:

$$\Delta S_+ \leq \min_{j=2,NY} \left[\frac{U_{i,j} \Delta Y}{\left| V_{i,j} + \frac{\left(N_{i,j-1} - N_{i,j+1}\right)}{2\Delta Y} \right|} \right] \tag{5.17}$$

A startling change became evident, as oscillations became negligible in some cases, and tended to diffuse and damp out in others. It was felt that, with subsequent refinement, this promised to be the cure to the instability problem.

The refinement consisted of including the lateral difference of effective conductivity also, so that

$$\Delta S_+ \leq \min_{j=2,NYJ} \left[\frac{U_{i,j} \Delta Y}{\left| V_{i,j} + \frac{FUNC}{2\Delta Y} \right|} \right] \tag{5.18}$$

where NYJ = max (NY, NYT) and

$$\text{FUNC} = \max\left[\left(N_{i,j-1} - N_{i,j+1}\right), \left(N_{H_{i,j-1}} - N_{H_{i,j+1}}\right)\right]$$

More details on the stability analysis are given in Appendix E.

Further, the turbulent viscosity and conductivity profiles were allowed to extend up to (NYJ + 2) i.e. 2 grid points beyond the jet boundary. This reduced the value of FUNC at the edge and allowed greater economy of computer time. A final touch of refinement to the method was given when a consistency check, limiting the difference between two successive streamwise step sizes, was provided.

The method is fast, and allowable step sizes (except for $Fr_o \to 0$ cases), are as high as 6-7% of the mixing layer width δ. In comparison, the implicit method of Patankar and Spalding allows 2% of δ [87]. A comment worth making is that, in general, the stability restrictions using the explicit method for the jet flow are far more severe than for the wall boundary layer, especially as $R \to 0$. This can be seen upon examining Eq. (5.18). (A similar form could be derived for wall-boundary layers). Close to the wall, even though $U_{i,j} = 0$, so is $V_{i,j}$ (except for flows with transpiration). In contrast, at the edge of the jet flow, even though $U_{i,j} = 0$ for quiescent ambient, a finite entrainment velocity $V_{i,j}$ exists. This could be one reason why stability problems were not encountered when the D-F scheme was applied to wall boundary layer flows [36] and confined flows [38]. An edge velocity $\simeq$ 5% of jet velocity was found to be adequate to speed up the computation. (The sensitivity analysis presented previously showed no significant error in results due to this operation.)

The method, refined as described above, was now free from problems

of instability, and was successfully used, without further modification, to solve past the zero buoyancy height and into the region of negative buoyancy for the problem of the vertical plume discharging into a stratified ambient.

6. THE HORIZONTAL OR INCLINED BUOYANT JET IN A QUIESCENT AMBIENT

Attention is now directed to the configuration in which the jet or plume follows a curved path. The aim and main challenge of a curved jet calculation is to predict the jet trajectory along with estimates of the flow properties. These results are then compared to available experimental data, and the results of other prediction methods wherever possible. Cases investigated were the buoyant jet discharging horizontally and at 45^{o} to the horizontal into a uniform, quiescent ambient.

6.1. Introduction

The most obvious practical application of this configuration is in the submerged, offshore outfalls from power plants. In more recent outfall construction it has been the practice to orient the ports so that the effluent is issued horizontally into the receiving water [1]. Compared with a buoyant vertical jet, a horizontal one undergoes greater dilution and thus greater cooling on its way to the surface [42,1]. A clear illustration of this can be obtained by looking at the experimental data of [72]. However, for most rapid mixing and dispersion of the effluent, an inclined discharge at 45^{o} to the horizontal might be preferred [10]. Choice of the discharge configuration would also depend on the exact requirements of the water quality standards at the proposed site of the power plant.

The characteristic of jets that issue horizontally or inclined to the horizontal into denser ambient fluid is that they follow a curved trajectory as they rise upwards due to buoyancy forces. They have been

experimentally studied by Cederwall [27], Bosanquet et al. [88], Frankel and Cumming [70], Anwar [89], Fan [16], and most recently, by Ryskiewich and Hafetz [72]. Bosanquet and Fan measured centerline trajectories; Frankel and Cumming measured the centerline concentration, but Anwar, and Ryskiewich and Hafetz measured both centerline trajectories and concentration (or temperature in case of Ryskiewich) for horizontal and inclined jets at different discharge Froude numbers. The study of Ryskiewich and Hafetz is probably the most complete of these, where they have also considered the vertical configuration and free surface effects. These measurements show that the jet rises more sharply for a smaller discharge Froude number.

The vertical jet experiments of Frankel and Cumming showed deviation from published experimental and theoretical data on vertical jets [28,69]. Abraham [13] observes that since similar deviation is exhibited between the horizontal jet experiments of Frankel and Cumming, and the experiments of Cederwall [27], he tends to agree with the results of the latter.

Theoretical analyses for the prediction of buoyant jets discharged to a quiescent medium can be found in Abraham [13], Bosanquet et al. [88], Fan [16], Anwar [89], and Hirst [9]. The approaches are all integral in nature. More recently, Chan and Kennedy [41] obtained closed form solutions restricted to the momentum-dominated regions of horizontally discharged submerged jets in infinite, uniform ambients, using one more assumption in addition to those common to integral methods. Differential methods for this problem have not been noted to date, and the work to be described in this chapter is an attempt to fill that

gap. The same explicit finite-difference scheme that was applied successfully for the non-buoyant jet analysis (see Chapter 4), and for analysis of the vertical buoyant jet in uniform and stratified ambients (see Chapter 5), is employed for this configuration as well. An additional equation, the conservation of transverse momentum, has to be solved.

6.2. Flow Configuration

Figure 6.1 shows the flow configuration for a buoyant jet discharging at angle θ_o to the horizontal. The jet is deflected upwards due to positive buoyancy forces. In general, this deflection is present even in the initial region, and is especially noticeable for smaller discharge Froude numbers. Fan, Hirst, etc. neglect this effect in their analyses. This assumption may be satisfactory for high Fr_o flows, but for low Fr_o flows, this assumption is incorrect, and may cause significant deviation in the predicted trajectory and centerline values. The natural (curvilinear) coordinate system is shown superimposed on the flow configuration. The jet grows as it rises and entrains ambient fluid.

One of the assumptions listed in Chapter 2 that underlies the present analysis, is that the jet cross section remains axisymmetric. For horizontal non-buoyant jets and vertical buoyant plumes this assumption is perfectly justified by experimental observation. For a buoyant, curved jet, however, the cross-section is probably never really axisymmetric, and it is assumed as such only to simplify the analysis. This has been a common practice with integral methods, and it is felt that, as long as the flow is not far from axisymmetric, this assumption could

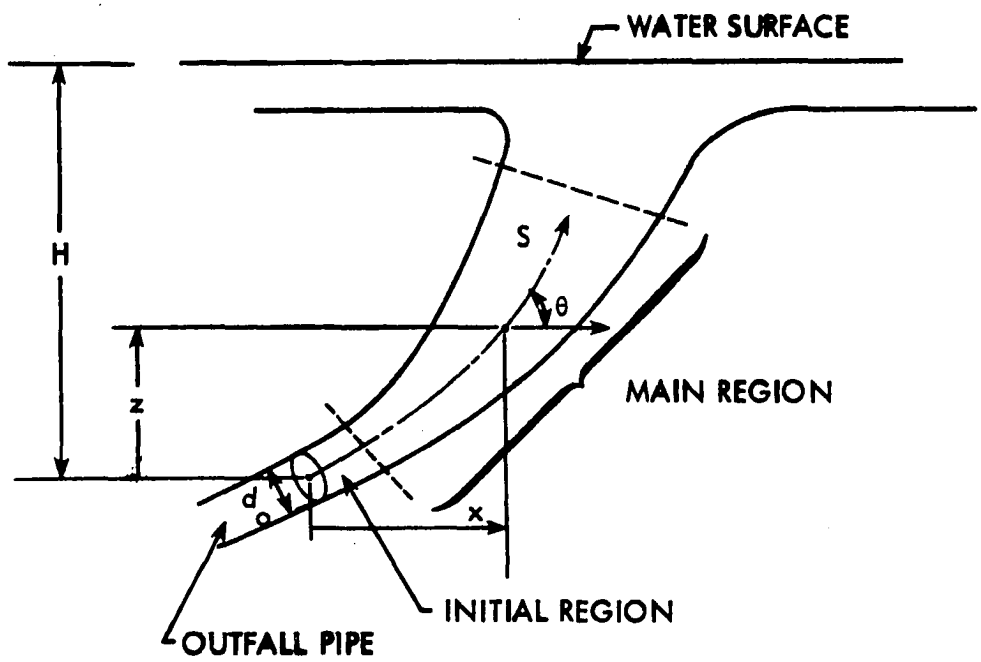

Fig. 6.1. Flow configuration for a submerged, inclined buoyant jet.

be a powerful way of reducing the complexity of the problem and lending it easily to analysis. The results of this chapter will show that the assumption is very satisfactory for the cases considered and might even be a good starting point in the analysis of jets subjected to ambient cross-flows, where the cross-section really appears quite distorted, more in the shape of a horseshoe [56,90] due to the presence of two counter-rotating vortices in the cross-section. Surely the approximation must have limits but within these limits the calculation procedure should prove useful for predictions in engineering design.

Buoyancy has negligible effect on the streamwise velocity in the initial region, contrary to what is observed for the vertical jet where an increase of 250% or more over discharge velocity is possible (see Chapter 5). However, as the jet turns, the component of buoyancy in the direction of flow begins to accelerate the flow, thereby slowing down the velocity decay process. Here also, as in the vertical jet analysis, the starting length is based, for convenience, on the plume centerline temperature.

Eventually, on rising, the jet will reach the surface, unless ambient stratification prevents it from doing so. In this study, emphasis was not placed on the spreading region close to the surface. One of the conclusions from the studies on potential environmental effects of offshore submerged nuclear power plants in [91] was as follows: "In every case, the thermal "mixing zone," as defined by the most stringent standards presently applied to coastal installations, ends before either a surface or subsurface field is established. This is an important finding, because any surface field that might result will be at a

temperature that is acceptable under these standards." Thus, the infinite ambient analysis is valid for most practical flows in the region of interest. This will be explained more completely later.

6.3. The Governing Equations

The differential equations governing the motion and dilution of the buoyant jet were presented as Eqs. (3.1) to (3.4) in the general formulation of Chapter 3. They are repeated here for convenience.

Continuity:

$$\frac{\partial}{\partial s}(uy) + \frac{\partial}{\partial y}(vy) = 0 \tag{6.1}$$

s-momentum:

$$u \frac{\partial u}{\partial s} + v \frac{\partial u}{\partial y} = \frac{1}{\rho y} \frac{\partial}{\partial y} (y\tau) + \frac{(\rho_\infty - \rho)}{\rho_o} g \sin\theta \tag{6.2}$$

y-momentum:

$$u^2 \frac{d\theta}{ds} = \frac{(\rho_\infty - \rho)}{\rho_o} g \cos\theta \tag{6.3}$$

Energy:

$$u \frac{\partial t}{ds} + v \frac{\partial t}{\partial y} = \frac{1}{\rho y c_p} \frac{\partial}{\partial y} (-yq) \tag{6.4}$$

As before,

$$\tau = \rho n \frac{\partial u}{\partial y} \quad , \quad n = \nu + \nu_T$$

$$q = - \rho c_p n_H \frac{\partial t}{\partial y} \, , \quad n_H = \alpha + \alpha_T$$

and

$$Pr_T = \frac{\nu_T}{\alpha_T} \tag{6.5}$$

Comparing this formulation with that of the vertical plume, one additional unknown, θ, is observed to be present, along with one additional equation, the conservation of transverse momentum. The y-momentum equation written in the form shown as Eq. (6.3) is simply a balance between the centrifugal force due to the jet turning, acting in the direction of the radius of curvature, and the component of buoyancy in the direction opposite to that of the centrifugal force.

$$\text{Centrifugal force} = \frac{u^2}{|\bar{R}|} = u^2 \frac{d\theta}{ds}$$

where

$\bar{R}$ is the radius of curvature of the trajectory.

The initial and boundary conditions, being the same as Eqs. (3.12) and (3.13), are listed here for the reader's convenience.

Initial conditions:

$$u(s_o,y) = f(y),\ t(s_o,y) = g(y),\ \theta(s_o) = \theta_o \tag{6.6}$$

θ_o for the cases investigated in this chapter is 0^o (0 radians) and 45^o (0.785715 radians).

Boundary conditions:

$$\frac{\partial u}{\partial y}(s,0) = \frac{\partial t}{\partial y}(s,0) = 0,\ v(s,0) = 0$$

$$\lim_{y\to\infty} u(s,y) = u_\infty,\quad \lim_{y\to\infty} t(s,y) = t_\infty \tag{6.7}$$

The non-dimensional forms and finite-difference equations have been presented in Chapter 3, and will not be repeated here.

6.4. Solution Method - Some Aspects

The techniques involved in the solution of the transverse momentum equation to generate the jet trajectory deserve further explanation. The normalized form of Eq. (6.3) appears in DuFort-Frankel formulation as follows:

$$(U_{i,j})^2 \left(\frac{\theta_{i+1} - \theta_{i-1}}{\Delta S_+ + \Delta S_-}\right) = \frac{(T_{i,j} - T_{\infty i})}{Re_o\ Fr_o} \cos\theta_i \tag{6.8}$$

One of the assumptions used in deriving the governing equations (see Appendix B) is that curvature changes over the cross-section are small enough to be neglected. This implies a constant θ over the cross-section. Also, sample calculations allowing θ to be variable over the cross-section showed no significant changes in the predicted results compared to solving Eq. (6.8) at just the centerline.

However, applying Eq. (6.8) only at the centerline to determine θ_{i+1} would mean using $(U_{i,1})^2$ and $(T_{i,1} - T_{\infty_i})$, and the solution thus obtained would give an estimate of θ at station $(i+1)$ based only on the behavior of the jet at the centerline, without considering the influence of the rest of the flow cross-section. It was felt that a better and more realistic estimate of θ at station $i+1$ could be obtained if Eq. (6.8) were representative of the entire flow cross-section at i. Hence, the equation was integrated (assuming constant θ over the cross-section) as follows:

$$\left(\frac{\theta_{i+1} - \theta_{i-1}}{\Delta S_+ + \Delta S_-}\right) \int_{0\ (j=1)}^{\delta_i\ (j=NYJ)} U_{i,j}^{\,2}\, Y_j\, dY$$

$$= \frac{\cos\theta_i}{Re_o} \int_{0\ (j=1)}^{\delta_i\ (j=NYJ)} \frac{\left(T_{i,j} - T_{\infty_i}\right)}{Fr_o}\, Y_j dY \qquad (6.9)$$

The $U_{i,j}$ and $T_{i,j}$ values used in the integration are obtained from the s-momentum and energy equations, respectively, at station i. Hence

this is a numerical integration, and no profile assumptions are made as is the case with integral methods.

The numerical integration was performed using Simpson's rule, which for the present formulation can be written as:

$$\int_{Y_j}^{Y_j+2\Delta Y} U_{i,j}^{\,2}\, Y_j\, dY$$

$$= \frac{\Delta Y}{3}\left[U_{i,j}^{\,2}\, Y_j + 4\, U_{i,j+1}^{\,2}\, Y_{j+1} + U_{i,j+2}^{\,2}\, Y_{j+2} \right]$$

and

$$\int_{Y_j}^{Y_j+2\Delta Y} \left(\frac{T_{i,j} - T_{\infty_i}}{Fr_o} \right) Y_j dY = \frac{\Delta Y}{3}\left[\left(\frac{T_{i,j} - T_{\infty_i}}{Fr_o} \right) Y_j \right.$$

$$\left. + 4\left(\frac{T_{i,j+1} - T_{\infty_i}}{Fr_o} \right) Y_{j+1} + \left(\frac{T_{i,j+2} - T_{\infty_i}}{Fr_o} \right) Y_{j+2} \right] \qquad (6.10)$$

The solution procedure was briefly explained in Chapter 3 with the help of Fig. 3.2.

With reference to that figure, θ_{i+1} is determined from the transverse momentum equation, as explained above, and then the coordinates of the trajectory are generated according to Eq. (3.31). This procedure is

illustrated in Fig. 6.2. The typical forward streamwise step shown is greatly exaggerated for clarity.

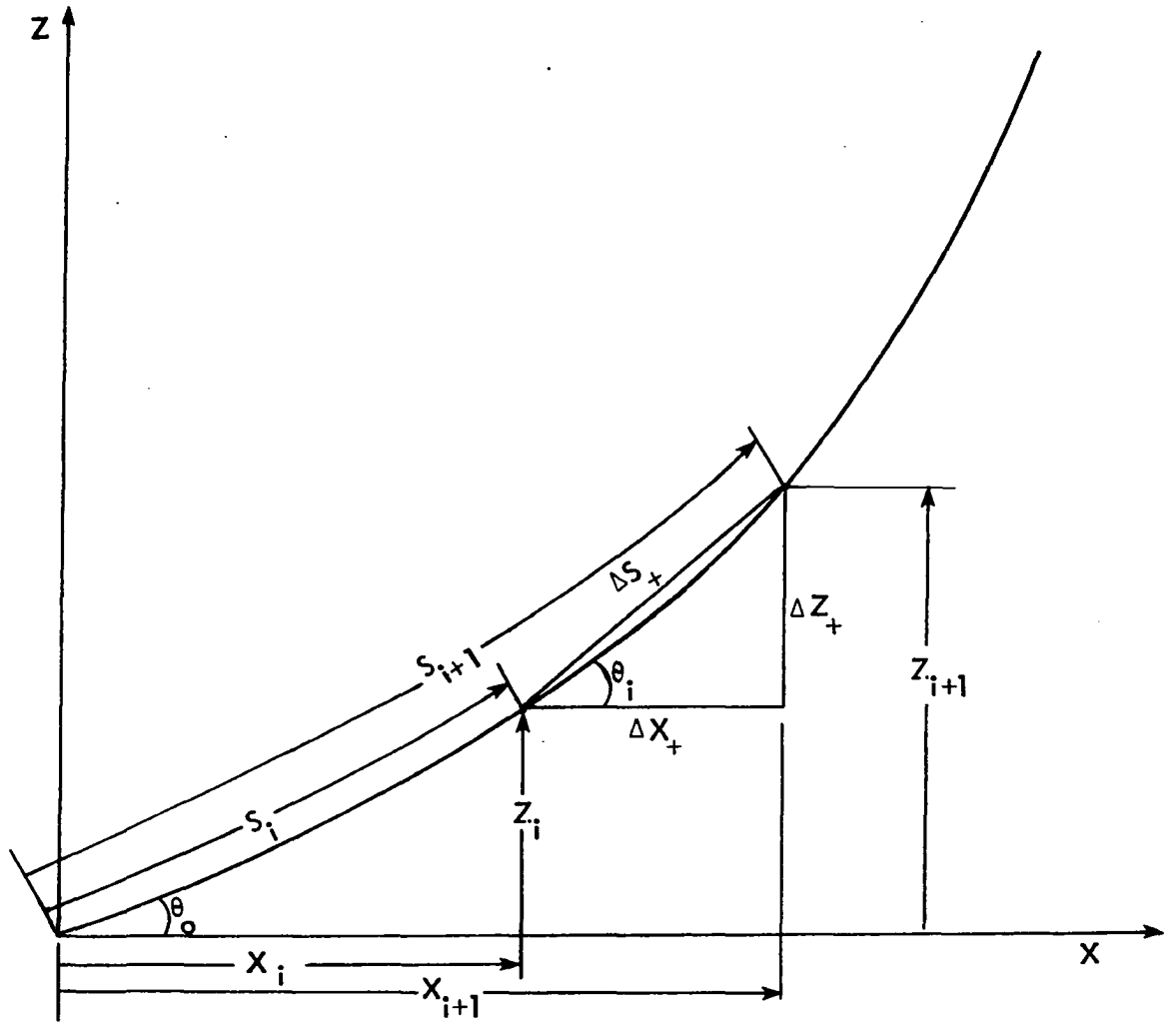

Fig. 6.2. Generation of jet trajectory.

6.5. Transport Model and Results

Once again, in the initial region, the simple mixing length model, Model A, was used to represent the turbulent viscosity, with mixing length $\ell = 0.0762\delta$ as before. Predictions of starting length and deflection using this formulation are consistent with results using Abraham's equations [42] (see Fig. 6.3).

In the main region of flow, first, calculations were made assuming that buoyancy had no effect on the effective viscosity and conductivity. Prandtl's constant viscosity model, Model F, that was used successfully in the vertical jet analysis, was employed here as well, with constant kept the same, i.e.

$$\nu_T = K_3 y_{1/2}(u_{max} - u_{min})$$

where

$$K_3 = 0.0246 \tag{6.11}$$

Figure 6.4 shows the results using this model (represented as $K_4 = 0$ in the figure) with the present method to predict the trajectory and centerline temperature values for a jet discharged horizontally at $Fr_o = 64$. The predicted trajectory compares very well with the measurements of Ryskiewich and Hafetz [72], but the centerline temperature decay is somewhat underpredicted.

Several references [35,92,93] and others mention the influence of buoyancy on mixing, and recommend modifying the mixing length to account

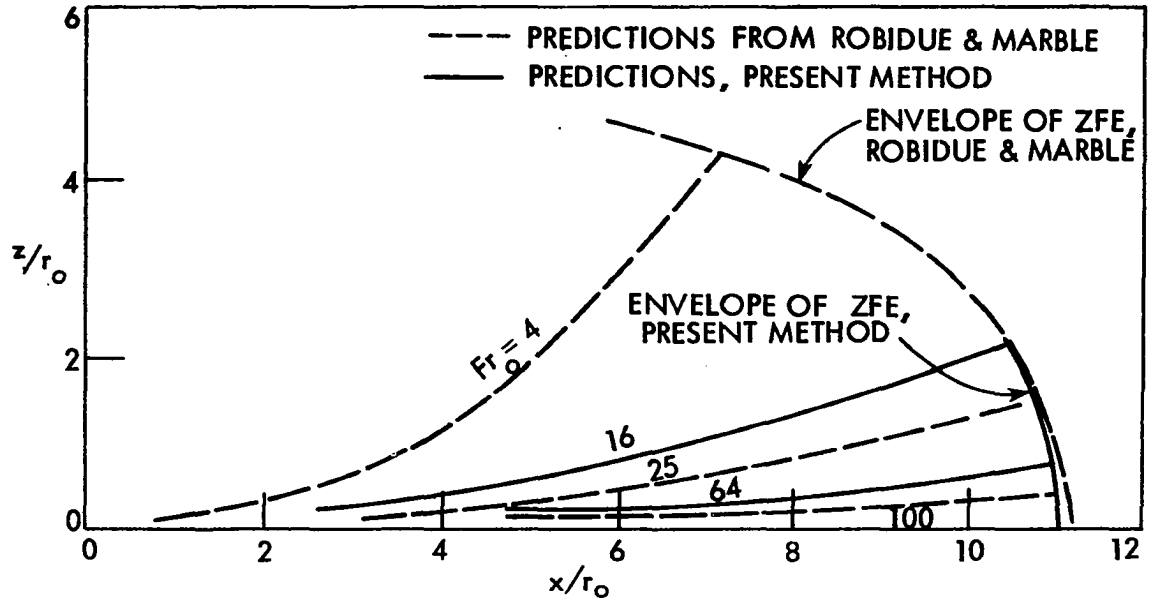

Fig. 6.3. Jet centerline path in zone of flow establishment (ZFE) for various values of Fr_o.

for this effect.

Bradshaw [92] gives a good discussion of buoyancy effects on turbulence intensity and presents some well-known empirical formulae which predict buoyancy effects as a function of a meteorological parameter, the Richardson number. The Monin-Oboukhov formula for the modification of the apparent mixing length by small buoyancy effects, one of the earliest of such formulae, is given in [92] as

$$\ell_o/\ell = 1/(1 - \beta' Ri) \tag{6.12}$$

where ℓ_o is the mixing length without buoyancy and ℓ is the modified mixing length. In unstable conditions ($Ri < 0$), β' is about 4.5 and in stable conditions ($Ri > 0$) it lies between 7 and 10.

Ri denotes the gradient Richardson number, which is the ratio of buoyancy to inertia forces, and is defined as:

$$Ri = \frac{g}{T_a} \left(\frac{\partial t}{\partial y} + \Gamma\right) \Big/ \left(\frac{\partial u}{\partial y}\right)^2$$

T_a is the ambient temperature at discharge in degrees absolute. Γ, the adiabatic lapse rate of the atmosphere, is negligible for most applications. Tennekes and Lumley [34] define Ri without this term. Thus.

$$Ri = \frac{g}{T_a} \left(\frac{\partial t}{\partial y}\right) \Big/ \left(\frac{\partial u}{\partial y}\right)^2 \tag{6.13}$$

For the present analysis, it was found more convenient to use a global representation of Ri as follows:

$$Ri = \frac{g}{T_a} \left(\frac{\Delta t_c}{\delta}\right) \Big/ \left(\frac{\Delta u_c}{\delta}\right)^2$$

$$= \frac{g}{T_a} (t_c - t_\infty) \times \frac{\delta}{u_c^2}$$

i.e., $$= \frac{g}{T_a} \frac{(t_c - t_\infty)\delta}{u_c^2} \qquad (6.14)$$

The Monin-Oboukhov formula is only valid for small buoyancy effects (or small Ri), and for larger negative Richardson numbers, typically in the range $-0.5 < Ri < 0$, the formula of Keyps [92] is mentioned as being commonly used instead. This is

$$\ell/\ell_o = (1 - 18\ Ri)^{0.25} \qquad (6.15)$$

In the present calculations, negative Ri values as large as -1.5 and even larger, were encountered, and so the "Keyps" formula was modified as follows:

$$\ell/\ell_o = (1 - K_4\ Ri)^{0.25} \qquad (6.16)$$

where $K_4 = 1.0$ was used for all calculations reported here.

It is worth noting that the Richardson number is effective in altering the turbulent mixing only as long as the gradients involved in Eq. (6.13) are in the direction of the earth's gravity. Anwar [89] notes that the phenomenon of the vertical plume does not depend on Ri

since no work is required to be done against gravity in entraining surrounding fluid. Indeed, this was seen to be approximately true from the vertical plume analysis of Chapter 5, where the deviation of predicted centerline decay values from experiment was not significant enough to suggest modifying the mixing length to include a Richardson number effect. (Naturally, there may be some secondary coupling effects in the turbulent motion which could be accounted for by more complex models.) However, this relative independence of Ri cannot be true for an inclined jet. Hence, to give Eq. (6.16) more generality, a cos θ term was introduced, as follows:

$$\ell = \ell_o \, (1 - K_4 \, Ri \cos \theta)^{0.25} \tag{6.17}$$

Here, θ is the local angle, so that as the jet turns upward, θ will increase, effectively reducing the effect of Ri on the mixing length.

Equation (6.17) was implemented in the model of Eq. (6.11) as follows:

$$\nu_T \text{ (based on } \ell_o) = \ell_o^2 \left|\frac{\partial u}{\partial y}\right| \approx K_3 \times (y_{1/2})^2 \times \frac{\Delta u_c}{y_{1/2}}$$

$$= K_3 \, y_{1/2} \left(u_{max} - u_{min}\right)$$

So that

$$\nu_T \text{ (based on } \ell) = \ell^2 \left|\frac{\partial u}{\partial y}\right| = \frac{\ell^2}{\ell_o^2} \times \ell_o^2 \left|\frac{\partial u}{\partial y}\right|$$

i.e., $$\nu_T = K_3 \, y_{1/2} \left(u_{max} - u_{min}\right)\left(1 - K_4 Ri \cos \theta\right)^{0.5} \tag{6.18}$$

where $K_3 = 0.0246$

The results using Eq. (6.18) and Eq. (6.11) (or Eq. (6.18) with $K_4 = 0.0$) to predict the trajectory and centerline temperature decay for the jet discharged horizontally at $Fr_o = 64$ are compared in Fig. 6.4. The predicted trajectory remains close to measurements in both cases, but using Eq. (6.18) with $K_4 = 1.0$ considerably improves predictions of centerline temperature. From this comparison Ri is seen to have a strong effect on centerline decay, but only marginal effect on the jet trajectory. This is an important finding because no references have been seen that give an observation or explanation of this effect for the buoyant curved jet. In Figs. 6.5 to 6.10, the predicted trajectories and centerline temperature values for buoyant jets discharged horizontally to a uniform ambient at $Fr_o = 16$ and 256, in addition to $Fr_o = 64$, are compared to the measurements of Ryskiewich and Hafetz [72], and the predictions of Hirst [10], Fan and Brooks (cited in [72]), and Abraham [13] where these have been available. The results from the present analysis show the best agreement with experiment.

The experiments of Anwar [89] agree closely with those of Ryskiewich and Hafetz for the buoyant jet discharging horizontally at $Fr_o = 16$, but for $Fr_o = 64$, there is significant deviation. The reasons for this discrepancy are not clear. If free surface effects were a factor, they would cause greater deviation in the data of Anwar, since in his experimental set-up, H/d_o varied from 27 to 70, whereas the results of Ryskiewich and Hafetz that have been used for comparison were obtained at $H/d_o = 80$.

Results for the inclined buoyant jet discharged at 45^o to a uniform quiescent ambient are presented in Figs. 6.11 to 6.14 for $Fr_o = 16$, 64,

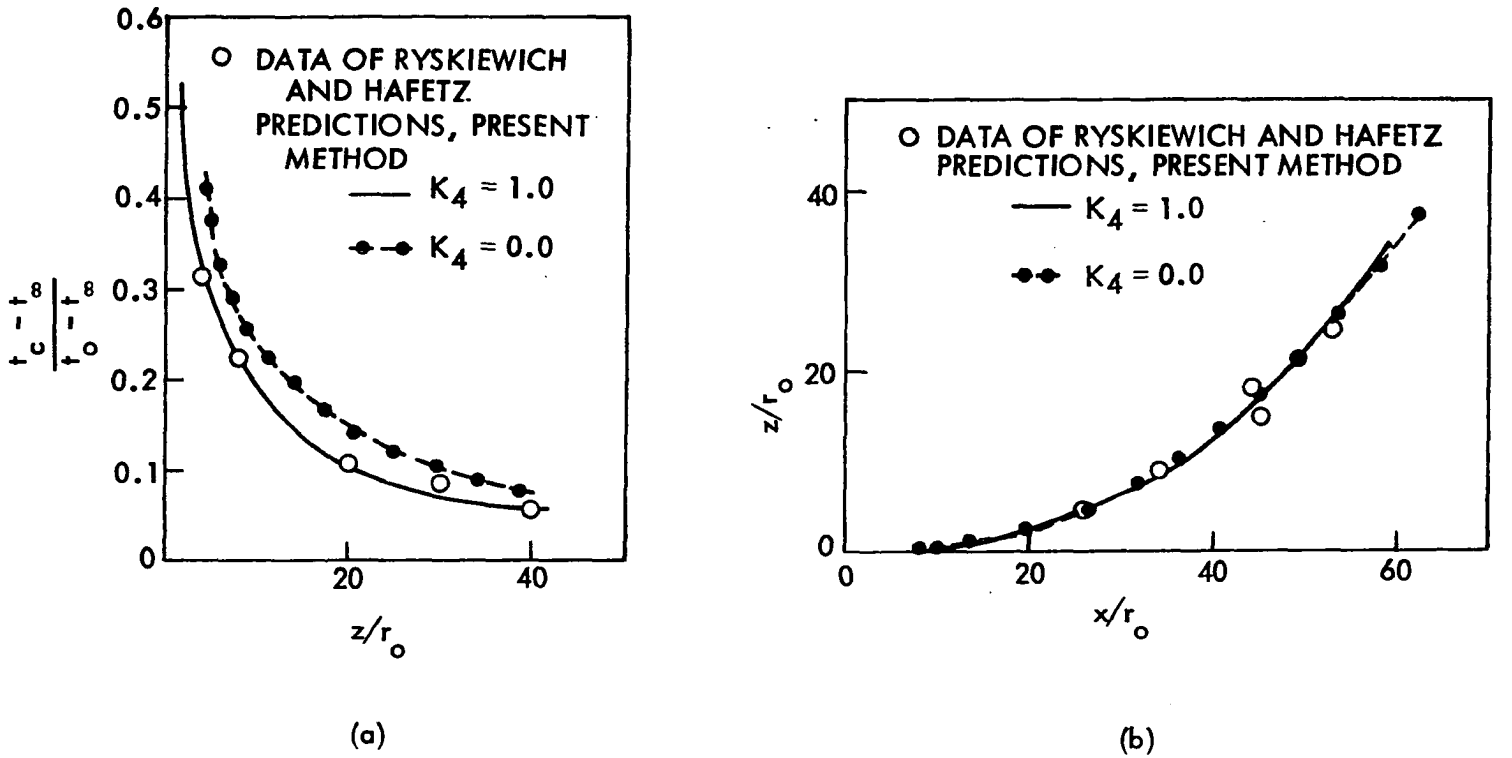

Fig. 6.4. Comparisons to show the influence of Ri on predictions for $Fr_o = 64$; buoyant jet discharged horizontally to a uniform ambient (a) decay of centerline temperature, (b) jet trajectory.

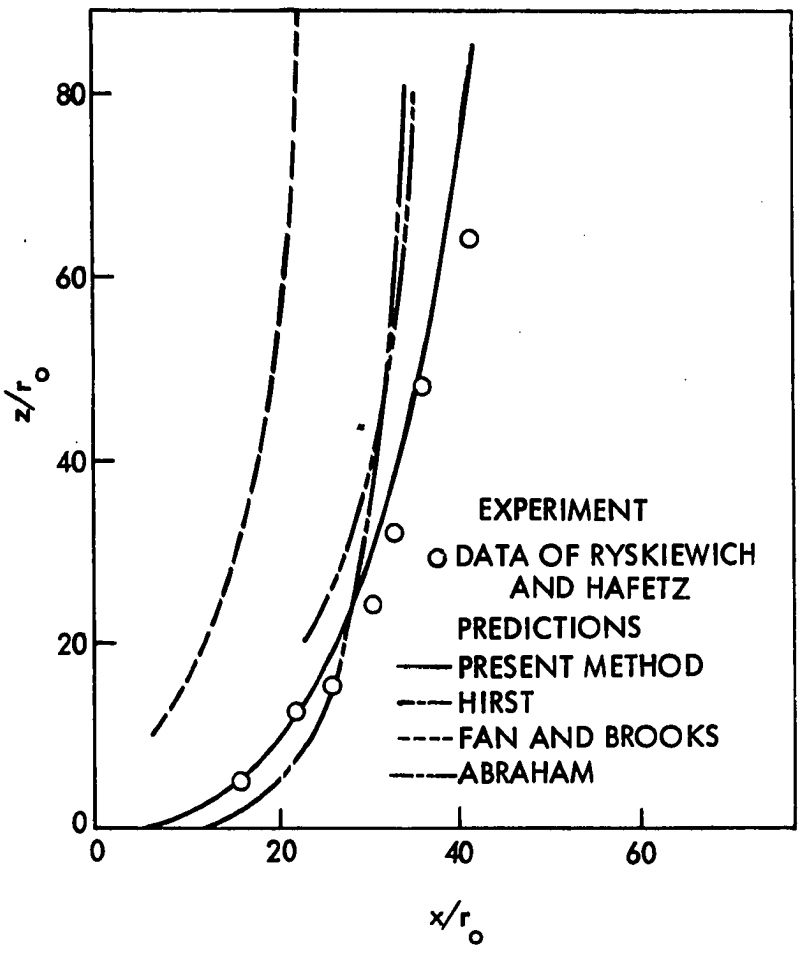

Fig. 6.5. Predicted and experimental trajectory for $Fr_o = 16$; buoyant jet discharged horizontally to a uniform ambient.

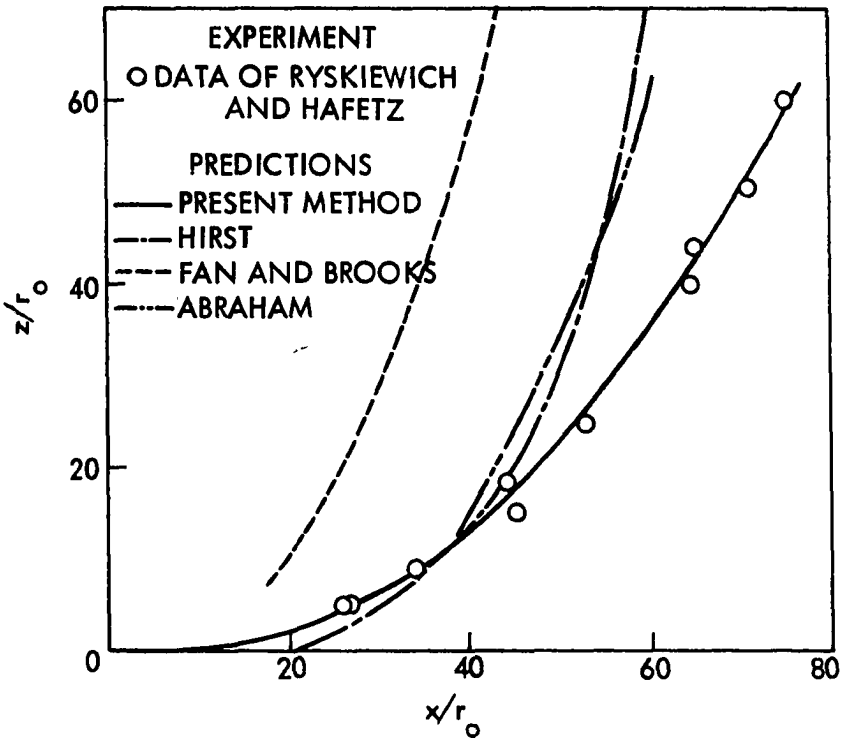

Fig. 6.6. Predicted and experimental trajectory for $Fr_o = 64$; buoyant jet discharged horizontally to a uniform ambient.

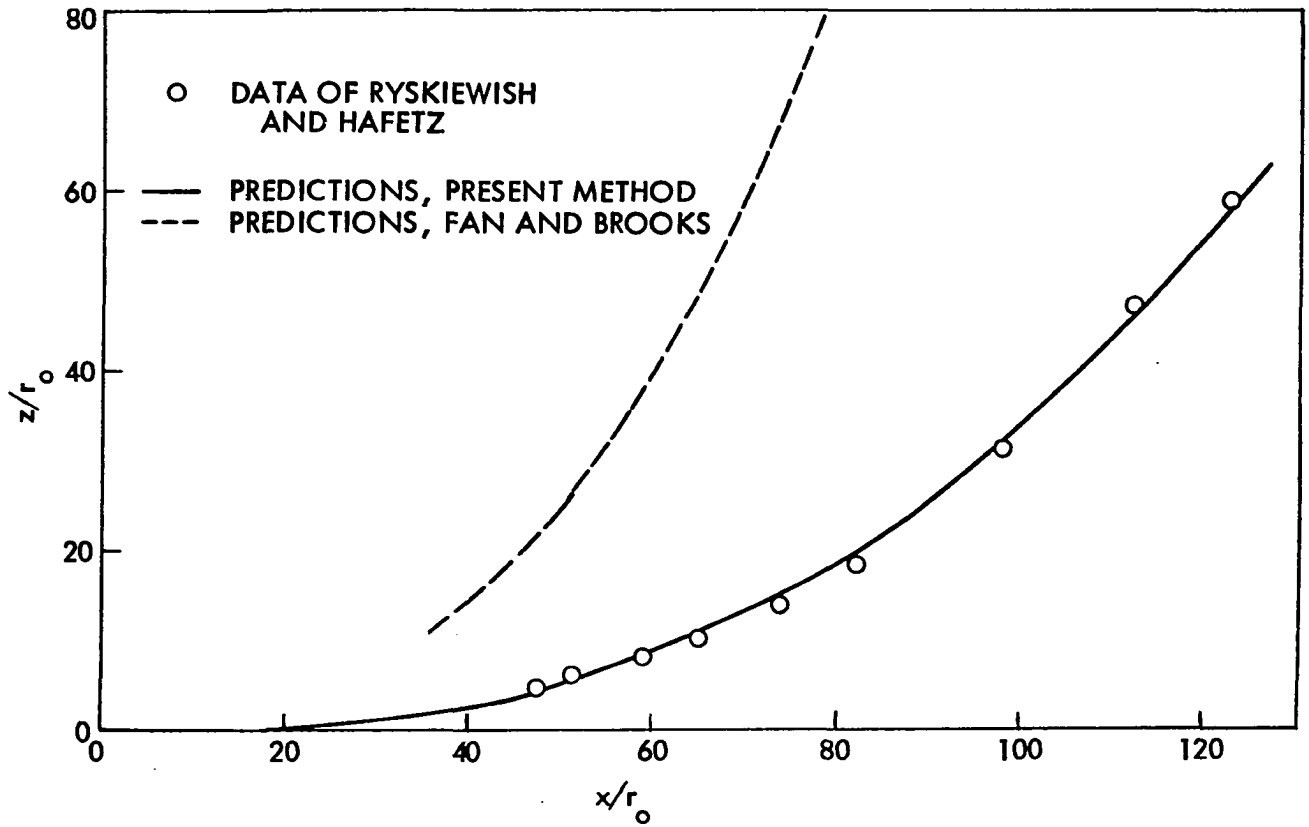

Fig. 6.7. Predicted and experimental trajectory for $Fr_o = 256$; buoyant jet discharged horizontally to a uniform ambient.

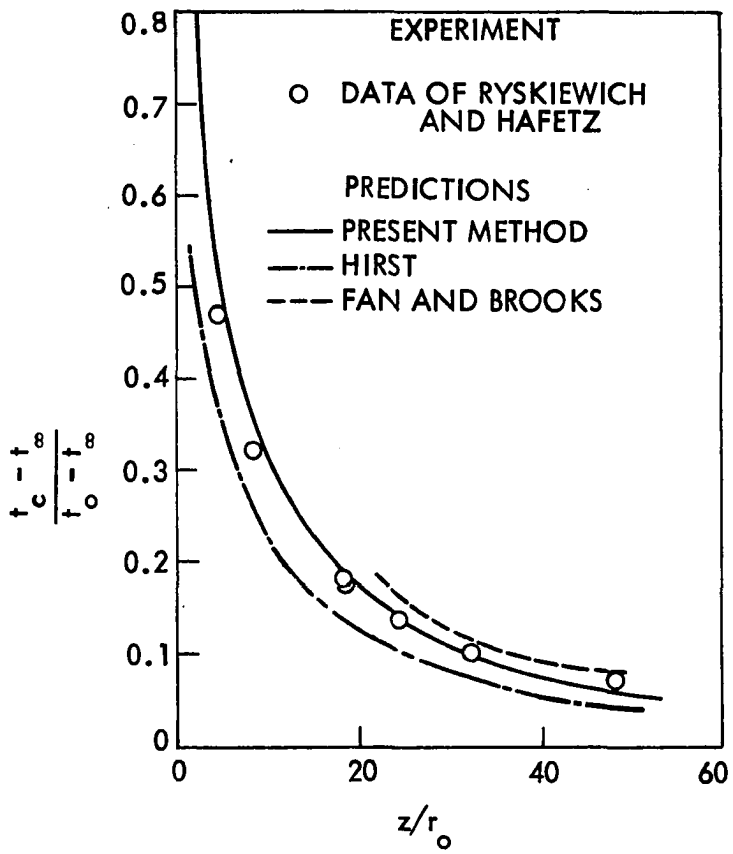

Fig. 6.8. Predicted and experimental decay of centerline temperature for $Fr_o = 16$; buoyant jet discharged horizontally to a uniform ambient.

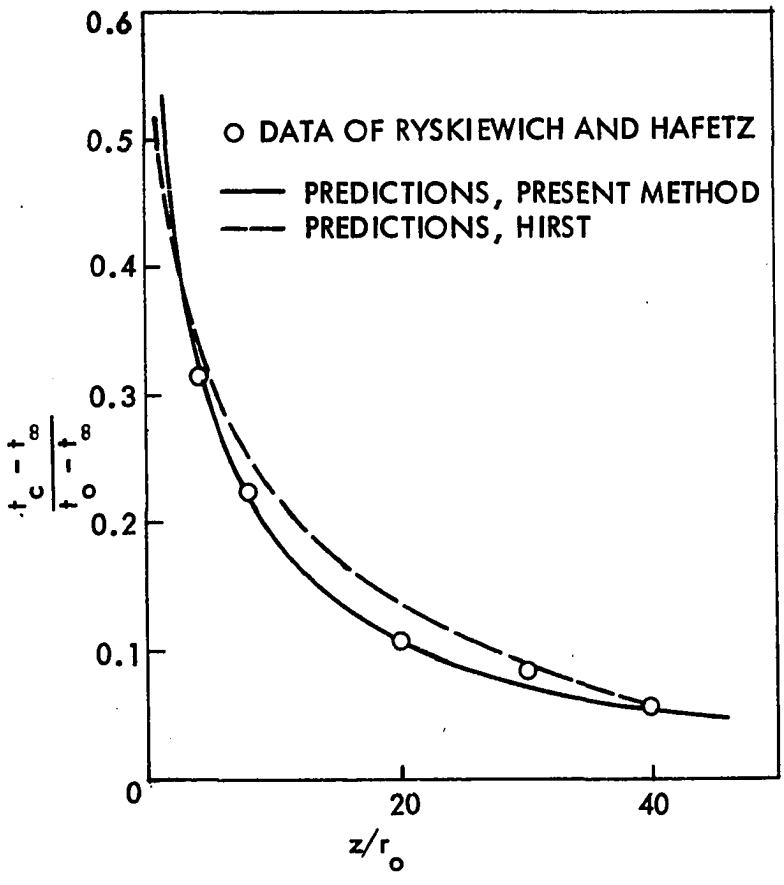

Fig. 6.9. Predicted and experimental decay of centerline temperature for $Fr_o = 64$; buoyant jet discharged horizontally to a uniform ambient.

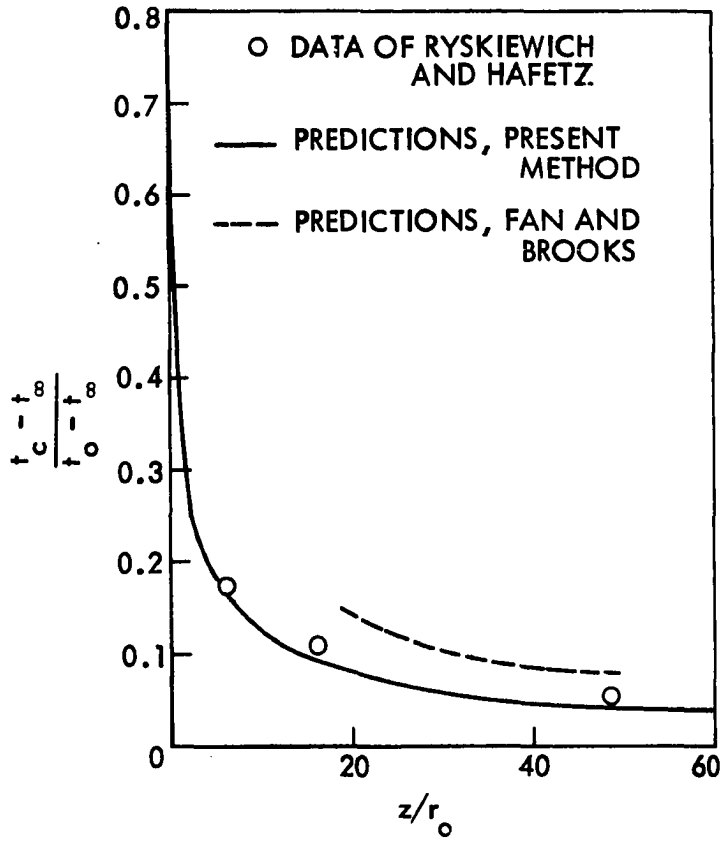

Fig. 6.10. Predicted and experimental decay of centerline temperature for $Fr_o = 256$; buoyant jet discharged horizontally to a uniform ambient.

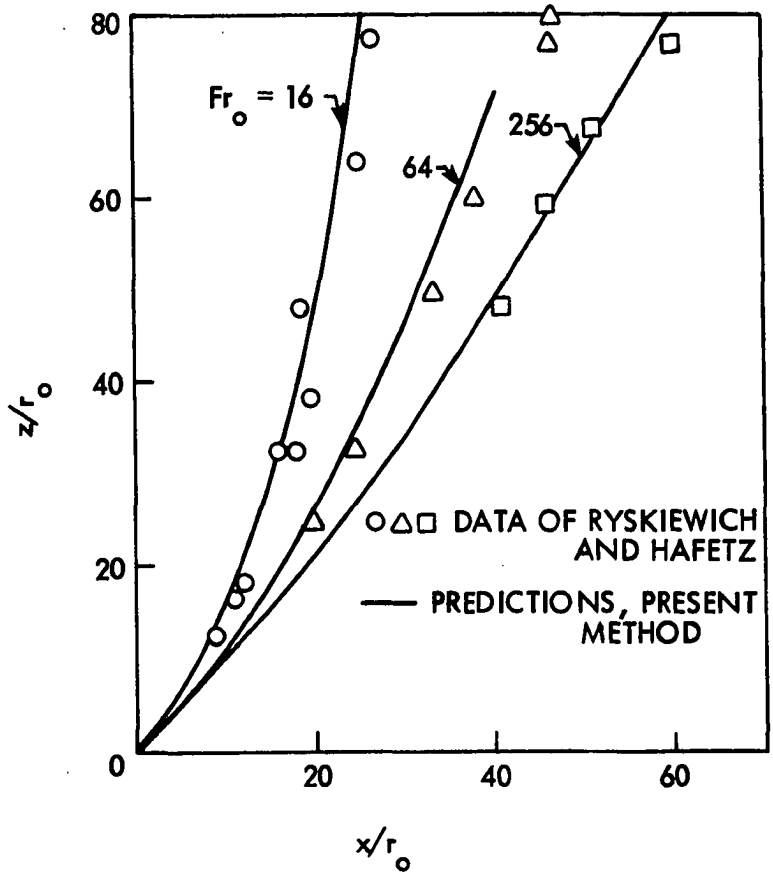

Fig. 6.11. Predicted and experimental trajectories for different discharge Froude numbers; buoyant jets discharged at 45° to a uniform ambient.

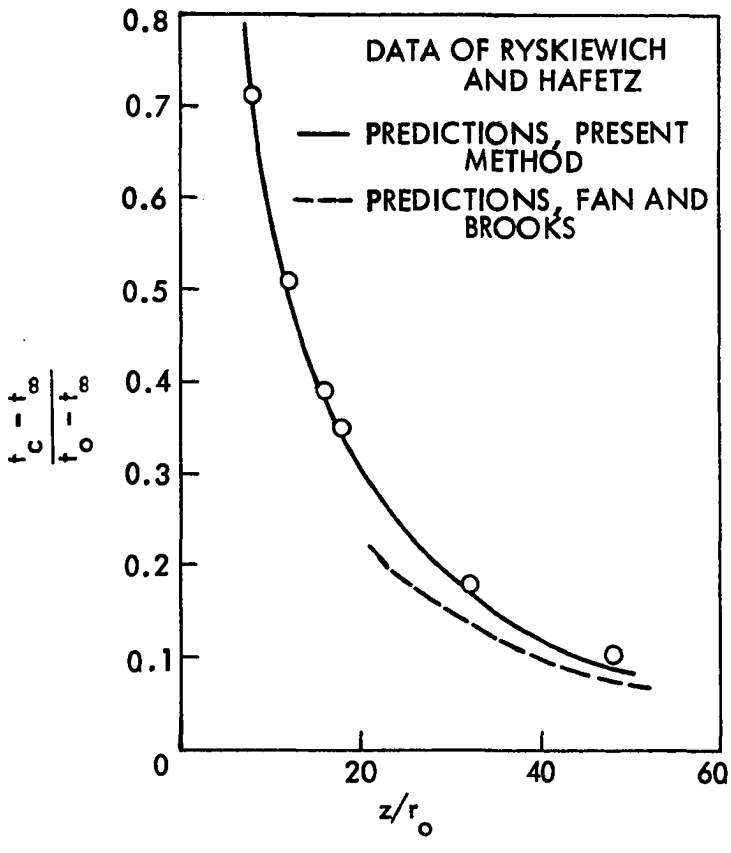

Fig. 6.12. Predicted and experimental decay of centerline temperature for $Fr_o = 16$; buoyant jet discharged at 45^o to a uniform ambient.

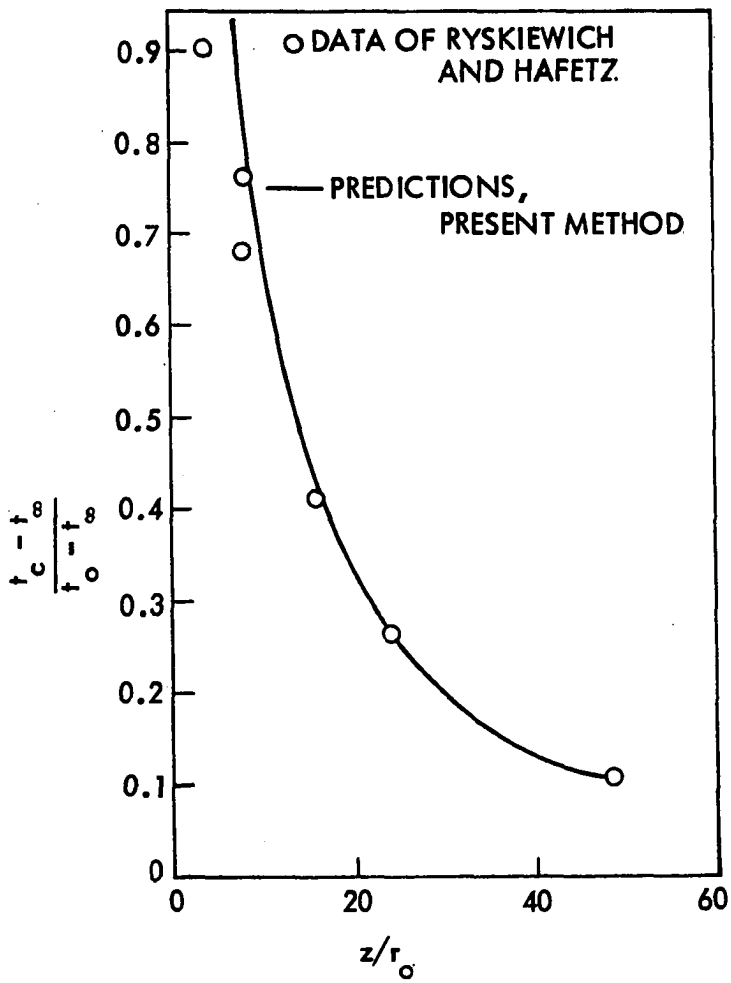

Fig. 6.13. Predicted and experimental decay of centerline temperature for $Fr_o = 64$; buoyant jet discharged at 45^o to a uniform ambient.

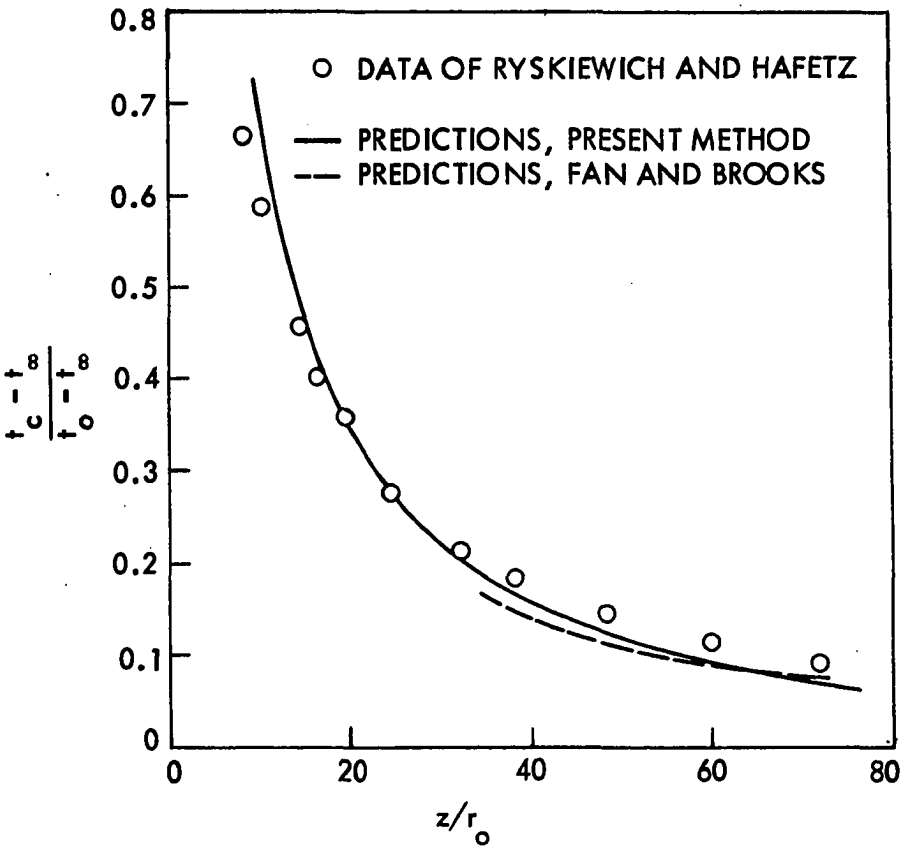

Fig. 6.14. Predicted and experimental decay of centerline temperature for Fr_o = 256; buoyant jet discharged at 45° to a uniform ambient.

and 256. In Fig. 6.11 the predicted plume trajectories are seen to compare very well with the measurements of Ryskiewich and Hafetz [72]. Figures 6.12 to 6.14 compare the centerline temperature values obtained by the present analysis with experimental data [72] and the predictions of Fan and Brooks as presented in [72]. Again, it can be seen that the present predictions show the best agreement with measurements.

6.6. Some Numerical Aspects

The stability criterion presented in Chapter 5 (Eq. (3.30)) was retained in the code and the solutions obtained were free of stability problems. Step sizes of the order of 6% of jet half-width, δ, were employed for most calculations of this configuration.

For one of the cases reported, namely, the horizontally discharged jet at $Fr_o = 256$, the jet had grown so as to use all the array areas allocated for the variables in the program, while the solution had not yet traversed a sufficient distance downstream for truly meaningful results to be obtained. The program could be made more efficient in general by incorporating the capability of doubling the transverse mesh size at some convenient point downstream, thereby increasing the allowable flow region and also reducing the required number of calculations at each station. However, lack of time prevented improvement of the code in this direction, and so recourse was taken to increasing the available array area for the program. Despite this, the calculation procedure was seen to be fast, and most calculations reported here have required little over

a minute of computer time on the IBM 360/65, with the one case described above requiring a little over two minutes.

6.7. Concluding Remarks

1. A simple turbulence model that includes important effects such as buoyancy, is shown to work well for analysis of the curved jet configuration. There is no evidence that a more complex model would do better for this configuration, but that could be one of the avenues to explore. For practical applications of interest to this investigation, such as the design of thermal discharge systems for power plants, however, a simple but well-tested model would be favored since much information such as initial shear stress profiles that would be required for a complex model (which is very sensitive to these values), is not available.

2. The infinite ambient analysis has been investigated for applicability to shallow water discharge. According to Marble and Robideau [42], this assumption is fine for the region of interest in outfall design, since surface effects are negligible there. However, the inclusion of surface effects in the prediction method could be a possible extension of this work.

3. The results of the previous section have justified the use of the axisymmetric assumption as a convenient and effective tool for simplifying the analysis without significant loss of accuracy for the cases considered. However, for jets in ambient cross-flows, this assumption may lead to inaccuracies in prediction, and an avenue of further research could be to relax this assumption.

4. Having been tested for the vertical, horizontal, and inclined configurations of the buoyant jet, this program can be used with confidence to predict the trajectory and flow properties of jets discharged at arbitrary angles to the horizontal. The thermal "mixing zone" can be determined by drawing isotherms until a temperature excess of either 5 ^{o}F (or whatever is the upper limit allowed by the local temperature standard) is reached. The same method can be used, without modification, to calculate arbitrary angles of discharge in the presence of ambient stratification. Sufficient time has not been available to carry out these calculations.

5. Interestingly, the present analysis is also applicable to ocean sewage outfalls, without requiring the additional solution of a species concentration equation. The reason for this generality is that the partial differential equation governing the concentration of effluent, in non-dimensional form, is the same as the non-dimensional energy equation. Also, the density difference could be due to salinity or temperature difference, and since the results are presented in non-dimensional form, the only step required is to use such initial temperatures that give the same initial density difference as is due to the salinity difference specified, and then, convert the non-dimensional temperature results to dimensional concentration rather than temperature.

7. CONCLUSIONS AND RECOMMENDATIONS

7.1. Concluding Remarks

Several specific conclusions were given in sections 4.6, 5.6, and 6.7; more general remarks and summarizing observations will be made here.

A differential approach has been presented for analysis of the behavior of turbulent, axisymmetric buoyant jets and plumes issuing into quiescent or flowing ambients. Special emphasis has been placed on configurations occurring in the thermal discharge from power plants and other sources into adjacent water bodies or the atmosphere with the hope that some of the prediction procedures developed would be useful in the discharge design process.

The governing differential equations of the flow in boundary layer form, derived in a curvilinear orthogonal coordinate system (see Appendix B) were solved numerically in the physical plane using an explicit finite-difference scheme of the DuFort-Frankel type.

The following flow categories were considered: (1) the non-buoyant jet discharging into a co-flowing or quiescent ambient; (2) the vertically discharging buoyant jet or plume in a uniform or stratified ambient; and (3) the buoyant jet discharging horizontally or inclined to the horizontal into a uniform quiescent ambient.

The Reynolds stress and turbulent heat flux terms in the governing equations were modeled using the "Boussinesq" concept of eddy viscosity. Reynolds analogy in the form of a turbulent Prandtl number (see Eq. (3.8)) was used to relate the turbulent exchange of heat and momentum. The value of Pr_T was kept constant = 0.7 for all calculations reported.

The calculation method utilized a turbulence model to evaluate the turbulent (eddy) diffusivities for heat and momentum.

The solution of the governing differential equations resulted in details such as the velocity and temperature fields, and, in addition, the jet trajectory in case of the buoyant curved jet. Predicted results were compared with available experimental data, and the results of other prediction methods wherever possible, for a number of test cases in all three flow categories. The present method was seen to provide improved predictions for most of the cases considered.

The first flow category provided a suitable test configuration for a verification study of the computational technique developed for the jet flow calculations, and as a first step in evaluating the different models for the turbulent transport. Several existing turbulence models for the non-buoyant jet in co-flowing and quiescent ambients were compared to experimental data, and some modifications were suggested and examined. A velocity ratio function, given by Eq. (4.13), was proposed which caused the simple eddy viscosity models to result in improved predictions for a wide range of velocity ratios, including the important case of jet into quiescent ambient flows.

For the second flow category, the calculation method was used to predict the velocity and temperature fields resulting from a vertically discharged buoyant jet or plume. In addition, when the ambient was stratified, the method was used to predict the zero buoyant height and the maximum height of rise of the plume. Comparisons were made for a wide range of Froude numbers and stratification parameters, believed to be of most practical interest in discharge design. Agreement was very

good. An eddy viscosity model for the turbulence, given by Eq. (4.15), was seen to be successful in analyzing the jet flow, for both uniform and stratified ambient cases. The inifinte ambient analysis of the present investigation was seen to be applicable for predicting shallow water discharges as well, over the entire range of Froude numbers of practical interest.

In the third flow category, the analysis was extended to predict the jet trajectory along with estimates of the flow properties for the configuration in which the jet or plume followed a curved path. No predicted results using differential methods have been noted to date for this flow category.

An extra equation, the normal or y-momentum equation had to be included in the governing system of equations. The simple eddy viscosity model of Eq. (4.15) gave good predictions of jet trajectory; however, the best predictions of both trajectory and centerline temperature values were obtained when the model was modified to include buoyancy effects on turbulent mixing in terms of a gradient Richardson number, Ri, defined by Eq. (6.14). The Richardson number used this way was found to have a strong effect on centerline decay values, but only marginal effect on the jet trajectory.

With the good agreement obtained for the test cases with different angles of discharge and different discharge Froude numbers, this program can be used with some confidence to predict the trajectory and flow properties of jets discharged at arbitrary angles to the horizontal under different buoyancy conditions.

Consistency and stability of the numerical scheme were studied. A new and more complete stability criterion for the DuFort-Frankel difference equations, given by Eq. (3.30), was derived by application of the Von Neumann stability analysis. This restriction was seen to allow streamwise step sizes several times larger than possible with the simple explicit scheme. The computational scheme was seen to be economical, almost all the calculations reported requiring less than 2 minutes of computational time on the IBM 360/65 machine.

The results presented in this investigation demonstrate (1) the viability of an explicit finite-difference scheme in the physical plane to accurately and economically predict the velocity and temperature fields and the location of the effluent plume resulting from a thermal discharge into the immediate environment, and (2) the suitability of simple models for the turbulent transport mechanism as applied to this problem.

It is felt that the present analysis can be applied with a fair degree of confidence in the design and analysis of thermal discharge systems, and should serve as a valuable stepping stone for the further application of differential approaches to analyze the general problem of turbulent buoyant jets and plumes.

7.2. Recommendations for Further Study

Several recommendations concerning the extension of this work can be suggested.

Attention could be directed to analysis of jets discharged to ambient cross flows, where relaxation of the axisymmetric assumption that was so successful in the present investigation may become necessary in order to get accurate predictions of the flow field. Surface effects could be included in the analysis for submerged, shallow water discharges and more complex turbulence models could be studied using the present calculation scheme.

Other related problems that can be attempted using the same general method are:

1. Discharge of effluent from large, multiport diffusers. The present round jet analysis can be used until the jets being to interact. The interaction could take place when 2δ becomes equal to $(L + 2r_o)$ where L is the spacing between two consecutive ports, or even before that. Once the jets merge, the analysis would shift to that of a slot jet.

2. A species concentration equation could be solved in addition to the energy equation. This would enable the present method to be useful in predicting the concentration and spread of sewage effluent, and brine effluents from desalination plants, and the concentration of pollutants from industrial chimney stacks.

3. Finally, the entire analysis could be extended to solve for jets and plumes with three-dimensional trajectories. This would involve two angles to be determined in tracing the jet trajectory; one in the horizontal plane, and the other in the plane perpendicular to the horizontal.

As regards the need for future experimental studies, there seems to be sufficient experimental data for flow category (1) above, but for categories (2) and (3), additional measurements are needed to compare the predicted jet growth and the associated velocity and temperature profiles. Experimental data for flows with three-dimensional trajectories seems to be non-existent. Intermittency measurements over the jet or plume cross-section are also needed, as they would be helpful in providing a physical basis for improving the turbulence models used to analyze the flow.

8. ACKNOWLEDGMENTS

The author wishes to express his most sincere gratitude to Dr. Richard H. Pletcher, his thesis advisor and committee chairman, who gave his valuable guidance, help, suggestions, encouragement and time with great generosity.

The author is indebted to his doctoral committee, Dr. Arthur E. Bergles, Professor Henry M. Black, Professor William F. Riley, and Dr. Donald F. Young, for their interest, cooperation, and helpful suggestions during the course of the study.

The author is thankful to the National Science Foundation Fluid Mechanics Program for sponsoring the research under grants GK-18810 and ENG 74-22193, and also to the Engineering Research Institute, Iowa State University, for providing partial support.

Thanks are also due to Dr. Mostafa A. Shirazi of the National Thermal Pollution Research Program, EPA, at Corvallis, Oregon, for his helpfulness in pointing out the recent experimental work of Pryputniewicz on buoyant vertical jets, and to Dr. Merwin D. Dougal of the Iowa State Water Resources Research Institute, for providing a copy of the report by Ryskiewich and Hafetz on their measurements in vertical and inclined buoyant jets.

Finally, the author is grateful to his parents, family and friends for their unfailing encouragement, and especially to his father, who died while this work was in progress and whose faith and selfless efforts linger in the author's memory. This thesis is dedicated to his memory.

9. REFERENCES

1. Baumgartner, D. J., and Trent, D. S., 'Ocean Outfall Design: Part I - Literature Review and Theoretical Development,' Corvallis, Oregon: U.S. Department of Interior, Federal Water Quality Control Administration, 1970.

2. Harleman, D. R. F., and Stolzenbach, K. D., 'Fluid Mechanics of Heat Disposal from Power Generation,' Annual Review of Fluid Mechanics (1972):7-31.

3. Parker, F. L., and Krenkel, P. A., 'Thermal Pollution: Status of the Art,' Report No. 3, Dept. of Environmental and Water Resources Engineering, Vanderbilt University, Dec. 1969.

4. Parker, F. L., and Krenkel, P. A., Engineering Aspects of Thermal Pollution, Nashville, Tenn.: Vanderbilt University Press, 1969.

5. Kolfat, T. D., 'Thermal Discharges - An Engineering Problem,' Paper #70-WA/PID-5. Presented at the ASME Winter Annual Meeting, New York, N. Y., 1970.

6. Di Luzio, F. C., 'Natural Resource Management,' Mechanical Engineering 91, No. 4 (April 1969):35.

7. Stanford Conference on Computation of Turbulent Boundary Layers, Proc. 1968 AFOSR-IFP, Vol. 1, Stanford University, 1969.

8. Langley Working Conference on Free Turbulent Shear Flows, Proc. NASA SP-321, Vol. 1, 1972.

9. Hirst, E. A., 'Buoyant Jets Discharged to Quiescent Stratified Ambients,' Journal of Geophysical Research 76, No. 30 (1971):7375-7384.

10. Hirst, E. A., 'Analysis of Round Turbulent, Buoyant Jets Discharged to Flowing Stratified Ambients,' Report No. ORNL-4585, Oak Ridge National Laboratory, 1971.

11. Campbell, J. F., and Schetz, J. A., 'Analysis of the Injection of a a Heated, Turbulent Jet into a Moving Mainstream, with Emphasis on a Thermal Discharge in a Waterway,' Report No. VPI-E-72-24, 1972, College of Engineering, Virginia Polytechnic Institute and State University.

12. Abraham, G., 'Jet Diffusion in Stagnant Ambient Fluid,' Delft Hydraulics Lab. No. 29, 1963.

13. Abraham, G., 'Horizontal Jets in Stagnant Fluid of Other Density,' ASCE Journal of Hydraulics Division 91, HY4 (1965):139-153.

14. Morton, B. R., 'Forced Plumes,' Journal of Fluid Mechanics 5 (1959): 151-163.

15. Morton, B. R., Taylor, G. I., and Turner, J. S., 'Turbulent Gravitational Convection from Maintained and Instantaneous Sources,' Proceedings of the Royal Society of London A234 (1956):1-23.

16. Fan, L. N., 'Turbulent Buoyant Jets into Stratified or Flowing Ambient Fluids,' Keck Lab. of Hydraulics and Water Resources, California Institute of Technology, Report No. KH-R-15, 1967.

17. Fan, L. N., and Brooks, N. H., 'Numerical Solutions of Turbulent Buoyant Jet Problems,' Keck Lab. of Hydraulics and Water Resources, California Institute of Technology, Report No. KH-R-18, 1969.

18. Schetz, J. A., 'Turbulent Mixing of a Jet in a Co-Flowing Stream,' AIAA Journal 6 (1968):2008-2010.

19. Fox, H., Sinha, R., and Weinberger, L., 'An Implicit Finite-Difference Solution for Jet and Wake Problems,' Astronautica Acta 17 (1972):265-278.

20. Zelazny, S. W., 'Eddy Viscosity in Quiescent and Co-Flowing Axisymmetric Jets,' AIAA Journal 9, No. 11 (1971):2292-2294.

21. Trent, D. S., and Welty, J. R., 'Numerical Thermal Plume Model for Vertical Outfalls in Shallow Water,' Report No. EPA-R2-73-162, Environmental Protection Agency (1973).

22. Trent, D. S., and Welty, J. R., 'Numerical Computation of Momentum Jets and Forced Plumes,' Computers and Fluids, Vol. 1, New York: Pergamon Press (1973):331-357.

23. Boussinesq, J., 'Sur la Maniere Dent les Vitesse; Dans Tube Cylindrique de Section Circulaire, Evase a son Entree, se Distribuent Depuis Cette Entree Jusq'aux Endroit ou se Trouve Establi un Regime Uniforme,' Comptes Rendus 113 (1891):49-59.

24. Ricou, F. P., and Spalding, D. B., 'Measurements of Entrainment by Axisymmetrical Turbulent Jets,' Journal of Fluid Mechanics 11 (1961): 21-32.

25. Rawn, A. M., Bowerman, F. R., and Brooks, N. H., 'Diffusers for Disposal of Sewage in Sea Water,' ASCE Journal of Sanitary Engineering Division (1960):65-105.

26. Hinze, J. O., Turbulence, New York: McGraw-Hill, 1959, pp. 376-439.

27. Cederwall, K., 'The Initial Mixing on Jet Disposal into a Recipient,' Chalmers Institute of Technology; Goteburg, Sweden, 1963 (in Swedish).

28. Pryputniewicz, R. J., 'An Experimental Study of the Free Surface Effects on a Submerged Vertical Buoyant Jet,' M.S. Thesis, University of Connecticut, 1974.

29. Tollmien, W., 'Grenzschichttheorie,' Handbuch der Experimentalphysik 4, Pt. 1 (1931):248.

30. Goldstein, S., Modern Developments in Fluid Dynamics, Vol. 1, Cambridge, England: Oxford University Press, 1938.

31. Dvorak, F. A., 'Calculation of Turbulent Boundary Layers and Wall Jets over Curved Surfaces,' AIAA Journal 11, No. 4 (1973):517-524.

32. Rastogi, A. K., and Whitelaw, J. H., 'Procedure for Predicting the Influence of Longitudinal Curvature on Boundary-Layer Flows,' Paper No. 71-WA/FE-37. Presented at the ASME Winter Annual Meeting, Washington, D.C., 1971.

33. Kreith, F., Principles of Heat Transfer, 3rd edition, New York: Intext Educational Publishers, 1973.

34. Tennekes, H., and Lumley, J. L., A First Course in Turbulence, Cambridge, Mass.: The MIT Press, 1972.

35. Launder, B. E., and Spalding, D. B., Mathematical Models of Turbulence, New York: Academic Press, 1972.

36. Pletcher, R. H., 'On a Finite-Difference Solution for the Constant-Property Turbulent Boundary Layer,' AIAA Journal 7, No. 2 (1969): 305-311.

37. Pletcher, R. H., 'Calculation Method for Compressible Turbulent Boundary Layer Flows with Heat Transfer,' AIAA Journal 10, No. 3 (1972):245-246.

38. Nelson, R. M., and Pletcher, R. H., 'An Explicit Scheme for the Calculation of Confined Turbulent Flows with Heat Transfer,' Proc. 1974 Heat Transfer and Fluid Mechanics Institute, Stanford, Calif.: Stanford University Press, 1974.

39. Schlichting, H., Boundary-Layer Theory, 6th edition, New York: McGraw-Hill, Inc., 1968.

40. Keffer, J. F., and Baines, W. D., 'The Round Turbulent Jet in a Cross-Wind,' Journal of Fluid Mechanics 15, No. 4 (1963):481-497.

41. Chan, D. T. L., and Kennedy, J. F., 'Submerged Buoyant Jets in Quiescent Fluids,' ASCE Journal of the Hydraulic Division 101, No. HY6 (1975):733.

42. Marble, R. W., and Robideau, R. F., 'Thermal Field Resulting from an Offshore-Submerged Nuclear Electric Power Generating Station,' Paper No. 71-WA/NE-3. Presented at the ASME Winter Annual Meeting, Washington, D.C., 1971.

43. DuFort, E. C., and Frankel, S. P., 'Stability Conditions in the Numerical Treatment of Parabolic Differential Equations,' Mathematical Tables Aid Computation 7 (1953):135-152.

44. Roache, P. J., Computational Fluid Dynamics, Albuquerque, N.M.: Hormosa Publishers, 1972.

45. Ames, W. F., Numerical Methods for Partial Differential Equations, New York: Barnes and Noble, Inc., 1969.

46. Wang, R. L., and duPlessis, M. P., 'An Explicit Numerical Method for the Solution of Jet Flows,' Paper No. 72-WA/FE-20. Presented at the ASME Winter Annual Meeting in New York, N. Y., 1972.

47. O'Brien, G. G., Hyman, M. A., and Kaplan, S., 'A Study of the Numerical Solution of Partial Differential Equations,' Journal of Mathematics and Physics 29 (1951):223-241.

48. Hornbeck, R. W., Numerical Marching Techniques for Fluid Flows with Heat Transfer, NASA SP-297, 1973, 339 p.

49. Richtmyer, R. D., and Morton, K. W., Difference Methods for Initial Value Problems, 2nd edition, New York: Wiley (Interscience), 1967.

50. Pletcher, R. H., 'An Analytic Study of Film Behavior in Horizontal Annular Two-Phase Flow,' Interim Report, ARO(D) Project No. 3199-E, Cornell University, 1965.

51. Nelson, R. M., 'An Explicit Finite-Difference Analysis for Developing Turbulent Internal Flows with Heat Transfer and Property Variations,' M.S. Thesis, Iowa State University, 1972.

52. Tollmien, W., 'Strahlverbreiterung,' Zeitschrift Fur Angewandte Mathematik Und Mechanik 6 (1926):468-478.

53. Kuethe, A. M., 'Investigations of the Turbulent Mixing Regions Formed by Jets,' Trans. ASME, Journal of Applied Mechanics 2 (1935): 87-95.

54. Squire, H. B., and Trouncer, J., 'Round Jets in a General Stream,' ARC Technical Report R & M No. 1974, 1944.

55. Pai, S. I., 'Axially Symmetrical Jet Mixing of a Compressible Fluid,' Quart. Applied Mathematics 10, No. 2 (1952):141-148.

56. Abramovich, G. N., The Theory of Turbulent Jets, translated by Scripts Technica, Cambridge, Mass.: MIT Press, 1963.

57. Albertson, M. L., Dai, Y. B., Jensen, R. A., and Rouse, H., 'Diffusion of Submerged Jets,' ASCE Trans. 115 (1950):637-697.

58. Forstall, W., and Shapiro, A. H., 'Momentum and Mass Transfer in Coaxial Gas Jets,' Trans. ASME, Journal of Applied Mechanics 17, No. 4 (1950):399-408.

59. Landis, F., and Shapiro, A. H., 'The Turbulent Mixing of Co-Axial Gas Jets,' Heat Transfer and Fluid Mechanics Institute, 1951.

60. Cebeci, T., 'Calculation of Compressible Turbulent Boundary Layers with Heat and Mass Transfer,' AIAA Journal 9 (1971):1091-1097.

61. Reynolds, W. C., 'Computation of Turbulent Flows - State-of-the-Art, 1970,' Report No. MD-27, Stanford University, 1970.

62. Launder, B. E., Morse, A., Rodi, W., and Spalding, D. B., 'Prediction of Free Shear Flows - A Comparison of the Performance of Six Turbulence Models,' Proc. Langley Working Conference on Free Turbulence Shear Flows, NASA SP-321, Vol. 1 (1972):361-422.

63. Schetz, J. A., 'Free Turbulent Mixing in a Co-Flowing Stream,' Proc. Langley Working Conference on Free Turbulent Shear Flows, NASA SP-321, Vol. 1 (1972):259-276.

64. Schubauer, G. B., and Tchen, C. M., 'Turbulent Flow,' Turbulent Flow and Heat Transfer, Vol. 5 of High Speed Aerodynamics and Jet Propulsion, Princeton, N. J.: Princeton Press (1959):165.

65. Morgenthaler, J. H., and Zelazny, S. W., 'Predictions of Axisymmetric Free Turbulent Shear Flows using a Generalized Eddy-Viscosity Approach,' Proc. Langley Working Conference on Free Turbulent Shear Flows, NASA SP-321, Vol. 1 (1972):277-326.

66. Cohen, L. S., 'A Kinematic Eddy Viscosity Model Including the Influence of Density Variations and Preturbulence,' Proc. Langley Working Conference on Free Turbulent Shear Flows, NASA SP-321, Vol. 1 (1972):139-189.

67. Patankar, S. V., and Spalding, D. B., Heat and Mass Transfer in Boundary Layers, 2nd edition, London: Intertext Books, 1970.

68. Karplus, W. J., 'An Electric Circuit Theory Approach to Finite-Difference Stability,' Trans. AIEE 77, No. 1 (1958).

69. Abraham, G., 'Jet Diffusion in Liquid of Greater Density,' ASCE Journal of Hydraulics Division 86, HY6 (1960):1-13.

70. Frankel, R. J., and Cumming, J. D., 'Turbulent Mixing Phenomena of Ocean Outfalls,' ASCE Journal of Sanitary Engineering Division, SA2 (1965):33-59.

71. Rouse, H., Yih, C. S., and Humphreys, H. W., 'Gravitational Convection from a Boundary Source,' Tellus 4 (1952):201-210.

72. Ryskiewich, B. S., and Hafetz, L., 'An Experimental Study of the Free Surface Effect on a Buoyant Jet,' General Dynamics Report No. U440-74-103, 1975.

73. Pryputniewicz, R. J., and Bowley, W. W., 'An Experimental Study of Vertical Buoyant Jets Discharged into Water of Finite Depth,' ASME Journal of Heat Transfer (May 1975):274-281.

74. Schmidt, W., 'Turbulente Ausbreiting Eines Stromes Erhitzter Luft,' Zietschrift Für Angewandte Mathematik Und Mechanik 21 (1941):265-278, 351-363.

75. Trent, D. S., 'A Numerical Model for Predicting Energy Dispersion in Thermal Plumes issuing from Large, Vertical Outfalls in Shallow Coastal Water,' Doctoral dissertation, Oregon State University, Corvallis, 1972.

76. Oosthuizen, P. H., 'Low Velocity Heated Air Jets,' presented at the Fourth Western Canadian Heat Transfer Conference, Winnipeg, Manitoba, 1972.

77. Hart, W. E., 'Jet Discharge into a Fluid with a Density Gradient,' ASCE Journal of Hydraulics Division 87, HY6 (1961):171-200.

78. Crawford, T. V., and Leonard, A. S., 'Observations of Buoyant Plumes in Calm Stably Stratified Air,' Journal of Applied Meteorology 1 (1962):251-256.

79. Abraham, G., and Eysink, W. D., "Jets Issuing into Fluid with a Density Gradient,' Journal of Hydraulic Research 7, No. 2 (1969): 145-175.

80. Fox, D. G., 'Forced Plume in a Stratified Fluid,' Journal of Geophysical Research 75, No. 33 (1970):6818-6835.

81. Priestley, C. H. B., and Ball, F. K., 'Continuous Convection from an Isolated Source of Heat,' Quart. J. Roy. Meteorol. Soc. 81 (1955):144-157.

82. Sneck, H. J., and Brown, D. H., 'Plume Rise from Large Thermal Sources Such as Cooling Towers,' General Electric Report No. 72GEN025, Nov. 1972.

83. Hirst, E. A., 'Analysis of Buoyant Jets within the Zone of Flow Establishment,' Report No. ORNL-TM-3470, Oak Ridge National Laboratory, 1971.

84. Briggs, G. A., Plume Rise, USAEC Division of Technical Information, 1969.

85. Robidue, R. F., 'The Discharge of Submerged Buoyant Jets into Water of Finite Depth,' General Dynamics Report No. U440-72-121, Nov. 1972.

86. Dancey, C. L., and Pletcher, R. H., 'A Boundary Layer Finite Difference Method for Calculating through the Separation Point and into the Region of Recirculation in Incompressible Laminar Flow,' Report No. HTL-2, ERI, Iowa State University, Ames, June 1974.

87. Gibson, M. M., and Launder, B. E., 'On the Calculation of Horizontal Non-Equilibrium Turbulent Shear Flows Under Gravitational Influence,' Imperial College of Science and Technology, Mechanical Engineering Report No. HTS/74/28, Sept. 1974.

88. Bosanquet, C. H., Horn, G., and Thring, M. W., 'The Effect of Density Differences on the Path of Jets,' Journal Roy. Soc. London A263 (1961):340-352.

89. Anwar, H. O., 'Behavior of Buoyant Jet in Calm Fluid,' ASCE Journal of the Hydraulics Division 91, HY4 (1969):139-153.

90. Gordier, R. L., 'Studies on Fluid Jets Discharging Normally into Moving Liquid,' University of Minnesota, St. Anthony Falls Hydraulic Lab., Tech. Paper No. 28, Series B, 1959.

91. Water Pollution Control Research Series, 'Potential Environmental Effects of an Offshore Submerged Nuclear Power Plant, Volume 1,' General Dynamics Report No. 16130 GFI 06/71, June 1971.

92. Bradshaw, P., 'The Analogy Between Streamline Curvature and Buoyancy in Turbulent Shear Slow,' Journal of Fluid Mechanics 36, part 1 (1969):177-191.

93. 'Turbulence Models and their Experimental Verification,' Lecture Series at the Pennsylvania State University, University Park, April 8-10, 1974.

94. Gebhart, G., Heat Transfer, 2nd edition, New York: McGraw-Hill, Inc., 1971.

95. Owczarek, J. A., Introduction to Fluid Mechanics, Scranton, Penn.: International Textbook Co., 1968.

96. Spiegel, M. R., Theory and Problems of Vector Analysis, Schaum's Outline Series, New York: McGraw-Hill, Inc., 1959.

97. Cebeci, T., and Smith, A. M. O., Analysis of Turbulent Boundary Layers, New York: Academic Press, 1974.

98. Hong, S. W., 'Laminar Flow Heat Transfer in Ordinary and Augmented Tubes,' Doctoral dissertation, Iowa State University, Ames, 1974.

10. APPENDIX A:

EXAMPLE COMPUTER PROGRAM

For the readers' convenience, this appendix contains a listing of the computer program that was used to solve the governing equations for the buoyant jet or plume discharged at arbitrary angles to the vertical (the configuration of Chapter 6). The same program can be used without modification to compute the vertical jet configuration of Chapter 5 as well. For the non-buoyant jet analysis, this program can be implemented either by having a large enough discharge Froude number, or by making the difference form of the y-momentum equation optional and specifying $\theta = 0^{o}$.

The computer code consists of a main program and 6 subroutines.

```
C     PROGRAM TO PREDICT THE GROWTH, LOCATION AND PROPERTIES OF A TURBULENT,
C     AXISYMMETRIC, BUOYANT JET OR PLUME
C
C     USING SIMPLE EXPLICIT FINITE DIFFERENCING SCHEME AS STARTING
C     METHOD,FOLLOWED BY THE DUFORT-FRANKEL SCHEME
C
C
C     THE FOLLOWING IS AN EXPLANATION OF THE INPUT PARAMETERS
C
C     INPUT   = 0 INDICATES SOLUTION WILL START AT DISCHARGE
C             = 1 MEANS SOLUTION WILL CONTINUE FROM A PREVIOUSLY CALCULATED
C                 STATION,USING INFORMATION FROM PUNCHED OUTPUT
C     LORT     GT.0 FOR TURBULENT FLOW CALCULATIONS
C              LE.0 FOR LAMINAR FLOW CALCULATIONS(NOT USED)
C     IQORC   = 0 FOR QUIESCENT AMBIENT
C             = 1 FOR COFLOWING(OR FLOWING) AMBIENT
C     IEND    = MAXIMUM NUMBER OF I STATIONS TO BE COMPUTED
C               THIS IS A SAFETY FEATURE AND SHOULD BE SET HIGHER THAN
C               EXPECTED NUMBER OF STEPS IN ANY CALCULATION
C     IOUT    = NUMBER OF I STEPS BETWEEN OUTPUTS.
C
C     NS      = VALUE OF I WHEN D-F SCHEME TAKES OVER
C     NVI     = NUMBER OF GRID SPACES OVER NOZZLE RADIUS
C     IPUNCH  = NUMBER OF I STEPS BETWEEN PUNCHED OUTPUTS
C     MULT     GT.0 MEANS IOUT=1 IRRESPECTIVE OF SPECIFIED IOUT
C             = 0 MEANS IOUT HAS ITS SPECIFIED VALUE
C     IAVG    = RESEARCH PARAMETER,NO LONGER USED
C     ISTAB    GT.0 ALLOWS STABILITY CRITERION TO BE USED IN DETERMINING
C               STEP SIZE
C             = 0 BYPASSES STABILITY CHECK
C     CONST1  = CONSTANT IN TURBULENCE MODEL FOR INITIAL REGION
C     CONST2  = CONSTANT IN TURBULENCE MODEL FOR MAIN REGION
C     CONST3  = CONSTANT IN RICHARDSON NUMBER MODIFICATION
C     FRAC    = FRACTION OF MAXIMUM ALLOWABLE STEPSIZE USED
C     DXFMIN  = RESEARCH PARAMETER,NO LONGER USED
C     DEC     = CHANGE IN STEPSIZE ALLOWED AS A FRACTION OF PREVIOUS
C               STEPSIZE
C     DENS    = DENSITY OF FLUID
C     ANU     = KINEMATIC VISCOSITY OF FLUID
C     USTART  = JET VELOCITY AT DISCHARGE
C     TSTART  = JET TEMPERATURE AT DISCHARGE
C     RAD     = RADIUS OF DISCHARGE PIPE
C     VAXIS   = LATERAL VELOCITY ALONG JET CENTERLINE
C     PRT     = TURBULENT PRANDTL NUMBER
C     UF      = FREE STREAM (AMBIENT) VELOCITY
C     UE      = VELOCITY AT EDGE OF JET
C     TF0     = AMBIENT TEMPERATURE AT DISCHARGE
C     TE0     = TEMPERATURE AT EDGE OF JET (AT DISCHARGE)
C     CP      = SPECIFIC HEAT AT CONSTANT PRESSURE
C     HTK     = THERMAL CONDUCTIVITY
C     THETA0  = INITIAL ANGLE OF DISCHARGE (IN RADIANS)
C     LAMDA   = DEGREE OF AMBIENT STRATIFICATION
C     BETA    = ISOBARIC VOLUME EXPANSIVITY OF FLUID
C     UFRAC   = PRESCRIBED EDGE VELOCITY AS FRACTION OF USTART
C     INCR    = STEPWIZE INCREASE IN DXF SPECIFIED AS MULTIPLIER OF DXF
C     DXFMAX  = MAXIMUM ALLOWABLE DXF SPECIFIED
C     INCR1   = VALUE OF INCR IN MAIN REGION
```

THE MAIN PROGRAM

The main program reads in the data and logic parameters, initializes all necessary quantities, co-ordinates the subroutines and calculates needed parameters, including the plume trajectory. It also contains the procedure for determining the streamwise stepsize with the DuFort-Frankel scheme.

The subroutines called (in order) are:

- SDELX
- UVEL
- VVEL
- TEMP
- EFVISC
- OUTPUT

```
C      MAIN PROGRAM
C
       REAL INCR,INCR1,LAMDA
       COMMON/AREA1/U(400),UP(400),UM(400),V(400),VP(400),VM(400),T(400),
      2TP(400),TM(400),FINV(400),FPINV(400),UTEST,UE,UF,TTEST,TE,TF,REO,
      3VAXIS,LORT,USTART,AL1,AL2,BL1,BL2,TSTART,TEO,TFO,THETA,THETAM,
      4THETAP
       COMMON/AREA2/DELXP,DELXM,DELXT,DELY,DELTA,TDELTA,Y(400),I,NS,NY,
      1NYT,EV(400),EK(400),ECONV,UCONV,XCONV,TCONV,FCONV,N,DELMIX,
      2EVP(400),EKP(400),DELHP,DELZP
       COMMON/AREA3/COEFP(400),COEFM(400),SMUP(400),SMUM(400),SKCP(400),
      3SKCM(400)
       COMMON/AREA4/XL,ANU,PRT,HTK,DENS,CP,ALPHA
       COMMON/AREA5/X,XO,H,Z,RAD,LT,STRAT
       COMMON/AREA6/CONST1,CONST2,FRAC,DXFMIN,CONST3
       COMMON/AREA7/YUHALF,YTHALF,YMAX,YCORE
       COMMON/AREA8/TC1,TC2,FRND
       COMMON/AREA9/JCORE,JJ,JINFL
       COMMON/AREA10/NYJ,NAVG,NBUOY
C
C      READING IN THE INPUT
C
       READ(5,8) INPUT
       READ(5,8) LORT
       READ(5,8) IQORC
    8  FORMAT(I6)
       READ(5,10) IEND,IOUT,NS,NYI,IPUNCH,MULT,IAVG,ISTAB
   10  FORMAT(8I6)
       WRITE(6,11) IEND,IOUT,NS,NYI,IPUNCH,MULT,IAVG,ISTAB
   11  FORMAT(' ',' IEND=',I4,10X,'IOUT=',I3,10X,'NS=',I2,10X,'NYI=',I3,
      110X,'IPUNCH=',I4, 5X,'MULT=',I4,5X,'IAVG=',I3,5X,'ISTAB=',I2)
       READ(5,12) CONST1,CONST2,FRAC,DXFMIN,DEC,CONST3
   12  FORMAT(6F12.5)
       WRITE(6,13) CONST1,CONST2,FRAC,DXFMIN,DEC,CONST3
   13  FORMAT(' ',' CONST1=',F12.5,3X,'CONST2=',F12.5,3X,'FRAC=',F12.5,
      13X,'DXFMIN=',F12.5,5X,'DEC=',F12.5,3X,'CONST3=',F12.5)
       READ(5,15) DENS,ANU,USTART,RAD,TSTART,VAXIS,PRT,UE,UF,TEO,TFO,CP,
      1HTK,THETAO,LAMDA,BETA,UFRAC
   15  FORMAT(6G12.5)
       WRITE(6,16) DENS,ANU,USTART,RAD,TSTART,VAXIS,PRT,UE,UF,TEO,TFO,CP,
      1HTK,THETAO,LAMDA,BETA,UFRAC
   16  FORMAT(' ',' DENS=',F12.5,5X,'ANU=',G12.5,5X,'USTART=',F12.5,5X,
      1'RAD=',F12.5,5X,'TSTART=',F12.5,5X,'VAXIS=',F12.5/' ',' PRT=',
      2F12.5,5X,'UE=',F12.5,5X,'UF=',F12.5,5X,'TE=',F12.5,5X,'TF=',F12.5,
      35X,'CP=',F12.5/' ',' HTK=',G12.5,5X,'THETAO=',F12.5,5X,'LAMDA=',
      4F12.5,5X,'BETA=',F12.5,5X,'UFRAC=',F12.5)
       READ(5,17) INCR,DXFMAX,INCR1
   17  FORMAT(3F12.5)
       WRITE(6,18) INCR,DXFMAX,INCR1
   18  FORMAT(' ',' INCR=',F12.5,5X,'DXFMAX=',F12.5,5X,'INCR1=',F12.5)
C
C      READING IN PUNCHED OUTPUT
C
  115  FORMAT(' ',5G15.8)
  120  FORMAT(' ',9I6)
       IF(IQORC.GT.0) GO TO 121
       UF=UFRAC*USTART
       UE=UFRAC*USTART
  121  IF(INPUT.GT.0) GO TO 105
       GO TO 28
```

```
  105 READ(5,115)  (UM(J),J=1,400)
      READ(5,115)  (VM(J),J=1,400)
      READ(5,115)  (TM(J),J=1,400)
      READ(5,115)  (U(J),J=1,400)
      READ(5,115)  (V(J),J=1,400)
      READ(5,115)  (T(J),J=1,400)
      READ(5,115)  (EV(J),J=1,400)
      READ(5,115)  (EK(J),J=1,400)
      READ(5,115)  (Y(J),J=1,400)
      READ(5,115) (FINV(J),J=1,400)
      READ(5,115) X,H,Z,DELXM,DELHM,DELZM,THETAM,THETA,DXF,DELTA,DELMIX,
     1DELY,TDELTA,YUHALF,YTHALF
      READ(5,120) I,IP,K,N,NY,NYT,M,NYJ ,NA
      GO TO 29
C
   28 R=UF/USTART
C
      WRITE(6,21) R
   21 FORMAT(' ','VELOCITY RATIO R=',G12.5)
      TE=TEO
      TF=TFO
C
C     NON-DIMENSIONALIZING
C
C     CONVERSION FACTORS
   29 XCONV=ANU/USTART
C
      G=32.2
C     FOR METRIC SYSTEM,USE APPROPRIATE VALUE OF G
C
      FCONV=(USTART*USTART)/(BETA*2.0*RAD*G*(TSTART-TFO))
      ECONV=ANU
      UCONV=USTART
      REO=USTART*2.0*RAD/ANU
      TC1=TEO
      TC2=(TSTART-TEO)
      STRAT=(-LAMDA*2.0*RAD)/(REO*TC2)
      IF(LAMDA.EQ.0.0) GO TO 23
      PARM1=RAD*(-LAMDA)/TC2
      PARM2=(-LAMDA*USTART*USTART*(TFO    +460.0))/(TC2*TC2*G)
      TEE=TC2/(RAD*(-LAMDA))
      WRITE(6,20) STRAT,PARM1,PARM2,TEE
   20 FORMAT(' ','STRAT=',G12.5,3X,'PARAMETER1=',G12.5,3X,'PARAMETER2=',
     1G12.5,3X,'TEE=',G12.5)
C
C     VARIABLES
   23 TEO=(TEO-TEO)/(TSTART-TEO)
      TFO=TEO
      TSTART=1.0
      FSTART=FCONV/TSTART
      WRITE(6,22) FSTART
   22 FORMAT(' ','STARTING FR.NO.=',G12.5)
      FINVO=1/FSTART
      UE=UE/UCONV
      UF=UF/UCONV
      USTART=USTART/UCONV
      RAD=RAD/XCONV
      ALPHA=(HTK/(DENS*CP))*1.0/ECONV
      IF(INPUT.GT.0) GO TO 67
C
```

```
C     Y-GRID SPACING
C
      DELY=RAD/NYI
C
C     STARTING PROFILES
C     ASSUMED UNIFORM
C
      I=0
      X=0.0
      H=0.0
      Z=0.0
      THETA=THETAO
      NNYI=NYI+1
      DO 25 J=1,NNYI
      Y(J)=(J-1)*DELY
      U(J)=1.0
      V(J)=0.0
      T(J)=1.0
      EV(J)=1.0
      EK(J)=ALPHA
      FINV(J)=FINVO
   25 CONTINUE
      NNNYI=NNYI+1
      DO 40 J=NNNYI,400
      Y(J)=(J-1)*DELY
      U(J)=UF
      V(J)=0.0
      T(J)=TFO
      EV(J)=1.0
      EK(J)=ALPHA
      FINV(J)=0.0
   40 CONTINUE
      DELTA=RAD
      TDELTA=RAD
      NY=NNYI
      NYT=NY
      DELMIX=0.0
C
C     BEGINNING OF COMPUTATION LOOP
C
C     SIMPLE EXPLICIT SCHEME
C
      IF(LORT.GT.0.0) GO TO 54
      WRITE (6,58)
   58 FORMAT('-',30X,'LAMINAR JET CASE')
      AL1=2.0
      AL2=2.0
      BL1=2.0*ALPHA
      BL2=2.0*ALPHA
   54 WRITE(6,55)
   55 FORMAT('-',15X,'SIMPLE EXPLICIT SCHEME')
      NY=NNYI
      N=1
      I=1
      LT=0.0
      GO TO 57
   56 I=I+1
      IF(I.GT.NS) GO TO 65
      LT=1.0
   57 CALL SDELX
```

```
      X=X+DELXP
      CALL UVEL
      DELHP=DELXP*COS(THETA)
      DELZP=DELXP*SIN(THETA)
      H=H+DELHP
      Z=Z+DELZP
      CALL VVEL
      CALL TEMP
      IF(LORT.GT.0.0) CALL EFVISC
      CALL OUTPUT
C
C     USUAL UPDATING
C
      DELXM=DELXP
       THETAM=THETA
      THETA=THETAP
      DO 60 J=1,400
      UM(J)=U(J)
      U(J)=UP(J)
      FINV(J)=FPINV(J)
      VM(J)=V(J)
      V(J)=VP(J)
      EV(J)=EVP(J)
      EK(J)=EKP(J)
      TM(J)=T(J)
   60 T(J)=TP(J)
      GO TO 56
C
C     DUFORT-FRANKEL SCHEME
C
   65 WRITE(6,66)
   66 FORMAT('-',15X,'DUFORT-FRANKEL SCHEME')
      N=1
      K=1
      M=1
      NA=1
      NBUOY=1
   51 DXF=DELXM/DELMIX
      WRITE(6,52) DXF
   52 FORMAT(' ','STARTING DXF=',G12.5)
   67 IF(T(1).LT.TSTART) GO TO 63
   68 DELXP=DXF*DELMIX
      ODELX=DELXP*XCONV
      WRITE(6,71) ODELX
      GO TO 61
   63 IF(K.EQ.1) GO TO 64
      GO TO 69
   64 DELXP=DELXM
      DXF=DELXP/DELTA
      GO TO 77
   69 DELXP=DXF*DELTA
      INCR=INCR1
      ODELX=DELXP*XCONV
      WRITE(6,71) ODELX
      GO TO 61
   77 DIST=X*XCONV
      HDIST=H*XCONV
      ZDIST=Z*XCONV
      WRITE(6,62) DIST,DXF,HDIST,ZDIST
   62 FORMAT('0','PRED. STARTING LENGTH=',G12.5,1X,'DXF=',G12.5,1X,
```

```
     1'ABSCISSA=',G12.5,1X,'ORDINATE=',G12.5)
      K=K+1
C
C     STABILITY CHECK
C
   61 IF(ISTAB.EQ.0) GO TO 127
   71 FORMAT(' ','DELXP=',G14.8)
      FUNC1=0.0
      DO 125 J=2,NYJ
      F1=(EV(J-1)-EV(J+1))/(2.0*DELY)
      F2=(EK(J-1)-EK(J+1))/(2.0*DELY)
      F1=ABS(V(J)+F1)
      F2=ABS(V(J)+F2)
      F1=AMAX1(F1,F2)
      F3=2.0*DELY*U(J)
      FUNC=F1/F3
      FUNC1=AMAX1(FUNC,FUNC1)
  125 CONTINUE
      DELXP1=0.5/FUNC1
      IF(DELXP.LE.(FRAC*DELXP1)) GO TO 127
      DELXP=FRAC*DELXP1
      ODELX=DELXP*XCONV
      WRITE(6,126) ODELX
  126 FORMAT(' ','STABILITY CORRECTED DELXP=',G14.8)
C
  127 IF(ABS((DELXP-DELXM)/DELXM).LE.DEC) GO TO 130
      IF(DELXP.GT.DELXM) GO TO 400
      DELXP=DELXM*(1.0-DEC)
      GO TO 401
  400 DELXP=DELXM*(1.0+DEC)
  401 ODELX=DELXP*XCONV
      WRITE(6,128) ODELX
  128 FORMAT(' ','CONSISTENCY CORRECTED DELXP=',G14.8)
  130 DELXT=DELXM+DELXP
      X=X+DELXP
  452 CALL UVEL
      DELHP=DELXP*COS(THETA)
      DELZP=DELXP*SIN(THETA)
      H=H+DELHP
      Z=Z+DELZP
      UCL=(UP(1)-UE)/(USTART-UE)
      IF(UCL.GT.0.05) GO TO 456
      DIST=X*XCONV
      HDIST=H*XCONV
      ZDIST=Z*XCONV
      WRITE(6,455) DIST,HDIST,ZDIST
  455 FORMAT(' ','ZERO MOMENTUM HEIGHT=',G12.5,1X,'ABSCISSA=',G12.5,
     1 1X,'ORDINATE=',G12.5)
      GO TO 100
  456 CALL VVEL
      CALL TEMP
   80 IF(LORT.GT.0.0) CALL EFVISC
      IN=I-NS
      II=IOUT*N
      IF(MULT.GT.0) GO TO 75
      IF(IN.EQ.II) GO TO 75
      GO TO 76
   75 CALL OUTPUT
C
C     USUAL UPDATING
```

```
   76 DO 70 J=1,400
  454 UM(J)=U(J)
      U(J)=UP(J)
      VM(J)=V(J)
      V(J)=VP(J)
      EV(J)=EVP(J)
      EK(J)=EKP(J)
      FINV(J)=FPINV(J)
      TM(J)=T(J)
   70 T(J)=TP(J)
      DELXM=DELXP
      DELHM=DELHP
      DELZM=DELZP
      THETAM=THETA
      THETA=THETAP
C
C     PUNCHING OUT VALUES
C
      IP=IPUNCH*M
      IPP=IP+1
      IF(I.EQ.IP) GO TO 110
      GO TO 74
  110 M=M+1
      WRITE(7,115) (UM(J),J=1,400)
      WRITE(7,115) (VM(J),J=1,400)
      WRITE(7,115) (TM(J),J=1,400)
      WRITE(7,115) (U(J),J=1,400)
      WRITE(7,115) (V(J),J=1,400)
      WRITE(7,115) (T(J),J=1,400)
      WRITE(7,115) (EV(J),J=1,400)
      WRITE(7,115) (EK(J),J=1,400)
      WRITE(7,115) (Y(J),J=1,400)
      WRITE(7,115) (FINV(J),J=1,400)
   74 DXF=INCR*DXF
      WRITE(6,101) INCR,DXF
  101 FORMAT(' ','INCR=',G14.8,5X,'DXF=',G14.8)
      I=I+1
      IF(DXF.GE.DXFMAX) GO TO 90
      GO TO 91
   90 DXF=DXFMAX
   91 IF(I.EQ.IPP) GO TO 96
      GO TO 95
   96 WRITE(7,115) X,H,Z,DELXM,DELHM,DELZM,THETAM,THETA,DXF,DELTA,
     1DELMIX,DELY,TDELTA,YUHALF,YTHALF
      WRITE(7,120) I,IP,K,N,NY,NYT,M,NVJ,NA
      GO TO 100
   95 IF(I.GT.IEND) GO TO 100
      GO TO 67
  100 STOP
      END
```

SUBROUTINE SDELX

This subroutine calculates the streamwise stepsize for the simple explicit scheme used to start the solution. This subroutine is called only for the first 10 or 20 steps during execution.

```
      SUBROUTINE SDELX
C
      COMMON/AREA1/U(400),UP(400),UM(400),V(400),VP(400),VM(400),T(400),
     2TP(400),TM(400),FINV(400),FPINV(400),UTEST,UE,UF,TTEST,TE,TF,REO,
     3VAXIS,LORT,USTART,AL1,AL2,BL1,BL2,TSTART,TEO,TFO,THETA,THETAM,
     4THETAP
      COMMON/AREA2/DELXP,DELXM,DELXT,DELY,DELTA,TDELTA,Y(400),I,NS,NY,
     1NYT,EV(400),EK(400),ECONV,UCONV,XCONV,TCONV,FCONV,N,DELM1X,
     2EVP(400),EKP(400),DELMP,DELZP
      COMMON/AREA3/COEFP(400),COEFM(400),SMUP(400),SMUM(400),SKCP(400),
     3SKCM(400)
      COMMON/AREA5/X,XO,H,Z,RAD,LT,STRAT
      COMMON/AREA6/CONST1,CONST2,FRAC,DXFMIN,CONST3
C
   11 Y(1)=0.0
      SMUP(1)=EV(1)+EV(2)
      SKCP(1)=EK(1)+EK(2)
      DO 4 J=2,199
      Y(J)=(J-1)*DELY
      YJ=Y(J)
      YJP=YJ+DELY
      YJM=Y(J-1)
      CC1=4.0*U(J)*YJ*DELY
  100 IF(LORT.LE.0.0) GO TO 30
      SMUP(J)=EV(J)+EV(J+1)
      SMUM(J)=EV(J)+EV(J-1)
      SKCP(J)=EK(J)+EK(J+1)
      SKCM(J)=EK(J)+EK(J-1)
   30 IF(U(J).EQ.0.0) GO TO 4
      COEFP(J)=(YJ+YJP)/(CC1*DELY)
      COEFM(J)=(YJ+YJM)/(CC1*DELY)
    4 CONTINUE
    9 IF(LORT.LE.0.0) GO TO 10
      IF(LT.EQ.0.0) GO TO 10
      GO TO 13
   10 DELXP= 5.0*DELY
      GO TO 12
   13 CC3=0.0
      DO 5 J=2,NY
      IF(LORT.LE.0.0) GO TO 22
      AL1=SMUP(J)
      AL2=SMUM(J)
      BL1=SKCP(J)
      BL2=SKCM(J)
   22 SPMAX=AMAX1(AL1,BL1)
      SMMAX=AMAX1(AL2,BL2)
      IF(CC1.EQ.0.0) GO TO 5
      CC2=(ABS(V(J)))/(U(J)*DELY)+COEFP(J)*SPMAX+COEFM(J)*SMMAX
      CC3=AMAX1(CC2,CC3)
    5 CONTINUE
   25 DELXP1=0.5/CC3
    6 IF(DELXP1.GT.( 0.9*DELXP)) GO TO 14
    8 DELXP=DELXP1
      GO TO 12
   14 DELXP= 0.9*DELXP
   12 RETURN
      END
```

SUBROUTINE UVEL

This subroutine calculates the axial velocity components $U_{i+1,j}$ for all j's by solving the finite-difference forms (simple explicit and DuFort-Frankel) of the s-momentum equation and determines the jet growth in terms of half-radius and nominal plume boundary. θ_{i+1} is also evaluated here from the y-momentum equation.

```
      SUBROUTINE UVEL
C
      DIMENSION  DER(400)
      COMMON/AREA1/U(400),UP(400),UM(400),V(400),VP(400),VM(400),T(400),
     2TP(400),TM(400),FINV(400),FPINV(400),UTEST,UE,UF,TTEST,TE,TF,REO,
     3VAXIS,LORT,USTART,AL1,AL2,BL1,BL2,TSTART,TEO,TFO,THETA,THETAM,
     4THETAP
      COMMON/AREA2/DELXP,DELXM,DELXT,DELY,DELTA,TDELTA,Y(400),I,NS,NY,
     1NYT,EV(400),EK(400),ECONV,UCONV,XCONV,TCONV,FCONV,N,DELMIX,
     2EVP(400),EKP(400),DELHP,DELZP
      COMMON/AREA3/COEFP(400),COEFM(400),SMUP(400),SMUM(400),SKCP(400),
     3SKCM(400)
      COMMON/AREA7/YUHALF,YTHALF,YMAX,YCORE
      COMMON/AREA9/JCORE,JJ,JINFL
      COMMON/AREA10/NYJ,NAVG,NBUOY
C
      L=1
      K=1
      M=1
      IM=1
      IF(I.GT.NS) GO TO 20
C
C     SIMPLE EXPLICIT EQUATIONS
C
      DO 19 J=2,199
      UJ=U(J)
      UJP=U(J+1)
      UJM=U(J-1)
      YJ=Y(J)
      VJ=V(J)
      IF(LORT.LE.0.0) GO TO 9
      AL1=SMUP(J)
      AL2=SMUM(J)
      VT=VJ*DELY
      SMUP(J)=0.5*(AL1+ABS(VT)+ABS(AL1-ABS(VT)))
      SMUM(J)=0.5*(AL2+ABS(VT)+ABS(AL2-ABS(VT)))
    9 IF(VJ.GT.0.0) GO TO 11
   10 UP(J)=UJ-DELXP*VJ*(UJP-UJ)/(DELY*UJ+DELXP* (COEFP(J)*SMUP(J)*
     1(UJP-UJ)-COEFM(J)*SMUM(J)*(UJ-UJM))+DELXP*SIN(THETA)*FINV(J)/(UJ*
     2REO)
      GO TO 34
   11 UP(J)=UJ-DELXP*VJ*(UJ-UJM)/(DELY*UJ+DELXP* (COEFP(J)*SMUP(J)*
     2(UJP-UJ)-COEFM(J)*SMUM(J)*(UJ-UJM))+DELXP*SIN(THETA)*FINV(J)/(UJ*
     2REO)
   34 UPJ=UP(J)
C
C     INCORPORATING BOUNDARY CONDITION
C
      IF(K.GT.1) GO TO 30
      GO TO 12
   30 IF(K.GT.2) GO TO 31
      UP(1)=(4.0*UP(2)-UP(3))/3.0
C
C     CALCULATING YUHALF
C
   31 IF(M.GT.1) GO TO 12
      UPMEAN=(UP(1)+UF)/2.0
      IF(UPJ.LE.UPMEAN) GO TO 32
      GO TO 12
   32 JJ=J
```

```
      JM=J-1
      UPJJ=UP(JJ)
      UPJM=UP(JM)
      YJJ=(JJ-1)*DELY
      YJM=(JM-1)*DELY
      YUHALF=YJM+((YJJ-YJM)/(UPJJ-UPJM))*(UPMEAN-UPJM)
      M=M+1
   12 K=K+1
C
C     CALCULATING YCORE
C
      IF(K.LT.3) GO TO 19
      IF(L.GT.1) GO TO 13
      IF(UPJ.LT.(0.9999*UP(1))) GO TO 14
      GO TO 13
   14 YCORE=(J-1)*DELY
      JCORE=J
      L=L+1
   13 IF(K.LT.3) GO TO 19
      UTEST=(UP(1)-UPJ)/(UP(1)-UF)
      IF(UTEST.GE.0.99   ) GO TO 27
   19 CONTINUE
C
      GO TO 29
C     DUFORT-FRANKEL EQUATIONS
   20 SMUP(1)=EV(1)+EV(2)
      DO 26 J=2,399
    5 YJ=Y(J)
      UJ=U(J)
      VJ=V(J)
      UJP=U(J+1)
      UJM=U(J-1)
      UMJ=UM(J)
      IF(LORT.LE.0.0) GO TO 25
      SMUP(J)=EV(J)+EV(J+1)
      SMUM(J)=EV(J)+EV(J-1)
      AL1=SMUP(J)
      AL2=SMUM(J)
      VT=VJ*DELY
      SMUP(J)=0.5*(AL1+ABS(VT)+ABS(AL1-ABS(VT)))
      SMUM(J)=0.5*(AL2+ABS(VT)+ABS(AL2-ABS(VT)))
   25 UA=UJ/DELXT
      UB=(Y(J+1)+YJ)*SMUP(J)/(8.0*YJ*DELY*DELY)
      UC=(YJ+Y(J-1))*SMUM(J)/(8.0*YJ*DELY*DELY)
      UD=UMJ*UA
      UH=-VJ*(UJP-UJM)/(2.0*DELY)
      UI=(UJP-0.5*UMJ)*UB*2.0
      UG=(UJM-0.5*UMJ)*UC*2.0
      UK=SIN(THETA)*FINV(J)/REO
C
      UP(J)=(UD+UH+UI+UG+UK)/(UA+UB+UC)
      UPJ=UP(J)
      IF(UPJ.GE.UF) GO TO 125
      UP(J)=UF
C
C     INCORPORATING BOUNDARY CONDITION
C
  125 IF(K.GT.1) GO TO 40
      GO TO 33
   40 IF(K.GT.2) GO TO 41
```

```
      UP(1)=(4.0*UP(2)-UP(3))/3.0
C
C     CALCULATING YUHALF
C
   41 IF(M.GT.1) GO TO 33
      UPMEAN=(UP(1)+UF)/2.0
      IF(UPJ.LE.UPMEAN) GO TO 42
      GO TO 33
   42 JJ=J
      JM=J-1
      UPJJ=UP(JJ)
      UPJM=UP(JM)
      YJJ=(JJ-1)*DELY
      YJM=(JM-1)*DELY
      YUHALF=YJM+((YJJ-YJM)/(UPJJ-UPJM))*(UPMEAN-UPJM)
      M=M+1
   33 K=K+1
      IF(K.LT.3) GO TO 22
      IF(UP(1).LT.U(1)) GO TO 22
C
C     CALCULATING YCORE
C
   21 IF(L.GT.1) GO TO 22
      JM=J-1
      UPJM=UP(JM)
      IF(UPJM.LT.(0.9999*UP(1))) GO TO 24
      GO TO 22
   24 YCORE=(JM-1)*DELY
      JCORE=JM
      L=L+1
   22 IF(K.LT.4) GO TO 26
      UTEST=(UP(1)-UP(J))/(UP(1)-UF)
C
C     CALCULATING INFLEXION
      DER(J-1)=ABS(UPJ-UP(J-2))
      DER(J-2)=ABS(UP(J-1)-UP(J-3))
      IF(IM.GT.1) GO TO 100
      IF(DER(J-1).LT.DER(J-2)) GO TO 105
      GO TO 100
  105 JINFL=J-2
      IM=IM+1
C
  100 IF(UTEST.GE.0.99   ) GO TO 27
   26 CONTINUE
   27 DELTM=DELTA
      NYO=NYT
      DELTA=(J-1)*DELY
       DELMIX=DELTA-YCORE
   35 NY=J
      UP(NY+1)=UF
      UP(NY+2)=UF
      NNY=NY+3
      DO 28 J=NNY,400
      EVP(J)=1.0
   28 UP(J)=UF
C
C     BOUNDARY CONDITIONS
C
      VP(1)=VAXIS
C
```

```
      IF(I.LE.NS) GO TO 36
      NY1=NYO/2
      NY2=(NYO+1)/2
      IF(NY1.EQ.NY2) GO TO 43
      NJ=NYO
      GO TO 44
   43 NJ=NYO+1
   44 SUM1=0.0
      SUM2=0.0
      COEF=2.0*(DELY/3.0)
      DO 45 J=1,NJ,2
      TERM1=U(J)*U(J)*Y(J)+4.0*U(J+1)*U(J+1)*Y(J+1)+U(J+2)*U(J+2)*Y(J+2)
      TERM2=FINV(J)*Y(J)+4.0*FINV(J+1)*Y(J+1)+FINV(J+2)*Y(J+2)
      SUM1=SUM1+TERM1
      SUM2=SUM2+TERM2
   45 CONTINUE
      DEL1=SUM1*COEF
      DEL2=SUM2*COEF
      THETAP=THETAM+DELXT*COS(THETA)*DEL2/(DEL1*REO)
      GO TO 29
C
   36 THETAP=THETA
C
   29 RETURN
      END
```

SUBROUTINE VVEL

The lateral velocity components $V_{i+1,j+1}$ are evaluated here for all j's by solving the finite-difference forms (simple explicit and DuFort-Frankel) of the continuity equation.

```
      SUBROUTINE VVEL
C
      COMMON/AREA1/U(400),UP(400),UM(400),V(400),VP(400),VM(400),T(400),
     2TP(400),TM(400),FINV(400),FPINV(400),UTEST,UE,UF,TTEST,TE,TF,REO,
     3VAXIS,LORT,USTART,AL1,AL2,BL1,BL2,TSTART,TEO,TFO,THETA,THETAM,
     4THETAP
      COMMON/AREA2/DELXP,DELXM,DELXT,DELY,DELTA,TDELTA,Y(400),I,NS,NY,
     1NYT,EV(400),EK(400),ECONV,UCONV,XCONV,TCONV,FCONV,N,DELMIX,
     2EVP(400),EKP(400),DELHP,DELZP
C
      IF(I.GT.NS) GO TO 20
C
C     SIMPLE EXPLICIT EQUATIONS
C
      DO 10 J=1,399
      YJ=Y(J)
      YJP=YJ+DELY
   10 VP(J+1)=YJ*VP(J)/YJP -(DELY/(4.0*DELXP*YJP))*(YJP+YJ)*(UP(J+1)+
     1UP(J)-U(J+1)-U(J))
      GO TO 25
C
C     DUFORT-FRANKEL EQUATIONS
C
   20 DO 21 J=1,399
      YJ=Y(J)
      YJP=YJ+DELY
   21 VP(J+1)=YJ*VP(J)/YJP-(DELY/(4.0*DELXT*YJP))*(YJP+YJ)*(UP(J+1)+
     2UP(J)-UM(J+1)-UM(J))
   25 RETURN
      END
```

SUBROUTINE TEMP

This subroutine calculates the temperatures in the plume $T_{i+1,j}$ for all j's by solving the finite-difference forms (simple explicit and DuFort-Frankel) of the energy equation. The zero buoyancy height in case of stratified ambient is evaluated here.

```
      SUBROUTINE TEMP
C
      COMMON/AREA1/U(400),UP(400),UM(400),V(400),VP(400),VM(400),T(400),
     2TP(400),TM(400),FINV(400),FPINV(400),UTEST,UE,UF,TTEST,TE,TF,REO,
     3VAXIS,LORT,USTART,AL1,AL2,BL1,BL2,TSTART,TEO,TFO,THETA,THETAM,
     4THETAP
      COMMON/AREA2/DELXP,DELXM,DELXT,DELY,DELTA,TDELTA,Y(400),I,NS,NY,
     1NYT,EV(400),EK(400),ECONV,UCONV,XCONV,TCONV,FCONV,N,DELMIX,
     2EVP(400),EKP(400),DELHP,DELZP
      COMMON/AREA3/COEFP(400),COEFM(400),SMUP(400),SMUM(400),SKCP(400),
     3SKCM(400)
      COMMON/AREA4/XL,ANU,PRT,HTK,DENS,CP,ALPHA
      COMMON/AREA5/X,XO,H,Z,RAD,LT,STRAT
      COMMON/AREA7/YUHALF,YTHALF,YMAX,YCORE
      COMMON/AREA10/NYJ,NAVG,NBUOY
C
      K=1
      M=1
      TF=STRAT*Z
      TE=TF
    6 IF(I.GT.NS) GO TO 20
C
C     SIMPLE EXPLICIT EQUATIONS
C
      DO 19 J=2,199
      TJ=T(J)
      TJP=T(J+1)
      TJM=T(J-1)
      YJ=Y(J)
      YJP=YJ+DELY
      YJM=Y(J-1)
      IF(LORT.LE.0.0) GO TO 9
      BL1=SKCP(J)
      BL2=SKCM(J)
    9 TP(J)=TJ-DELXP*V(J)*(TJ-TJM)/(DELY*U(J))+DELXP* (COEFP(J)*  BL1   *
     1(TJP-TJ)-COEFM(J)* BL2 *(TJ-TJM))
      FPINV(J)=(TP(J)-TF)/FCONV
      TPJ=TP(J)
C
C     INCORPORATING BOUNDARY CONDITION
C
      IF(K.GT.1) GO TO 30
      GO TO 12
   30 IF(K.GT.2) GO TO 31
      TP(1)=(4.0*TP(2)-TP(3))/3.0
      FPINV(1)=(TP(1)-TF)/FCONV
C
C     CALCULATING YTHALF
C
   31 IF(M.GT.1) GO TO 12
      TPMEAN=(TP(1)+TE)/2.0
      IF(TPJ.LE.TPMEAN) GO TO 32
      GO TO 12
   32 JJ=J
      JM=J-1
      TPJJ=TP(JJ)
      TPJM=TP(JM)
      YJJ=(JJ-1)*DELY
      YJM=(JM-1)*DELY
      YTHALF=YJM+((YJJ-YJM)/(TPJJ-TPJM))*(TPMEAN-TPJM)
```

```
      M=M+1
   12 K=K+1
      IF(K.LT.3) GO TO 19
      TTEST=(TP(1)-TPJ)/(TP(1)-TF)
      IF(TTEST.GE.0.99) GO TO 27
   19 CONTINUE
      GO TO 27
C
C     DUFORT-FRANKEL EQUATIONS
C
   20 SKCP(1)=EK(1)+EK(2)
      DO 26 J=2,399
      YJ=Y(J)
      TJ=T(J)
      TJP=T(J+1)
      TJM=T(J-1)
      TMJ=TM(J)
      IF(LORT.LE.0.0) GO TO 25
      SKCP(J)=EK(J)+EK(J+1)
      SKCM(J)=EK(J)+EK(J-1)
      BL1=SKCP(J)
      BL2=SKCM(J)
   25 TA=U(J)/DELXT
      TB=(Y(J+1)+YJ)*  BL1  /(8.0*YJ*DELY*DELY)
      TC=(YJ+Y(J-1))*  BL2  /(8.0*YJ*DELY*DELY)
      TD=TMJ*TA
      TH=-V(J)*(TJP-TJM)/(2.0*DELY)
      TI=(TJP-0.5*TMJ)*TB*2.0
      TG=(TJM-0.5*TMJ)*TC*2.0
C
      TP(J)=(TD+TH+TI+TG)/(TA+TB+TC)
      FPINV(J)=(TP(J)-TF)/FCONV
      TPJ=TP(J)
      IF(TPJ.GE.TEO) GO TO 125
      TP(J)=TEO
C
C     INCORPORATING BOUNDARY CONDITION
C
  125 IF(K.GT.1) GO TO 40
      GO TO 33
   40 IF(K.GT.2) GO TO 21
      TP(1)=(4.0*TP(2)-TP(3))/3.0
      FPINV(1)=(TP(1)-TF)/FCONV
C
C     CALCULATING YTHALF
   21 IF((TP(1)-TF).GT.0.01) GO TO 41
      GO TO 33
C
   41 IF(M.GT.1) GO TO 33
      TPMEAN=(TP(1)+TE)/2.0
      IF(TPJ.LE.TPMEAN) GO TO 42
      GO TO 33
   42 JJ=J
      JM=J-1
      TPJJ=TP(JJ)
      TPJM=TP(JM)
      YJJ=(JJ-1)*DELY
      YJM=(JM-1)*DELY
      YTHALF=YJM+((YJJ-YJM)/(TPJJ-TPJM))*(TPMEAN-TPJM)
      M=M+1
```

```
33 K=K+1
   IF(K.LT.3) GO TO 26
   IF(TP(1).LT.TSTART) GO TO 45
   GO TO 46
45 YCORE=0.0
   JCORE=1
46 TTEST=(TP(1)-TP(J))/(TP(1)-TF)
   IF(TTEST.GE.0.99) GO TO 27
26 CONTINUE
27 TDELTA=(J-1)*DELY
   DELMIX=DELTA-YCORE
35 NYT=J
36 TP(NYT+1)=TF
   TP(NYT+2)=TF
   FPINV(NYT+1)=(TP(NYT+1)-TF)/FCONV
   FPINV(NYT+2)=(TP(NYT+2)-TF)/FCONV
   NNYT=NYT+3
   DO 28 J=NNYT,400
   FPINV(J)=0.0
   EKP(J)=ALPHA
28 TP(J)=TF
   UCL=(UP(1)-UE)/(USTART-UE)
   WRITE(6,5) TF,TP(1),UCL
 5 FORMAT(' ','TSTREAM=',G12.5,3X,'TCENTER=',G12.5,3X,'UCENTER=',
  1G12.5)
29 IF((TP(1)-TF).LE.0.01) GO TO 49
   GO TO 60
49 IF(NBUOY.EQ.1) GO TO 50
   GO TO 60
50 DIST=X*XCONV
   HDIST=H*XCONV
   ZDIST=Z*XCONV
   WRITE(6,51) DIST,HDIST,ZDIST
51 FORMAT('0','ZERO BUOYANCY HT.=',G12.5,1X,'ABSCISSA=',G12.5,1X,
  1'ORDINATE=',G12.5)
   NBUOY=NBUOY+1
60 RETURN
   END
```

SUBROUTINE EFVISC

This subroutine computes the effective viscosities and thermal diffusivities appearing in the s-momentum and energy equations, respectively. Different models for the turbulent transport can be incorporated into the calculation method simply by altering this subroutine.

```
      SUBROUTINE EFVISC
C
      DIMENSION  FUNC(400)
      COMMON/AREA1/U(400),UP(400),UM(400),V(400),VP(400),VM(400),T(400),
     2TP(400),TM(400),FINV(400),FPINV(400),UTEST,UE,UF,TTEST,TE,TF,REO,
     3VAXIS,LORT,USTART,AL1,AL2,BL1,BL2,TSTART,TEO,TFO,THETA,THETAM,
     4THETAP
      COMMON/AREA2/DELXP,DELXM,DELXT,DELY,DELTA,TDELTA,Y(400),I,NS,NY,
     1NYT,EV(400),EK(400),ECONV,UCONV,XCONV,TCONV,FCONV,N,DELMIX,
     2EVP(400),EKP(400),DELHP,DELZP
      COMMON/AREA4/XL,ANU,PRT,HTK,DENS,CP,ALPHA
      COMMON/AREA5/X,XO,H,Z,RAD,LT,STRAT
      COMMON/AREA6/CONST1,CONST2,FRAC,DXFMIN,CONST3,CONST4
      COMMON/AREA7/YUHALF,YTHALF,YMAX,YCORE
      COMMON/AREA8/TC1,TC2,FRNO
      COMMON/AREA9/JCORE,JJ,JINFL
      COMMON/AREA10/NYJ,NAVG,NBUOY
    9 FRNO=UP(1)*UP(1)*RAD/(USTART*USTART*DELTA*FPINV(1))
      G=32.2
      TC3=TC1+460.0
      FRI=(G*ANU*TC2)/(TC3*UCONV*UCONV*UCONV)
      RI=FRI*((TF-TP(1))*DELTA)/(UP(1)*UP(1))
      WRITE(6,3)  RI
    3 FORMAT(' ','RICH NO=',G10.3)
   30 IF(NY.GT.NYT) GO TO 35
      GO TO 36
   35 NYJ=NY
      GO TO 4
   36 NYJ=NYT
    4 IF(TP(1).LT.TSTART) GO TO 8
    5 XL=CONST1*DELMIX
      GO TO 40
    8 FBUOY=(1.0-CONST3*RI*COS(THETA))**0.25
      EV2=(CONST2*YUHALF*UP(1))*FBUOY*FBUOY
      EK2=EV2*1/PRT
      NYJ2=NYJ+2
      DO 20 J=1,NYJ2
      GAMMA=1.0
   15 EVP(J)=EV2*GAMMA
      EKP(J)=EK2*GAMMA
   20 CONTINUE
      GO TO 50
   40 EVP(1)=1.0
      EKP(1)=ALPHA
      NYJ2=NYJ+2
      DO 45 J=2,NYJ2
      UGRAD=(UP(J+1)-UP(J-1))/(2.0*DELY)
   44 EVP(J)=1.0+(XL*XL)*ABS(UGRAD)
      EVPJ=EVP(J)
      EKP(J)=ALPHA+(EVPJ-1.0)*1/PRT
   45 CONTINUE
   50 RETURN
      END
```

SUBROUTINE OUTPUT

Here all the important numerical results are printed out in the form most suited for comparisons.

```
      SUBROUTINE OUTPUT
C
      COMMON/AREA1/U(400),UP(400),UM(400),V(400),VP(400),VM(400),T(400),
     2TP(400),TM(400),FINV(400),FPINV(400),UTEST,UE,UF,TTEST,TE,TF,REO,
     3VAXIS,LORT,USTART,AL1,AL2,BL1,BL2,TSTART,TEO,TFO,THETA,THETAM,
     4THETAP
      COMMON/AREA2/DELXP,DELXM,DELXT,DELY,DELTA,TDELTA,Y(400),I,NS,NY,
     1NYT,EV(400),EK(400),ECONV,UCONV,XCONV,TCONV,FCONV,N,DELMIX,
     2EVP(400),EKP(400),DELHP,DELZP
      COMMON/AREA5/X,XO,H,Z,RAD,LT,STRAT
      COMMON/AREA6/CONST1,CONST2,FRAC,DXFMIN,CONST3
      COMMON/AREA7/YUHALF,YTHALF,YMAX,YCORE
      COMMON/AREA8/TC1,TC2,FRNO
C
      N=N+1
      NNY=NY+1
      NNYT=NYT+1
      IF(NNY.GE.NNYT) GO TO 22
      GO TO 23
   22 NNJ=NNY
      GO TO 24
   23 NNJ=NNYT
   24 WRITE(6,10)
   10 FORMAT('0')
      DIST=X*XCONV
      HDIST=H*XCONV
      ZDIST=Z*XCONV
      DDEL=DELTA*XCONV
      DTDEL=TDELTA*XCONV
      XBAR=X/(2.0*RAD)
      HBAR=H/(2.0*RAD)
      ZBAR=Z/(2.0*RAD)
      WRITE(6,15) I,DIST,DDEL,DTDEL,HDIST,ZDIST
   15 FORMAT(' ',1X,'I=',I4,2X,'X DIST=',G10.3,2X,'HALF-WIDTH=',G10.3,
     12X,'THERML HF-WIDTH=',G10.3,2X,'ABSCISSA=',G10.3,2X,'ORDINATE=',
     2G10.3)
      RUHALF=YUHALF/RAD
      RTHALF=YTHALF/RAD
      UCL=(UP(1)-UE)/(USTART-UE)
      TCL=TP(1)
      ANGLE=THETA*(180.*7./22.)
      WRITE(6,16) XBAR,HBAR,ZBAR,RUHALF,RTHALF,UCL,TCL,FRNO,ANGLE
   16 FORMAT('0',2X,'XBAR=',G10.3,1X,'HBAR=',G10.3,1X,'ZBAR=',G10.3,1X,
     1'RUHLF=',G10.3,1X,'RTHLF=',G10.3,1X,'UCL=',G10.3,1X,'TCL=',G10.3,/
     22X,'FR NO=',G10.3,1X,'THETA(DEG)=',G10.3)
      FEV2=CONST2*YUHALF*UP(1)
      DFEV=FEV2*ECONV
      DEV=EVP(1)*ECONV
      WRITE(6,20) DFEV,DEV
   20 FORMAT('0',2X,'VISC1=',G10.3,2X,'VISC2=',G10.3)
   18 WRITE(6,21)
   21 FORMAT(' ',7X,'J',5X,'Y DISTANCE',7X,'U VELO',8X,'V VELO',
     18X,'VISCOSITY',4X,'JET TEMP',6X,'CONDUCTIVITY')
      DO 40 J=1,NNJ
      DUJ=UP(J)*UCONV
      DVJ=VP(J)*UCONV
      DTJ=TP(J)*TC2+TC1
      DEVJ=EVP(J)*ECONV
      DEKJ=EKP(J)*ECONV
      YDIST=Y(J)*XCONV
```

```
      WRITE(6,26) J,YDIST,DUJ,DVJ,DEVJ,DTJ,DEKJ
   26 FORMAT(' ',5X,I3,5X,G12.5,3X,G12.5,3X,G12.5,3X,G12.5,3X,G12.5,3X,
     1G12.5)
   40 CONTINUE
      RETURN
      END
```

11. APPENDIX B:

DERIVATION OF THE GOVERNING EQUATIONS

11.1. The General Equations in Vector Form

The basic equations governing the development of the jet as it moves through the ambient are the conservation equations of mass, momentum and energy. In general vector form, they can be written as [94,95]:

$$\frac{\partial \rho}{\partial \tau} + \nabla \cdot (\rho \vec{v}) = 0 \tag{B.1}$$

$$\rho \frac{D\vec{v}}{D\tau} = \rho \vec{F} - \nabla p + \nabla \cdot (\mu \nabla \vec{v}) \tag{B.2}$$

$$\rho c_p \frac{Dt}{D\tau} = \nabla \cdot (k \nabla t) + \beta T_a \frac{Dp}{D\tau} + \mu \Phi \tag{B.3}$$

In this appendix, τ refers to time. Elsewhere in this work, τ refers to the overall shear stress appearing in the s-momentum equation (see Chapter 3). Φ is the dissipation function, and T_a is the fluid temperature in degrees absolute.

By the definition of substantial derivative,

$$\frac{D\vec{v}}{D\tau} = \frac{\partial \vec{v}}{\partial \tau} + \vec{v} \cdot (\nabla \vec{v})$$

$$\frac{Dt}{D\tau} = \frac{\partial t}{\partial \tau} + \vec{v} \cdot (\nabla t)$$

$$\frac{Dp}{D\tau} = \frac{\partial p}{\partial \tau} + \vec{v} \cdot (\nabla p) \tag{B.4}$$

Equations (B.1) to (B.3) can be simplified based on the assumptions listed in Chapter 2. For steady flow, $\frac{\partial ( )}{\partial \tau} = 0$.

For a Boussinesq fluid, ρ is assumed constant except in the buoyancy term, thus

$\nabla \cdot (\rho\vec{v}) = \rho \nabla \cdot \vec{v}$ and Eq. (B.1)

simplifies to

$$\nabla \cdot \vec{v} = 0 \tag{B.5}$$

The term $\vec{v} \cdot (\nabla p)$ in Eq. (B.3) depends on both velocity and pressure gradient. Pressure gradients are neglected within the jet flow (boundary layer assumption), and outside the jet boundaries, the pressure gradient is purely hydrostatic. Also, since the ambient flow velocity is always zero in the direction of the earth's gravity, $\vec{v} \cdot (\nabla p)$ can be eliminated. Further, viscous dissipation is assumed negligible.

Thus, Eq. (B.3) reduces to

$$\rho c_p \vec{v} \cdot (\nabla t) = \nabla \cdot (k \nabla t) \tag{B.6}$$

The body force term in Eq. (B.2) is

$$\rho\vec{F} = \rho\vec{g}$$

and the pressure gradient, assumed purely hydrostatic (due to the weight of the ambient fluid), is

$$\nabla p = \rho_\infty \vec{g}$$

Thus, Eq. (B.2) reduces to

$$\rho\vec{v} \cdot (\nabla\vec{v}) = (\rho - \rho_\infty)\vec{g} + \nabla \cdot (\mu \nabla\vec{v}) \tag{B.7}$$

Equations (B.5) to (B.7) are in terms of the gradient and divergence. These vector differential operators have to be defined for the curvilinear orthogonal co-ordinate system.

11.2. Differential Operators in Terms of s, y, ϕ

This section will follow the approach given in Hirst [10].

The scale factors, h_s, h_y, and h_ϕ, are:

$$h_s = \frac{\partial \vec{R}}{\partial s} \cdot \vec{i}_s$$

$$h_y = \frac{\partial \vec{R}}{\partial y} \cdot \vec{i}_y$$

$$h_\phi = \frac{\partial \vec{R}}{\partial \phi} \cdot \vec{i}_\phi \qquad \text{(B.8)}$$

where $\vec{R} = s\vec{i}_s + y\vec{i}_y$ is the position vector of any point in the jet. The scale factors relate the differential distances to the differentials of the co-ordinates. These will be evaluated in terms of the cartesion co-ordinate system for which the scale factors are constant.

The relationships among the unit vectors in the cartesion and curvilinear co-ordinate systems as applied to the configuration of Chapter 6, are [10]:

$$\vec{i}_s = \vec{i}\cos\theta + \vec{k}\sin\theta$$

$$\vec{i}_y = \vec{i}(-\sin\phi\sin\theta) + \vec{j}\cos\phi + \vec{k}\sin\phi\cos\theta$$

$$\vec{i}_\phi = \vec{i}(-\cos\phi\sin\theta) + \vec{j}(-\sin\phi) + \vec{k}\cos\phi\cos\theta \qquad \text{(B.9)}$$

Using Eqs. (B.8), (B.9) and the definition of $\vec{R}$, the scale factors are evaluated as:

$$h_s = 1 - e \qquad \text{where } e = y\frac{d\theta}{ds}\sin\phi \qquad \text{(B.10)}$$

$$h_y = 1$$

$$h_\phi = y$$

From [10,96], the gradient of a scalar is

$$\nabla a = \frac{1}{h_s}\frac{\partial a}{\partial s}\vec{i}_s + \frac{1}{h_y}\frac{\partial a}{\partial y}\vec{i}_y + \frac{1}{h_\phi}\frac{\partial a}{\partial \phi}\vec{i}_\phi \tag{B.11}$$

where a is any scalar, and the divergence of a vector $\vec{a}$ is:

$$\nabla \cdot \vec{a} = \frac{1}{h_s h_y h_\phi}\left[\frac{\partial}{\partial s}(h_y h_\phi a_s) + \frac{\partial}{\partial y}(h_\phi h_s a_y) + \frac{\partial}{\partial \phi}(h_s h_y a_\phi)\right]$$

$$\text{where } \vec{a} = a_s\vec{i}_s + a_y\vec{i}_y + a_\phi\vec{i}_\phi \tag{B.12}$$

Substituting the scale factor expressions into Eqs. (B.11) and (B.12) yields:

$$\nabla a = \frac{1}{1-e}\frac{\partial a}{\partial s}\vec{i}_s + \frac{\partial a}{\partial y}\vec{i}_y + \frac{1}{y}\frac{\partial a}{\partial \phi}\vec{i}_\phi \tag{B.13}$$

$$\nabla \cdot \vec{a} = \frac{1}{1-e}\frac{\partial a_s}{\partial_s} + \frac{1}{y}\frac{\partial (y a_y)}{\partial y} + \frac{1}{y}\frac{\partial a_\phi}{\partial \phi} - \frac{a_y}{1-e}\left[\frac{e}{y}\right] - \frac{a_\phi}{1-e}\left[\frac{1}{y}\frac{\partial e}{\partial \phi}\right] \tag{B.14}$$

11.3. The Equations in Terms of s, y, ϕ

If u, v, w are the components of $\vec{v}$ in the s, y, and ϕ directions, respectively, Eq. (B.7) can be written for each co-ordinate direction, as:

s-momentum [Eq. (B.7) $\cdot \frac{\vec{i}_s}{\rho}$]:

$$\vec{v} \cdot (\nabla u) = \frac{-(\rho - \rho_\infty)}{\rho} g\vec{k} \cdot \vec{i}_s + \nabla \cdot \left(\frac{\mu}{\rho}\nabla u\right)$$

i.e., $$\vec{v} \cdot (\nabla u) = \frac{-(\rho - \rho_\infty)}{\rho_o} g \sin\theta + \nabla \cdot (\frac{\mu}{\rho} \nabla u) \qquad (B.15)$$

The Boussinesq assumption for density permits $\frac{(\rho - \rho_\infty)}{\rho}$ to be written as $\frac{(\rho - \rho_\infty)}{\rho_o}$.

y-momentum [Eq. (B.7) $\cdot \frac{\vec{i}_y}{\rho}$]:

$$\vec{v} \cdot (\nabla v) = \frac{-(\rho - \rho_\infty)}{\rho_o} g \sin\phi \cos\theta + \nabla \cdot (\frac{\mu}{\rho} \nabla v) \qquad (B.16)$$

ϕ-momentum [Eq. (B.7) $\cdot \frac{\vec{i}_\phi}{\rho}$]:

$$\vec{v} \cdot (\nabla w) = \frac{-(\rho - \rho_\infty)}{\rho_o} g \cos\phi \cos\theta + \nabla \cdot (\frac{\mu}{\rho} \nabla w) \qquad (B.17)$$

Now, substituting Eqs. (B.13) and (B.14) into Eqs. (B.5), (B.6), (B.15) to (B.17) and using the axisymmetric assumption that $w = 0$ and $\frac{\partial(\,)}{\partial\phi} = 0$, yields:

Continuity:

$$\frac{1}{1-e} \frac{\partial u}{\partial s} + \frac{1}{y} \frac{\partial}{\partial y}(vy) - \frac{v}{1-e} \frac{e}{y} = 0 \qquad (B.18)$$

s-momentum:

$$\frac{u}{1-e} \frac{\partial u}{\partial s} + v \frac{\partial u}{\partial y} = \frac{(\rho_\infty - \rho)}{\rho_o} g \sin\theta + \frac{1}{(1-e)y} \left[\frac{\partial}{\partial s} \left(\frac{y\nu}{1-e} \frac{\partial u}{\partial s} \right) + \frac{\partial}{\partial y} \left(y\nu(1-e) \frac{\partial u}{\partial y} \right) \right] \qquad (B.19)$$

y-momentum:

$$\frac{u}{1-e}\frac{\partial v}{\partial s} + v\frac{\partial v}{\partial y} = \frac{(\rho_\infty - \rho)}{\rho_o} g \sin\phi\cos\theta + \frac{1}{(1-e)y}\left[\frac{\partial}{\partial s}\left(\frac{y\nu}{1-e}\frac{\partial v}{\partial s}\right) + \frac{\partial}{\partial y}\left(y\nu(1-e)\frac{\partial v}{\partial y}\right)\right] \tag{B.20}$$

The ϕ-momentum equation is no longer necessary because of the axisymmetric assumption.

Energy:

$$\frac{u}{1-e}\frac{\partial t}{\partial s} + v\frac{\partial t}{\partial y} = \rho c_p \frac{1}{(1-e)y}\left[\frac{\partial}{\partial s}\left(\frac{yk}{1-e}\frac{\partial t}{\partial s}\right) + \frac{\partial}{\partial y}\left(yk(1-e)\frac{\partial t}{\partial y}\right)\right] \tag{B.21}$$

Making further use of the boundary layer assumption that gradients in the streamwise direction are negligible compared to those in the cross-stream direction [39,97], the leading term on the right hand side of Eqs. (B.19) to (B.21) can be neglected. Since molecular action is negligible in turbulent jet flow, except near the nozzle where gradients in the streamwise direction are extremely small and sharp gradients in the cross-stream direction can be expected, this procedure is further justified.

To eliminate any ϕ terms in the equations, Eqs. (B.18), (B.19), (B.21) are integrated with respect to ϕ from 0 to 2π (after multiplying by $(1-e)$). This yields

Continuity:

$$\frac{\partial u}{\partial s} + \frac{1}{y}\frac{\partial}{\partial y}(vy) = 0 \tag{B.22}$$

s-momentum:

$$u\frac{\partial u}{\partial s} + v\frac{\partial u}{\partial y} = \frac{(\rho_\infty - \rho)}{\rho_o} g \sin\theta + \frac{1}{y}\frac{\partial}{\partial y}\left(y\nu\frac{\partial u}{\partial y}\right) \tag{B.23}$$

Energy:

$$u\frac{\partial t}{\partial s} + v\frac{\partial t}{\partial y} = \frac{1}{\rho c_p y}\frac{\partial}{\partial y}\left(yk\frac{\partial t}{\partial y}\right) \tag{B.24}$$

To obtain a simple form for Eq. (B.20), the equation is multiplied by $(1 - e)\sin\phi$ and then integrated. This gives

y-momentum:

$$\left(u^2 - \frac{vy}{2}\frac{\partial v}{\partial y}\right)\frac{d\theta}{ds} = \frac{(\rho_\infty - \rho)}{\rho_o} g \cos\theta \,. \tag{B.25}$$

11.4. The Equations for Turbulent Flow

So far, the derivation has not explicitly included the effects of turbulence, and the equations are equally valid for laminar and turbulent flows. According to Cebeci and Smith [97], although turbulent shear flows generally spread more rapidly than the corresponding laminar flows at the same Reynolds number, it is found empirically that Prandtl's boundary-layer approximations are also fairly good in turbulent cases and become better as Reynolds number increases.

Equations (B.22) to (B.25) will now be written for turbulent flow in terms of average and fluctuating quantities, that is

$$a = \bar{a} + a'$$

where $\bar{a}$ is the time-averaged value of a dependent variable a, defined as

$$\bar{a} = \lim_{\tau \to \infty} \left(\frac{1}{2\tau} \int_{-\tau}^{+\tau} a \, d\tau \right),$$

and a' is the fluctuating component of a. Substituting average and fluctuating components for the dependent variables u, v, t in Eqs. (B.22) to (B.25), and time averaging the equations remembering that

$$\bar{\bar{a}} = \bar{a}, \qquad \overline{a+b} = \bar{a} + \bar{b}, \qquad \overline{\bar{a} \cdot b} = \bar{a} \cdot \bar{b}$$

where b is another dependent variable, yields

Continuity:

$$\frac{\partial \bar{u}}{\partial s} + \frac{1}{y} \frac{\partial (\bar{v}y)}{\partial y} = 0 \tag{B.26}$$

s-momentum:

$$\bar{u} \frac{\partial \bar{u}}{\partial s} + \bar{v} \frac{\partial \bar{u}}{\partial y} = \frac{(\rho_\infty - \bar{\rho})}{\rho_o} g \sin\theta + \frac{1}{y} \frac{\partial}{\partial y} \left(y\nu \frac{\partial \bar{u}}{\partial y} \right) - \left[\frac{\partial (\overline{u'^2})}{\partial s} + \frac{1}{y} \frac{\partial}{\partial y} (y\overline{u'v'}) \right] \tag{B.27}$$

y-momentum:

$$\left[\bar{u}^2 - \frac{y}{2} \left(\bar{v} \frac{\partial \bar{v}}{\partial y} + \frac{1}{2} \frac{\partial}{\partial y} (\overline{v'^2}) \right) \right] \frac{d\theta}{ds} = \frac{(\rho_\infty - \bar{\rho})}{\rho_o} g \cos\theta . \tag{B.28}$$

Energy:

$$\bar{u}\frac{\partial \bar{t}}{\partial s} + \bar{v}\frac{\partial \bar{t}}{\partial y} = \frac{1}{\rho c_p y}\frac{\partial}{\partial y}\left(yk\frac{\partial \bar{t}}{\partial y}\right) - \left[\frac{\partial}{\partial s}(\overline{u't'}) + \frac{1}{y}\frac{\partial}{\partial y}(y\overline{v't'})\right] \tag{B.29}$$

(Fluctuations in the molecular diffusion terms have been neglected, see Ref. 97, p. 73.)

Based on the boundary layer assumptions for fluctuating quantities, it can be shown [97] that all double correlations such as $\overline{u'v'}$, $\overline{u'^2}$, $\overline{v't'}$, etc. are at most of order δ, where δ is the width of the boundary layer, in this case, the jet half-width. Also in accordance with the laminar boundary layer approximations [97], ρ, u, t, $\frac{\partial}{\partial s}$ are all of order L, $\frac{\partial}{\partial y}$ is of order δ^{-1}, v is of order δ, and ν,k are of order δ^2. Here, $\frac{\delta}{L} \ll 1$, L being a reference length. Using these relations to carry out an order-of-magnitude analysis of Eqs. (B.26) to (B.29) results in the following equations where terms of order L (or greater) are retained and terms of order δ and δ^2 are neglected.

Continuity (rewritten as):

$$\frac{\partial}{\partial s}(\bar{u}y) + \frac{\partial}{\partial y}(\bar{v}y) = 0 \tag{B.30}$$

s-momentum:

$$\bar{u}\frac{\partial \bar{u}}{\partial s} + \bar{v}\frac{\partial \bar{u}}{\partial y} = \frac{(\rho_\infty - \bar{\rho})}{\rho_o} g \sin\theta + \frac{1}{y}\frac{\partial}{\partial y}\left(y\nu\frac{\partial \bar{u}}{\partial y}\right)$$

$$- \frac{1}{y}\frac{\partial}{\partial y}(y\overline{u'v'}) \tag{B.31}$$

y-momentum:

$$\bar{u}^2 \frac{d\theta}{ds} = \frac{(\rho_\infty - \bar{\rho})}{\rho_o} g \cos\theta \tag{B.32}$$

Energy:

$$\bar{u} \frac{\partial \bar{t}}{\partial s} + \bar{v} \frac{\partial \bar{t}}{\partial y} = \frac{1}{\rho c_p y} \frac{\partial}{\partial y} \left(yk \frac{\partial \bar{t}}{\partial y} \right) - \frac{1}{y} \frac{\partial}{\partial y} (y\overline{v't'}) \tag{B.33}$$

Finally, removing the bars over mean quantities and rearranging yields:

Continuity:

$$\frac{\partial}{\partial s}(uy) + \frac{\partial}{\partial y}(vy) = 0 \tag{B.34}$$

s-momentum:

$$u \frac{\partial u}{\partial s} + v \frac{\partial u}{\partial y} = \frac{(\rho_\infty - \rho)}{\rho_o} g \sin\theta + \frac{1}{\rho y} \frac{\partial}{\partial y} \left[y \left(\rho\nu \frac{\partial u}{\partial y} - \rho\overline{u'v'} \right) \right] \tag{B.35}$$

y-momentum:

$$u^2 \frac{d\theta}{ds} = \frac{(\rho_\infty - \rho)}{\rho_o} g \cos\theta \tag{B.36}$$

Energy:

$$u \frac{\partial t}{\partial s} + v \frac{\partial t}{\partial y} = \frac{1}{\rho c_p y} \frac{\partial}{\partial y} \left[y \left(k \frac{\partial t}{\partial y} - \rho c_p \overline{v't'} \right) \right] \tag{B.37}$$

These are the same as Eqs. (3.1) to (3.6) of Chapter 3.

12. APPENDIX C:

DERIVATION OF NON-DIMENSIONAL FORMS

12.1. Governing Equations

The variables appearing in the governing equations [Eqs. (3.1) to (3.4)] are non-dimensionalized as follows:

$$U = \frac{u}{u_o}, \quad V = \frac{v}{u_o}, \quad T = \frac{t - t_{\infty_o}}{t_o - t_{\infty_o}}, \quad S = \frac{su_o}{\nu}, \quad Y = \frac{yu_o}{\nu},$$

$$N = \frac{n}{\nu}, \quad N_H = \frac{n_H}{\nu} \tag{C.1}$$

Combining Eq. (3.2) and Eq. (3.7), and using the Boussinesq assumption (see Chapter 2), yields the s-momentum equation in the following form:

$$u\frac{\partial u}{\partial s} + v\frac{\partial u}{\partial y} = \frac{1}{y}\frac{\partial}{\partial y}\left(yn\frac{\partial u}{\partial y}\right) + \frac{(\rho_\infty - \rho)}{\rho_o} g \sin\theta . \tag{C.2}$$

Introducing the non-dimensional relations of Eq. (C.1) into Eq. (C.2), gives

$$\frac{u_o^3}{\nu}\left(U\frac{\partial U}{\partial S} + V\frac{\partial U}{\partial Y}\right) = \frac{u_o^3}{\nu}\frac{1}{Y}\frac{\partial}{\partial Y}\left(YN\frac{\partial U}{\partial Y}\right) + \frac{(\rho_\infty - \rho)}{\rho_o} g \sin\theta$$

or

$$U\frac{\partial U}{\partial S} + V\frac{\partial U}{\partial Y} = \frac{1}{Y}\frac{\partial}{\partial Y}\left(YN\frac{\partial U}{\partial Y}\right) + \frac{\nu}{u_o^3}\frac{(\rho_\infty - \rho)}{\rho_o} g \sin\theta . \tag{C.3}$$

The equation of state, Eq. (3.10), is

$$\rho = \rho_{ref}\left[1 - \beta(t - t_{ref})\right]$$

or

$$\frac{\rho}{\rho_{ref}} = [1 - \beta(t - t_{ref})] \tag{C.4}$$

ρ is density at any point, and ρ_{ref} refers to the value of density at a reference point.

Thus, from Eq. (C.4), the following relations are obtained:

$$\frac{\rho_\infty}{\rho_o} = [1 - \beta(t_\infty - t_o)] \tag{C.5}$$

and

$$\frac{\rho}{\rho_o} = [1 - \beta(t - t_o)] \tag{C.6}$$

Subtracting Eq. (C.6) from Eq. (C.5) yields

$$\frac{\rho_\infty - \rho}{\rho_o} = \beta(t - t_\infty) \tag{C.7}$$

Equation (C.7) also appears in Chapter 3 as Eq. (3.11). In the same way,

$$\frac{(\rho_{\infty_o} - \rho_o)}{\rho_o} = \beta(t_o - t_{\infty_o}) \tag{C.8}$$

The discharge Froude number is defined as

$$Fr_o = \frac{u_o^2}{d_o g \dfrac{(\rho_{\infty_o} - \rho_o)}{\rho_o}}$$

Or, from Eq. (C.8)

$$Fr_o = \frac{u_o^2}{d_o g \beta (t_o - t_{\infty_o})} \tag{C.9}$$

Also, the buoyancy term in Eq. (C.3) can be expressed as

$$\frac{\nu}{u_o^3}\frac{(\rho_\infty - \rho)}{\rho_o} g \sin\theta = \frac{\nu}{u_o^3}\beta(t - t_\infty) g \sin\theta . \qquad (C.10)$$

The right hand side of Eq. (C.8) can be written as

$$\frac{\nu}{u_o d_o} \times \frac{d_o}{u_o^2} \times \beta\left[T(t_o - t_{\infty_o}) + t_{\infty_o} - (T_\infty[t_o - t_{\infty_o}] + t_{\infty_o})\right]$$

$$\times g \sin\theta$$

i.e.,

$$\frac{1}{Re_o} \times \frac{d_o}{u_o^2}\beta[T - T_\infty](t_o - t_{\infty_o}) g \sin\theta$$

or

$$\frac{1}{Re_o} \times \frac{(T - T_\infty)\sin\theta}{u_o^2 \Big/ [d_o g \beta (t_o - t_{\infty_o})]}$$

which finally gives

$$\frac{\nu}{u_o^3}\frac{(\rho_\infty - \rho)}{\rho_o} g \sin\theta = \frac{(T - T_\infty)}{Re_o Fr_o}\sin\theta . \qquad (C.11)$$

Introducing this into Eq. (C.3) yields

$$U\frac{\partial U}{\partial S} + V\frac{\partial U}{\partial Y} = \frac{1}{Y}\frac{\partial}{\partial Y}\left(YN\frac{\partial U}{\partial Y}\right) + \frac{(T - T_\infty)\sin\theta}{Re_o Fr_o} \qquad (C.12)$$

This is the non-dimensional form of the s-momentum equation presented in Chapter 3 as Eq. (3.16). Equations (3.15), (3.17) and (3.18) are derived in a similar manner.

θ is a dimensionless quantity and hence does not need to be redefined for the non-dimensional forms.

12.2. Stratification Boundary Condition

When the ambient temperature stratification is specified as λ, the degree of stratification, where

$$\lambda = - \frac{\Delta t_\infty}{\Delta z}$$

this can be rearranged as

$$\Delta t = - \lambda \Delta z$$

or

$$t_\infty - t_{\infty_o} = - \lambda (z - z_o) = - \lambda z . \qquad (C.13)$$

Introducing the non-dimensional variables of Eq. (C.1) and the variable $Z = \frac{z u_o}{\nu}$ into Eq. (C.13) gives

$$T_\infty (t_o - t_{\infty_o}) + t_{\infty_o} = t_{\infty_o} - \lambda \frac{Z \nu}{u_o}$$

or

$$T_\infty = - \lambda \frac{\nu}{u_o} \frac{Z}{(t_o - t_{\infty_o})}$$

or

$$T_\infty = \frac{- \lambda d_o}{Re_o (t_o - t_{\infty_o})} Z \qquad (C.14)$$

This is the same as Eq. (3.21) presented earlier.

13. APPENDIX D:

TRUNCATION ERROR OF THE DUFORT-FRANKEL DIFFERENCE EQUATIONS

Consistency is generally studied by expanding the dependent variables in Taylor series and observing the difference between the partial differential equations and the finite-difference representation. This difference, as mentioned in Chapter 3, is due to the neglected terms and is known as the truncation error associated with the difference scheme. A scheme is said to be consistent if this error vanishes as the mesh size approaches zero.

The truncation error of Eqs. (3.22) to (3.25), assuming (ΔY) constant, is obtained as follows: For Eq. (3.23), the variable U is expanded in Taylor series about the point (i,j) to give:

$$U_{i+1,j} = U_{i,j} + \left(\frac{\partial U}{\partial S}\right)_{i,j} (\Delta S_+) + \left(\frac{\partial^2 U}{\partial S^2}\right)_{i,j} \frac{(\Delta S_+)^2}{2} + \left(\frac{\partial^3 U}{\partial S^3}\right)_{i,j} \frac{(\Delta S_+)^3}{6} + \ldots.$$

$$U_{i-1,j} = U_{i,j} - \left(\frac{\partial U}{\partial S}\right)_{i,j} (\Delta S_-) + \left(\frac{\partial^2 U}{\partial S^2}\right)_{i,j} \frac{(\Delta S_-)^2}{2} - \left(\frac{\partial^3 U}{\partial S^3}\right)_{i,j} \frac{(\Delta S_-)^3}{6} + \ldots.$$

$$U_{i,j+1} = U_{i,j} + \left(\frac{\partial U}{\partial Y}\right)_{i,j} (\Delta Y) + \left(\frac{\partial^2 U}{\partial Y^2}\right)_{i,j} \frac{(\Delta Y)^2}{2} + \left(\frac{\partial^3 U}{\partial Y^3}\right)_{i,j} \frac{(\Delta Y)^3}{6} + \ldots.$$

$$U_{i,j-1} = U_{i,j} - \left(\frac{\partial U}{\partial Y}\right)_{ij} (\Delta Y) + \left(\frac{\partial^2 U}{\partial Y^2}\right)_{i,j} \frac{(\Delta Y)^2}{2}$$

$$- \left(\frac{\partial^3 U}{\partial Y^3}\right)_{i,j} \frac{(\Delta Y)^3}{6} + \ldots.$$

Substituting these expansions into Eq. (3.23) yields

$$\frac{U_{i,j}}{(\Delta S_+ + \Delta S_-)} \left[\left(\frac{\partial U}{\partial S}\right)_{i,j} (\Delta S_+ + \Delta S_-) + \left(\frac{\partial^2 U}{\partial S^2}\right)_{i,j} \frac{[(\Delta S_+)^2 - (\Delta S_-)^2]}{2}\right.$$

$$\left. + \left(\frac{\partial^3 U}{\partial S^3}\right)_{i,j} \frac{[(\Delta S_+)^3 + (\Delta S_-)^3]}{6} + \ldots\right]$$

$$+ \frac{V_{i,j}}{2\Delta Y} \left[2 \left(\frac{\partial U}{\partial Y}\right)_{i,j} (\Delta Y) + 2\left(\frac{\partial^3 U}{\partial Y^3}\right)_{i,j} \frac{(\Delta Y)^3}{6} + \ldots\right]$$

$$= \frac{1}{Y_j \Delta Y} \left\{\frac{\left(Y_{j+1} + Y_j\right)\left(N_{i,j} + N_{i,j+1}\right)}{4\Delta Y} \times \left[\left(U_{i,j} + \left(\frac{\partial U}{\partial Y}\right)_{i,j} \Delta Y + \right.\right.\right.$$

$$+ \left(\frac{\partial^2 U}{\partial Y^2}\right)_{i,j} \frac{(\Delta Y)^2}{2} + \left(\frac{\partial^3 U}{\partial Y^3}\right)_{i,j} \frac{(\Delta Y)^3}{6} - 0.5 \left(2U_{i,j}\right.$$

$$+ \left(\frac{\partial U}{\partial S}\right)_{i,j} (\Delta S_+ - \Delta S_-) + \left(\frac{\partial^2 U}{\partial S^2}\right)_{i,j} \frac{[(\Delta S_+)^2 + (\Delta S_-)^2]}{2}$$

$$\left.\left.\left. + \left(\frac{\partial^3 U}{\partial S^3}\right)_{i,j} \frac{[(\Delta S_+)^3 - (\Delta S_-)^3]}{6} + \ldots\right)\right]$$

$$- \frac{\left(Y_j + Y_{j-1}\right)\left(N_{i,j} + N_{i,j-1}\right)}{4\Delta Y} \times \left[0.5 \left(2U_{i,j} + \left(\frac{\partial U}{\partial S}\right)_{i,j} (\Delta S_+ - \Delta S_-)\right.\right.$$

$$\left.\left. + \left(\frac{\partial^2 U}{\partial S^2}\right)_{i,j} \frac{[(\Delta S_+)^2 + (\Delta S_-)^2]}{2} + \left(\frac{\partial^3 U}{\partial S^3}\right)_{i,j} \frac{[(\Delta S_+)^3 - (\Delta S_-)^3]}{6} + \ldots\right)\right.$$

$$- \left(U_{i,j} - \left(\frac{\partial U}{\partial Y}\right)_{i,j} \Delta Y + \left(\frac{\partial^2 U}{\partial Y^2}\right)_{i,j} \frac{(\Delta Y)^2}{2} - \left(\frac{\partial^3 U}{\partial Y^3}\right)_{i,j} \frac{(\Delta Y)^3}{6} + \ldots \right) \Bigg] \Bigg\}$$

$$+ \frac{\left(T_{i,j} - T_{\infty_j}\right)}{Re_o Fr_o} \sin \theta_i$$

The use of turbulence models introduces a level of approximation, but it hardly seems worthwhile to associate a truncation error with them.

To simplify the analysis, the following is assumed:

$$\frac{\left(Y_j + Y_{j+1}\right)\left(N_{i,j} + N_{i,j+1}\right)}{4} = Y_j N_{i,j} = \frac{\left(Y_j + Y_{j-1}\right)\left(N_{i,j} + N_{i,j-1}\right)}{4}$$

This assumption is justified by expanding $\left(Y_j + Y_{j+1}\right)\left(N_{i,j} + N_{i,j+1}\right)$ and $\left(Y_j + Y_{j-1}\right)\left(N_{i,j} + N_{i,j-1}\right)$ in Taylor series above (i,j). No new terms will appear that will alter the truncation error equation to reduce the accuracy of the difference equation.

This gives

$$U_{i,j} \left[\left(\frac{\partial U}{\partial S}\right)_{i,j} + \left(\frac{\partial^2 U}{\partial S^2}\right)_{i,j} \frac{(\Delta S_+ - \Delta S_-)}{2} + \left(\frac{\partial^3 U}{\partial S^3}\right)_{i,j} \frac{\left[(\Delta S_+)^3 + (\Delta S_-)^3\right]}{6(\Delta S_+ + \Delta S_-)} \right]$$

$$+ V_{i,j} \left[\left(\frac{\partial U}{\partial Y}\right)_{i,j} + \left(\frac{\partial^3 U}{\partial Y^3}\right)_{i,j} \frac{(\Delta Y)^2}{6} + \ldots \right]$$

$$= \frac{1}{Y_j} \Bigg\{ Y_j N_{i,j} \Bigg[\left(\left(\frac{\partial^2 U}{\partial Y^2}\right)_{i,j} + \left(\frac{\partial^4 U}{\partial Y^4}\right)_{i,j} \frac{(\Delta Y)^2}{12} + \ldots \right)$$

$$- 0.5 \left(2\left(\frac{\partial U}{\partial S}\right)_{i,j} \frac{(\Delta S_+ - \Delta S_-)}{(\Delta Y)^2} + \left(\frac{\partial^2 U}{\partial S^2}\right)_{i,j} \frac{\left[(\Delta S_+)^2 + (\Delta S_-)^2\right]}{(\Delta Y)^2} \right.$$

$$\left. + \left(\frac{\partial^3 U}{\partial S^3}\right)_{i,j} \frac{\left[(\Delta S_+)^3 - (\Delta S_-)^3\right]}{3(\Delta Y)^2} + \ldots \right) \Bigg] \Bigg\} + \frac{(T_{i,j} - T_{\infty i})}{Re_o Fr_o} \sin \theta_i$$

Defining T_{SM} as the truncation error of Eq. (3.23), i.e., the difference equation minus the partial differential equation, gives:

$$T_{SM} = U_{i,j}\left(\frac{\partial^2 U}{\partial S^2}\right)_{i,j}\frac{(\Delta S_+ - \Delta S_-)}{2} + U_{i,j}\left(\frac{\partial^3 U}{\partial S^3}\right)_{i,j}\frac{[(\Delta S_+)^3 + (\Delta S_-)^3]}{6(\Delta S_+ + \Delta S_-)}$$

$$+ V_{i,j}\left(\frac{\partial^3 U}{\partial Y^3}\right)_{i,j}\frac{(\Delta Y)^2}{6} - \left(\frac{\partial^4 U}{\partial Y^4}\right)_{i,j}\frac{(\Delta Y)^2}{12}$$

$$+ N_{i,j}\left(\frac{\partial U}{\partial S}\right)_{i,j}\frac{(\Delta S_+ - \Delta S_-)}{(\Delta Y)^2} + N_{i,j}\left(\frac{\partial^2 U}{\partial S^2}\right)_{i,j}\frac{[(\Delta S_+)^2 + (\Delta S_-)^2]}{2(\Delta Y)^2}$$

$$+ N_{i,j}\left(\frac{\partial^3 U}{\partial S^3}\right)_{i,j}\frac{[(\Delta S_+)^3 - (\Delta S_-)^3]}{3(\Delta Y)^2} + \ldots. \qquad (D.1)$$

$$= 0(\Delta S_+ - \Delta S_-) + 0(\Delta Y)^2 + 0\left[\frac{(\Delta S_+ - \Delta S_-)}{(\Delta Y)^2}\right] + \text{etc.}$$

ΔS_+ can be expressed as

$$\Delta S_+ = K\Delta S_- \quad (K \neq 1)$$

$$\text{Thus, } T_{SM} = 0(\Delta S_-) + 0\left[\frac{(\Delta S_-)}{(\Delta Y)^2}\right] + 0(\Delta Y)^2 + 0(\Delta S_-)^2 + 0\left(\frac{\Delta S_-}{\Delta Y}\right)^2 \qquad (D.2)$$

From the original expression for truncation error, Eq. (D.1), it can be seen that, for

$$\Delta S_+ \simeq \Delta S_- ,$$

$$T_{SM} = U_{i,j}\left(\frac{\partial^3 U}{\partial S^3}\right)_{i,j}\frac{(\Delta S)^2}{6} + V_{i,j}\left(\frac{\partial^3 U}{\partial Y^3}\right)_{i,j}\frac{(\Delta Y)^2}{6}$$

$$- \left(\frac{\partial^4 U}{\partial Y^4}\right)_{i,j}\frac{(\Delta Y)^2}{12} + N_{i,j}\left(\frac{\partial^2 U}{\partial S^2}\right)_{i,j}\left(\frac{\Delta S}{\Delta Y}\right)^2$$

$$= O(\Delta S)^2 + O(\Delta Y)^2 + O\left(\frac{\Delta S}{\Delta Y}\right)^2 . \qquad (D.3)$$

The significance of the term $O\left(\frac{\Delta S}{\Delta Y}\right)^2$ in the truncation error has been discussed in Chapter 3. Comparing Eqs. (D.2) and (D.3), it can be seen that there is an advantage to preserving the central-differencing nature of the D-F scheme, in terms of improving the truncation error of the scheme. This can be achieved, at least approximately, by not allowing two successive stepsizes to differ significantly. Procedures for modifying the difference equations to eliminate the first two terms of truncation error in Eq. (D.2) are available [39,98]. A similar procedure was tried but seemed unimportant for these calculations.

The truncation error of Eq. (3.25) is found in a similar manner and the result, in terms of order of the truncation error, is the same as Eq. (D.3), i.e.,

$$T_E = O(\Delta S)^2 + O(\Delta Y)^2 + O\left(\frac{\Delta S}{\Delta Y}\right)^2 \qquad (\text{if } \Delta S_+ \simeq \Delta S_-)$$

where T_E denotes the truncation error of the energy equation in difference form.

For Eq. (3.24), θ is expanded about (i,j) to give:

$$\theta_{i+1,j} = \theta_{i,j} + \left(\frac{d\theta}{dS}\right)_{i,j} (\Delta S_+) + \left(\frac{d^2\theta}{dS^2}\right)_{i,j} \frac{(\Delta S_+)^2}{2} + \left(\frac{d^3\theta}{dS^3}\right)_{i,j} \frac{(\Delta S_+)^3}{6} + \ldots$$

$$\theta_{i-1,j} = \theta_{i,j} - \left(\frac{d\theta}{dS}\right)_{i,j} (\Delta S_-) + \left(\frac{d^2\theta}{dS^2}\right)_{i,j} \frac{(\Delta S_-)^2}{2}$$

$$- \left(\frac{d^3\theta}{dS^3}\right)_{i,j} \frac{(\Delta S_-)^3}{6} + \ldots .$$

Substituting in Eq. (3.24) gives

$$(U_{i,j})^2 \left[\left(\frac{d\theta}{dS}\right)_{i,j} + \left(\frac{d^2\theta}{dS^2}\right)_{i,j} \frac{(\Delta S_+ - \Delta S_-)}{2} + \left(\frac{d^3\theta}{dS^3}\right)_{i,j} \frac{[(\Delta S_+)^3 + (\Delta S_-)^3]}{6(\Delta S_+ + \Delta S_-)} \right]$$

$$= \frac{T_{i,j} - T_{\infty i}}{Re_o Fr_o} \cos \theta_i$$

Subtracting the partial differential equation from the above gives:

$$T_{YM} = O(\Delta S_+ - \Delta S_-) = O(\Delta S_-)$$

Or, if $\Delta S_+ \simeq \Delta S_-$,

$$T_{YM} = O(\Delta S)^2 \ . \qquad \text{(D.4)}$$

For the difference form of the continuity equation (Eq. (3.22)), U, V are expanded about the point $[(i + 1), (j + 1/2)]$. This gives

$$U_{i+1,j+1} = U_{i+1,j+1/2} + \left(\frac{\partial U}{\partial Y}\right)_{i+1,j+1/2} \left(\frac{\Delta Y}{2}\right) + \frac{1}{2}\left(\frac{\partial^2 U}{\partial Y^2}\right)\left(\frac{\Delta Y}{2}\right)^2 + \frac{1}{6}\left(\frac{\partial^3 U}{\partial Y^3}\right)\left(\frac{\Delta Y}{2}\right)^3 + \ldots .$$

$$U_{i+1,j} = U_{i+1,j+1/2} - \left(\frac{\partial U}{\partial Y}\right)_{i+1,j+1/2} \left(\frac{\Delta Y}{2}\right) + \frac{1}{2}\left(\frac{\partial^2 U}{\partial Y^2}\right)\left(\frac{\Delta Y}{2}\right)^2 - \frac{1}{6}\left(\frac{\partial^3 U}{\partial Y^3}\right)\left(\frac{\Delta Y}{2}\right)^3 + \ldots .$$

$$U_{i-1,j+1} = U_{i+1,j+1/2} + \left(-(2\Delta S_-)\frac{\partial}{\partial S} + \frac{\Delta Y}{2}\frac{\partial}{\partial Y}\right) U_{i+1,j+1/2} + \frac{1}{2}\left(-(2\Delta S_-)\frac{\partial}{\partial S} + \frac{\Delta Y}{2}\frac{\partial}{\partial Y}\right)^2 U_{i+1,j+1/2} + \ldots .$$

$$U_{i-1,j} = U_{i+1,j+1/2} + \left(-(2\Delta S_-)\frac{\partial}{\partial S} - \frac{\Delta Y}{2}\frac{\partial}{\partial Y}\right) U_{i+1,j+1/2}$$

$$+ \frac{1}{2}\left(-(2\Delta S_-) - \frac{\Delta Y}{2}\frac{\partial}{\partial Y}\right)^2 U_{i+1,j+1/2} + \cdots$$

$$V_{i+1,j+1} = V_{i+1,j+1/2} \left(\frac{\partial V}{\partial Y}\right)_{i+1,j+1/2}\left(\frac{\Delta Y}{2}\right) + \frac{1}{2}\left(\frac{\partial^2 V}{\partial Y^2}\right)\left(\frac{\Delta Y}{2}\right)^2$$

$$+ \frac{1}{6}\left(\frac{\partial^3 V}{\partial Y^3}\right)\left(\frac{\Delta Y}{2}\right)^3 + \cdots.$$

$$V_{i+1,j} = V_{i+1,j+1/2} - \left(\frac{\partial V}{\partial Y}\right)_{i+1,j+1/2}\left(\frac{\Delta Y}{2}\right) + \frac{1}{2}\left(\frac{\partial^2 V}{\partial Y^2}\right)\left(\frac{\Delta Y}{2}\right)^2$$

$$- \frac{1}{6}\left(\frac{\partial^3 V}{\partial Y^3}\right)\left(\frac{\Delta Y}{2}\right)^3 + \cdots.$$

Substituting into Eq. (3.22) yields,

$$T_C = \frac{Y_{j+1/2}}{4(\Delta S_+ + \Delta S_-)}\left[-4(\Delta S_-)^2\frac{\partial^2 U}{\partial S^2}\right] - \frac{Y_{j+1/2}}{\Delta Y}\left[\frac{1}{3}\left(\frac{\partial^3 V}{\partial Y^3}\right)\left(\frac{\Delta Y}{2}\right)^3\right]$$

$$= \frac{O(\Delta S_-)^2}{(\Delta S_+ + \Delta S_-)} + O(\Delta Y)^2$$

Assuming $\Delta S_+ = k\Delta S_-$, yields

$$T_C = O(\Delta S_-) + O(\Delta Y)^2 . \qquad (D.5)$$

This remains the same even if $\Delta S_+ \simeq \Delta S_-$

By examining Eqs. (D.3), (D.4), (D.5), it is seen that the overall truncation error of the difference scheme is no smaller than

$$O(\Delta S) + O(\Delta Y)^2 + O\left(\frac{\Delta S}{\Delta Y}\right)^2 .$$

It is necessary that any truncation error be at most $O(\Delta Y)$ or $O(\Delta S)$ to satisfy consistency, and this is seen to be true for the present scheme, except for the presence of the term $O\left(\frac{\Delta S}{\Delta Y}\right)^2$, which would require the mesh to be refined such that $\lim_{\Delta S, \Delta Y \to 0} \left(\frac{\Delta S}{\Delta Y}\right) = 0$ in order to maintain consistency. However, as was explained in Chapter 3, the entire term in the truncation error is really $\left(\frac{\Delta S}{\Delta Y}\right)^2 \frac{\partial^2 U}{\partial S^2}$ and, for boundary-layer flows, $\frac{\partial^2 U}{\partial S^2}$ is negligibly small as compared to $\frac{\partial^2 U}{\partial Y^2}$ or other terms in the boundary-layer equations, causing the entire truncation error term to be negligible small.

14. APPENDIX E:

STABILITY OF THE DUFORT-FRANKEL DIFFERENCE SCHEME

To illustrate the stability analysis technique, the Von Neumann method will be applied to Eq. (3.23), i.e., the DuFort-Frankel difference form of the s-momentum equation. Equation (3.25), i.e., the difference form of the energy equation, can be treated in the same manner.

Let the exact solution of the difference equation be D and let the solution actually obtained by numerical calculations be $D + \delta'$, where δ' is the error at a point due to accumulation of round-off errors. $D + \delta'$ must also satisfy the difference equation (3.23). Substituting $D + \delta'$ for the dependent variable $U_{i,j}$ in Eq. (3.23) and subtracting the equation for D leaves the equation satisfied by δ' at any point.

The error equation at the point (i,j) is thus:

$$\frac{U_{i,j}}{(\Delta S_+ + \Delta S_-)}\left(\delta'_{i+1,j} - \delta'_{i-1,j}\right) + \frac{V_{i,j}}{(\Delta Y_+ + \Delta Y_-)} \times \left(\delta'_{i,j+1} - \delta'_{i,j-1}\right) = \frac{2}{Y_j(\Delta Y_+ + \Delta Y_-)} \times \left\{\left[\frac{(Y_{j+1} + Y_j)(N_{i,j} + N_{i,j+1})}{4} \times \frac{(\delta'_{i,j+1} - 0.5\,\delta'_{i+1,j} + \delta'_{i-1,j})}{\Delta Y_+}\right]\right\} - \left[\frac{(Y_j + Y_{j-1})(N_{i,j} + N_{i,j-1})}{4}\right.$$

$$\times \frac{\left(0.5\left[\delta'_{i+1,j} + \delta'_{i-1,j}\right] - \delta'_{i,j-1}\right)}{\Delta Y_-} \Bigg]\Bigg\} \qquad \text{(E.1)}$$

The coefficients of the derivative terms remain unchanged in this operation as they are assumed locally constant or error-free. This is a simplification and gives rise to a 'local' stability criterion, but if the requirement is checked at each grid point, then it is reasoned that an instability could not originate.

The Von Neumann condition assumes an error of the form

$$\delta'_{i,j} = e^{\alpha' S} e^{i\beta' Y}$$

This error, $\delta'_{i,j}$, is then substituted in the derivative terms for the dependent variable, U. At any instant, $\Delta S_+ \approx \Delta S_-$ and $\Delta Y_+ \approx \Delta Y_-$ and they will be assumed equal in order to simplify the analysis.

ΔY is assumed small enough so that

$$\frac{Y_{j+1} + Y_j}{2} \approx Y_j \approx \frac{Y_{j-1} + Y_j}{2}$$

Equation (E.1) then becomes

$$\frac{U_{i,j}}{2\Delta S_+}\left(e^{\alpha'(S+\Delta S)} e^{i\beta' Y} - e^{\alpha'(S-\Delta S)} e^{i\beta' Y}\right) + \frac{V_{i,j}}{2\Delta Y}$$

$$\times \left(e^{\alpha' S} e^{i\beta'(Y+\Delta Y)} - e^{\alpha' S} e^{i\beta'(Y-\Delta Y)}\right)$$

$$= \frac{1}{Y_j \Delta Y}\left\{\left[\frac{2Y_j\left(N_{i,j} + N_{i,j+1}\right)}{4}\right.\right.$$

$$\times\left(\frac{e^{\alpha' S} e^{i\beta'(Y+\Delta Y)} - 0.5\left[e^{\alpha'(S+\Delta S)} e^{i\beta' Y} + e^{\alpha'(S-\Delta S)} e^{i\beta' Y}\right]}{\Delta Y}\right)\Bigg]$$

$$-\left[\frac{2Y_j\left(N_{i,j} + N_{i,j-1}\right)}{4} \times \left(0.5\left[e^{\alpha'(S+\Delta S)} e^{i\beta' Y} + e^{\alpha'(S-\Delta S)} e^{i\beta' Y}\right]\right.\right.$$

$$\left.\left.\left. - e^{\alpha' S} e^{i\beta'(Y-\Delta Y)}\right)\right]\right\}$$

The term $\left(\frac{T_{i,j} - T_{\infty,i}}{Re_o\, Fr_o}\right)\sin\theta_i$ does not appear in the error equation, as it does not have any derivatives and is therefore assumed not to contribute any errors. Taking $e^{\alpha' S} e^{i\beta' Y}$ common,

$$\frac{U_{i,j}}{2\Delta S_+}\left(e^{\alpha'\Delta S} - e^{-\alpha'\Delta S}\right) + \frac{V_{i,j}}{2\Delta Y}\left(e^{i\beta'\Delta Y} - e^{-i\beta'\Delta Y}\right)$$

$$= \frac{1}{2(\Delta Y)^2}\left\{\left[\left(N_{i,j} + N_{i,j+1}\right) \times \left(e^{i\beta'\Delta Y} - 0.5\left[e^{\alpha'\Delta S} + e^{-\alpha'\Delta S}\right]\right)\right]\right.$$

$$\left. - \left[\left(N_{i,j} + N_{i,j-1}\right) \times \left(0.5\left[e^{\alpha'\Delta S} + e^{-\alpha'\Delta S}\right] - e^{i\beta'\Delta Y}\right)\right]\right\} \quad \text{(E.2)}$$

R.H.S. of Eq. (E.2) =

$$\frac{1}{2(\Delta Y)^2}\left\{\left(N_{i,j} + N_{i,j+1}\right) e^{i\beta'\Delta Y} + \left(N_{i,j} + N_{i,j-1}\right) e^{-i\beta'\Delta Y}\right.$$

$$- \frac{\left(N_{i,j+1} + 2N_{i,j} + N_{i,j-1}\right)}{2} e^{\alpha'\Delta S}$$

$$\left. - \frac{\left(N_{i,j+1} + 2N_{i,j} + N_{i,j-1}\right)}{2} e^{-\alpha'\Delta S}\right\}$$

Transposing, Eq. (E.2) becomes:

$$\frac{U_{i,j}}{2\Delta S_+}\left(e^{\alpha'\Delta S} - e^{-\alpha'\Delta S}\right)$$

$$+ \frac{1}{4(\Delta Y)^2}\left(N_{i,j+1} + 2N_{i,j} + N_{i,j-1}\right)\left(e^{\alpha'\Delta S} + e^{-\alpha'\Delta S}\right)$$

$$+ \frac{V_{i,j}}{2\Delta Y}\left(e^{i\beta'\Delta Y} - e^{-i\beta'\Delta Y}\right)$$

$$= \frac{1}{2(\Delta Y)^2}\left[\left(N_{i,j} + N_{i,j+1}\right) e^{i\beta'\Delta Y} + \left(N_{i,j} + N_{i,j-1}\right) e^{-i\beta'\Delta Y}\right]$$

or

$$e^{2\alpha\Delta S} - 1 + \frac{\Delta S_+}{2U_{i,j}(\Delta Y)^2}\left(N_{i,j+1} + 2N_{i,j} + N_{i,j-1}\right)\left(e^{2\alpha'\Delta S} + 1\right)$$

$$+ \frac{V_{i,j}\,\Delta S_+}{\Delta Y\, U_{i,j}}\, e^{\alpha'\Delta S}\left(e^{i\beta'\Delta Y} - e^{-i\beta'\Delta Y}\right)$$

$$= \frac{\Delta S_+\, e^{\alpha'\Delta S}}{(\Delta Y)^2\, U_{i,j}}\left[\left(N_{i,j} + N_{i,j+1}\right) e^{i\beta'\Delta Y}\right.$$

$$\left. + \left(N_{i,j} + N_{i,j-1}\right) e^{-i\beta'\Delta Y}\right]$$

Let $\bar{N} = \frac{N_{i,j+1} + 2N_{i,j} + N_{i,j-1}}{4}$, $N_+ = \frac{N_{i,j} + N_{i,j+1}}{2}$, $N_- = \frac{N_{i,j} + N_{i,j-1}}{2}$

$$A = \frac{V_{i,j}\Delta S_+}{\Delta Y U_{i,j}}, \qquad B = \frac{2\Delta S_+}{U_{i,j}(\Delta Y)^2} \tag{E.3}$$

This gives

$$e^{2\alpha'\Delta S} \times (1 + B\bar{N}) + (B\bar{N} - 1) + A e^{\alpha'\Delta S} 2i \sin \beta'\Delta Y$$

$$= B e^{\alpha'\Delta S} \left[N_+ e^{i\beta'\Delta Y} + N_- e^{-i\beta'\Delta Y}\right]$$

or

$$e^{2\alpha'\Delta S} (1 + B\bar{N}) + e^{\alpha'\Delta S} \left(2A i \sin \beta'\Delta Y - BN_+ e^{i\beta'\Delta Y}\right.$$

$$\left. - BN_- e^{-i\beta'\Delta Y}\right) + B\bar{N} - 1 = 0$$

or

$$e^{2\alpha'\Delta S} (1 + B\bar{N}) + e^{\alpha'\Delta S}\left[2A i \sin \beta'\Delta Y - BN_+ \left(\cos \beta'\Delta Y\right.\right.$$

$$\left.\left. + i \sin \beta'\Delta Y\right) - BN_- \left(\cos \beta'\Delta Y - i \sin \beta'\Delta Y\right)\right] + B\bar{N} - 1 = 0$$

Now, $N_+ + N_- = 2\bar{N}$

$$e^{2\alpha'\Delta S} (1 + B\bar{N}) + e^{\alpha'\Delta S}\left[2A i \sin \beta'\Delta Y - 2B\bar{N} \cos \beta'\Delta Y\right.$$

$$\left. + i \sin \beta'\Delta Y (-BN_+ + BN_-)\right] + B\bar{N} - 1 = 0$$

or

$$e^{2\alpha'\Delta S} (1 + B\bar{N}) + e^{\alpha'\Delta S}\left[-2B\bar{N} \cos \beta'\Delta Y +\right.$$

$$\left. + i \sin \beta'\Delta Y (2A + BN_- - BN_+)\right] + B\bar{N} - 1 = 0$$

Let $X = e^{\alpha' \Delta S}$

and

$$C = 2A + BN_{-} - BN_{+} \tag{E.4}$$

This gives

$$X^2(1 + B\bar{N}) + X\left[-2B\bar{N}\cos \beta' \Delta Y + i\, C \sin \beta' \Delta Y\right] + B\bar{N} - 1 = 0$$

This is a quadratic in X.

Hence,

$$e^{\alpha \Delta S} =$$

$$\frac{2B\bar{N}\cos \beta' \Delta Y - i\, C \sin \beta' \Delta Y \pm \sqrt{(-2B\bar{N}\cos \beta' \Delta Y + i\, C \sin \beta' \Delta Y)^2 - 4(1+B\bar{N})(B\bar{N}-1)}}{2(1+B\bar{N})}$$

(E.5)

Stability of the numerical solution requires that $\left|e^{\alpha' \Delta S}\right| \leq 1$.

The nature of $e^{\alpha' \Delta S}$ can easily be studied for extreme values of $\cos \beta' \Delta Y$ and $\sin \beta' \Delta Y$.

Extreme 1

$$\cos\beta'\Delta Y = +1, \quad \sin\beta'\Delta Y = 0$$

This yields from Eq. (E.5)

$$e^{\alpha'\Delta S} = \frac{2B\bar{N} \pm \sqrt{4B^2\bar{N}^2 - 4(B^2\bar{N}^2 - 1)}}{2(1+B\bar{N})} = \frac{(2B\bar{N} \pm 2)}{2(1+B\bar{N})} = \frac{B\bar{N} \pm 1}{B\bar{N} + 1}$$

And $|e^{\alpha'\Delta S}| \leq 1$ requires that

$$\left|\frac{B\bar{N} \pm 1}{B\bar{N} + 1}\right| \leq 1$$

Since B, $\bar{N}$ are both positive, the above condition is always satisfied.

Extreme 2

$$\cos\beta'\Delta Y = -1, \quad \sin\beta'\Delta Y = 0$$

This yields,

$$e^{\alpha'\Delta S} = \frac{-2B\bar{N} \pm \sqrt{4B^2\bar{N}^2 - (4B^2\bar{N}^2 - 4)}}{2(1 + B\bar{N})} = -\frac{2BN \pm 2}{2(1 + B\bar{N})} = -\frac{B\bar{N} + 1}{B\bar{N} + 1}$$

And, the condition $|e^{\alpha'\Delta S}| \leq 1$ gives

$$\left|-\frac{(B\bar{N} \mp 1)}{(B\bar{N} + 1)}\right| = \left|\frac{B\bar{N} \mp 1}{B\bar{N} + 1}\right| \leq 1$$

This is also always satisfied, as before.

Extreme 3

$$\cos\beta'\Delta Y = 0, \quad \sin\beta'\Delta Y = +1$$

This yields,

$$e^{\alpha'\Delta S} = \frac{-iC \pm \sqrt{-C^2 - 4B^2\bar{N}^2 + 4}}{2(1 + B\bar{N})}$$

(i) If $-C^2 - 4B^2\bar{N}^2 + 4 > 0$,

$|e^{\alpha'\Delta S}| \leq 1$ implies $\sqrt{R^2 + Im^2} \leq 1$.

i.e. $R^2 + Im^2 \leq 1$.

Or,

$$\frac{C^2 \pm (-C^2 - 4B^2\bar{N}^2 + 4)}{4(1 + B\bar{N})^2} \leq 1 \qquad \text{(E.6)}$$

a) $\frac{-4B^2\bar{N}^2 + 4}{4(1 + B\bar{N})^2} \leq 1$.

or $B^2\bar{N}^2 + 1 \leq 1 + 2B\bar{N} + B^2\bar{N}^2$.

or $(1 - 2B\bar{N}) \leq 1$.

or $B\bar{N} \geq 0$

Since B, $\bar{N}$ are both positive, this condition is always satisfied.

b) $\frac{2C^2 + 4B^2\bar{N}^2 - 4}{4(1 + B\bar{N})^2} \leq 1$

or $2C^2 + 4B^2\bar{N}^2 - 4 \leq 4 + 8B\bar{N} + 4B^2\bar{N}^2$

i.e., $2C^2 - 8B\bar{N} \leq 8$

or $C^2 \leq 4(1 + B\bar{N})$ (E.7)

Later, this condition will be seen to be satisfied.

(ii) If $-C^2 - 4B^2\bar{N}^2 + 4 < 0$, then $\sqrt{-C^2 - 4B^2\bar{N}^2 + 4}$ is imaginary, and can be replaced by $i\sqrt{+C^2 + 4B^2\bar{N}^2 - 4}$

Thus, $|e^{\alpha'\Delta S}| \leq 1$ implies

$$\left| \frac{i(-C \pm \sqrt{C^2 + 4B^2\bar{N}^2 - 4})}{2(1 + B\bar{N})} \right| \leq 1$$

Since $(1 + B\bar{N}) > 0$

This gives,

$$|i(-C \pm \sqrt{C^2 + 4B^2\bar{N}^2 - 4})| \leq 2(1 + B\bar{N})$$

or $$\left(-C \pm \sqrt{C^2 + 4B^2\bar{N}^2 - 4}\right)^2 \leq 4(1 + B\bar{N})^2 \qquad \text{(E.8)}$$

or $$C^2 + C^2 + 4B^2\bar{N}^2 - 4 \pm 2C\sqrt{C^2 + 4B^2\bar{N}^2 - 4} \leq 4\left(1 + 2B\bar{N} + B^2\bar{N}^2\right)$$

i.e., $$2C^2 - 4 \pm 2C\sqrt{C^2 + 4B^2\bar{N}^2 - 4} \leq 4(1 + 2B\bar{N}).$$

or $$\pm 2C\sqrt{C^2 + 4B^2\bar{N}^2 - 4} \leq 8(1 + B\bar{N}) - 2C^2$$

$$C^2(C^2 + 4B^2\bar{N}^2 - 4) \leq [4(1 + B\bar{N}) - C^2]^2$$

$$\leq 16(1 + B\bar{N})^2 - 8(1 + B\bar{N})C^2 + C^4$$

i.e. $$C^4 + 4B^2C^2\bar{N}^2 - 4C^2 \leq 16 + 32B\bar{N} + 16B^2\bar{N}^2 - 8C^2 - 8B\bar{N}C^2 + C^4$$

or $$C^2(1 + 2B\bar{N} + B^2\bar{N}^2) \leq 4(1 + B\bar{N})^2$$

or $$C^2(1 + B\bar{N})^2 \leq 4(1 + B\bar{N})^2$$

i.e., $$C^2 \leq 4.$$

or $$|C| \leq 2.$$

This yields,

$$\left| \frac{2V_{i,j}\Delta S_+}{U_{i,j}\Delta Y} + \frac{2\Delta S_+}{(\Delta Y)^2 U_{i,j}} \left(\frac{N_{i,j-1} - N_{i,j+1}}{2} \right) \right| \leq 2 .$$

i.e.,

$$\frac{\Delta S_+}{U_{i,j}\Delta Y} \left| V_{i,j} + \left(\frac{N_{i,j-1} - N_{i,j+1}}{2} \right) \right| \leq 1 .$$

or

$$\Delta S_+ \leq \frac{U_{i,j}\Delta Y}{\left| V_{i,j} + \left(\frac{N_{i,j-1} - N_{i,j+1}}{2} \right) \right|} \qquad \text{(E.9)}$$

which is the required stability constraint on the forward stepsize.

Also, since $4(1 + B\bar{N}) \geq 4$, the condition $C^2 \leq 4$ implies $C^2 \leq 4(1 + B\bar{N})$. Hence, Eq. (E.8) is satisfied.

Extreme 4

4 $\cos\beta'\Delta Y = 0$, $\sin\beta'\Delta Y = -1$

This yields,

$$e^{\alpha\Delta S} = \frac{iC \pm \sqrt{-C^2 - 4B^2\bar{N}^2 + 4}}{2(1 + B\bar{N})} .$$

(i) If $-C^2 - 4B^2\bar{N}^2 + 4 > 0$

$|e^{\alpha'\Delta S}| \leq 1$ gives

$$\frac{C^2 \pm (-C^2 - 4B^2\bar{N}^2 + 4)}{4(1 + B\bar{N})^2} \leq 1 .$$

which is the same as Eq. (E-6).

(ii) If $-C^2 - 4B^2\bar{N}^2 + 4 < 0$

$$\left|e^{\alpha'\Delta S}\right| \leq 1 \quad \text{gives}$$

$$\left| \frac{i\left(C \pm \sqrt{C^2 + 4B^2\bar{N}^2 - 4}\right)}{2(1 + B\bar{N})} \right| \leq 1$$

or $$\left(C \pm \sqrt{C^2 + 4B^2\bar{N}^2 - 4}\right)^2 \leq 4(1 + B\bar{N})^2$$

This is the same as Eq. (E.8).

The constraint of Eq. (E.9) has to be satisfied on all grid points of the jet width, and the most stringent requirement at each streamwise station would therefore be given by:

$$\Delta S_+ \leq \min_{j=2,NY}\left[\frac{U_{i,j}\Delta Y}{\left|V_{i,j} + \frac{N_{i,j-1} - N_{i,j+1}}{2\Delta Y}\right|}\right] \tag{E.10}$$

It is worth noting that the condition $C^2 \leq 4$ automatically satisfies $C^2 \leq 4\ (1 + B\bar{N})$ (Eq. E-8), since $4(1 + B\bar{N}) > 4$.

A similar analysis of the energy equation in difference form (Eq. (3.24)) yields

$$\Delta S_+ \leq \min_{j=2,NYT}\left[\frac{U_{i,j}\Delta Y}{\left|V_{i,j} + \frac{N_{H_{i,j-1}} - N_{H_{i,j+1}}}{2\Delta Y}\right|}\right] \tag{E.11}$$

Combining Eqs. (E.10) and (E.11) yields the final form of the stability constraint on the forward streamwise stepwise as follows:

$$\Delta S_+ \leq \min_{J=2,NYJ}\left[\frac{U_{i,j}\Delta Y}{\left|V_{i,j} + \frac{FUNC}{2\Delta Y}\right|}\right] \tag{E.12}$$

where NYJ = max (NY,NYT), and

$$FUNC = \max\left[\left(N_{i,j-1} - N_{i,j+1}\right), \left(N_{H_{i,j-1}} - N_{H_{i,j+1}}\right)\right]$$

This is the form shown in Chapter 3 as Eq. (3.30).

As a check, the stability criterion for laminar flow can be obtained from Eq. (E.12) by letting $N_{i,j-1} = N_{i,j+1} = \nu$

and $$N_{H_{i,j-1}} = N_{H_{i,j+1}} = \alpha.$$

This gives

$$\Delta S_+ \leq \min_{j=2,NYJ}\left[\frac{U_{i,j}\Delta Y}{|V_{i,j}|}\right] \tag{E.13}$$

In the computer code, the forward stepsize was calculated as $\Delta S_+ = 0.7 \times \Delta S_+)_{max}$ where $\Delta S_+)_{max}$ is the right hand side of Eq. (E.12). 0.7 is a safety factor to account for any approximations that have been used in the stability analysis.

15. APPENDIX F:

THE SIMPLE EXPLICIT DIFFERENCE SCHEME

The difference equations:

The simple explicit forms of Eqs. (3.14) to (3.17) are:

Continuity:

$$\frac{Y_{j+1} + Y_j}{4\Delta S_+}\left[U_{i+1,j+1} + U_{i+1,j} - U_{i,j+1} - U_{i,j}\right] + \frac{\left(Y_{j+1}V_{i+1,j+1} - Y_jV_{i+1,j}\right)}{\Delta Y_+} = 0 \qquad (F.1)$$

s-momentum:

$$\frac{U_{i,j}}{\Delta S_+}\left(U_{i+1,j} - U_{i,j}\right) + \frac{V_{i,j}}{\Delta Y_-}\left(U_{i,j} - U_{i,j-1}\right)^* = \frac{2}{Y_j(\Delta Y_+ + \Delta Y_-)}\left\{\left[\frac{\left(Y_{j+1} + Y_j\right)\left(N_{i,j} + N_{i,j+1}\right)}{4} \times \frac{\left(U_{i,j+1} - U_{i,j}\right)}{\Delta Y_+}\right] - \left[\frac{\left(Y_j + Y_{j-1}\right)\left(N_{i,j} + N_{i,j-1}\right)}{4} \times \frac{\left(U_{i,j} - U_{i,j-1}\right)}{\Delta Y_-}\right]\right\} + \frac{\left(T_{i,j} - T_{\infty i}\right)}{Re_o Fr_o}\sin\theta_i \qquad (F.2)$$

The starred term is used when $V_{i,j}$ is positive, otherwise it is replaced by:

$$\frac{V_{i,j}}{\Delta Y_+}\left(U_{i,j+1} - U_{i,j}\right)$$

y - momentum:

$$\frac{\left(U_{i,j}\right)^2}{\Delta S_+}\left(\theta_{i+1} - \theta_i\right) = \frac{\left(T_{i,j} - T_{\infty i}\right)}{Re_o Fr_o}\cos\theta_i \qquad (F.3)$$

Energy:

$$\frac{U_{i,j}}{\Delta S_+}\left(T_{i+1,j} - T_{i,j}\right) + \frac{V_{i,j}}{\Delta Y_-}\left(T_{i,j} - T_{i,j-1}\right)$$

$$= \frac{2}{Y_j(\Delta Y_+ + \Delta Y_-)}\left\{\left[\frac{\left(Y_{j+1} + Y_j\right)\left(N_{H_{i,j}} + N_{H_{i,j+1}}\right)}{4} \times \frac{\left(T_{i,j+1} - T_{i,j}\right)}{\Delta Y_+}\right]\right.$$

$$\left. - \left[\frac{\left(Y_j + Y_{j-1}\right)\left(N_{H_{i,j}} + N_{H_{i,j-1}}\right)}{4} \times \frac{\left(T_{i,j} - T_{i,j-1}\right)}{\Delta Y_-}\right]\right\} \qquad (F.4)$$

Stability restriction on stepsize:

The Von Neumann analysis, when applied to the simple explicit equations, reveals the following constraint [93]:

$$(\Delta S_+) \times \left[\frac{|V_{i,j}|}{U_{i,j}\Delta Y_-} + \frac{\left(Y_j + Y_{j+1}\right)_{FUNC^+}}{2U_{i,j}Y_j\Delta Y_+(\Delta Y_+ + \Delta Y_-)}\right.$$

$$\left. + \frac{\left(Y_j + Y_{j-1}\right)_{FUNC^-}}{2U_{i,j}Y_j\,\Delta Y_-(\Delta Y_+ + \Delta Y_-)}\right] \leq 1 \qquad (F.5)$$

where $FUNC^+ = \text{Max}\left[\left(N_{i,j} + N_{i,j+1}\right), \left(N_{H_{i,j}} + N_{H_{i,j+1}}\right)\right]$

$FUNC^- = \text{Max}\left[\left(N_{i,j} = N_{i,j-1}\right), \left(N_{H_{i,j}} + N_{H_{i,j-1}}\right)\right]$

Making use of the assumptions in Appendix E, Eq. (F.5) simplifies to:

$$\Delta S_+ \leq \frac{U_{i,j}\Delta Y}{\underset{j=2,NY}{\text{Max}}\left[|V_{i,j}| + \frac{\overline{FUNC}}{2\Delta Y}\right]} \tag{F.6}$$

where $\overline{FUNC} = \text{Max}\left[\left(N_{i,j+1} + 2N_{i,j} + N_{i,j-1}\right), \left(N_{H_{i,j+1}} + 2N_{H_{i,j}} + N_{H_{i,j-1}}\right)\right]$

A preliminary comparison of Eqs. (E.12) and (F.6) shows that while the denominator in the former depends only on the lateral difference in viscosity or conductivity values, the latter depends on the absolute values of the viscosities and conductivities, making the stability restriction on the forward stepsize far more severe for the simple explicit scheme than for the DuFort-Frankel formulation, except very near the jet discharge.